SURFACE DISPLACEMENT MEASUREMENTS STRAIN AND VIBRATIONAL ANALYSIS USING SPECKLE METROLOGY TECHNIQUES

Alan Bernard Lerchbacker

NAVAL POSTGRADUATE SCHOOL
Monterey, California

THESIS

SURFACE DISPLACEMENT MEASUREMENTS,
STRAIN AND VIBRATIONAL ANALYSIS
USING SPECKLE METROLOGY TECHNIQUES

by

Alan Bernard Lerchbacker

March 1980

Thesis Advisor: A. E. Fuhs

APPROVED FOR PUBLIC RELEASE; DISTRIBUTION UNLIMITED

REPORT DOCUMENTATION PAGE

READ INSTRUCTIONS BEFORE COMPLETING FORM

1. REPORT NUMBER	2. GOVT ACCESSION NO. / 3. RECIPIENT'S CATALOG NUMBER
4. TITLE (and Subtitle): Surface Displacement Measurements, Strain And Vibrational Analysis Using Speckle Metrology Techniques	5. TYPE OF REPORT & PERIOD COVERED: Master's Thesis March 1980 / 6. PERFORMING ORG. REPORT NUMBER
7. AUTHOR(s): Alan Bernard Lerchbacker	8. CONTRACT OR GRANT NUMBER(s)
9. PERFORMING ORGANIZATION NAME AND ADDRESS: Naval Postgraduate School, Monterey, California 93940	10. PROGRAM ELEMENT, PROJECT, TASK AREA & WORK UNIT NUMBERS
11. CONTROLLING OFFICE NAME AND ADDRESS: Naval Postgraduate School, Monterey, California 93940	12. REPORT DATE: March 1980 / 13. NUMBER OF PAGES: 153
14. MONITORING AGENCY NAME & ADDRESS(if different from Controlling Office)	15. SECURITY CLASS. (of this report): Unclassified / 15a. DECLASSIFICATION/DOWNGRADING SCHEDULE

16. DISTRIBUTION STATEMENT (of this Report)

Approved for public release; distribution unlimited.

17. DISTRIBUTION STATEMENT (of the abstract entered in Block 20, if different from Report)

18. SUPPLEMENTARY NOTES

19. KEY WORDS (Continue on reverse side if necessary and identify by block number)

Speckle, Laser, Metrology, Translation, Vibrations, Strain, Double-exposures.

20. ABSTRACT (Continue on reverse side if necessary and identify by block number)

Double-exposure specklegrams were made of aluminum 2024-T4 rectangular plates. The double-exposure speckle technique was applied to the aluminum plate to measure in-plane translation and rotation and out-of-plane tilt. Strain and vibrational analyses were also conducted. The vibrational results were compared with results previously obtained using double-exposure time average holography to ascertain their

Block 20 continued...

applicability to Naval Engineering.

Background in Fourier transforms, wave theory, Fraunhofer diffdiffraction theory, and other areas of physical optics were investigated to enhance the development of speckle metrology techniques.

Results of the experiments indicate that speckle metrology used in conjunction with holography has significant potential for Naval Engineering applications. Further research is required to develop these techniques. These procedures currently are being utilized extensively in the aerospace industry and automotive research and development areas.

Approved For Public Release; Distribution Unlimited

SURFACE DISPLACEMENT MEASUREMENTS, STRAIN AND VIBRATIONAL ANALYSIS USING SPECKLE METROLOGY TECHNIQUES

by

Alan Bernard Lerchbacker
Lieutenant, United States Navy
B.S., United States Naval Academy, 1974

Submitted In Partial Fulfillment Of The
Requirements For The Degree Of

MASTER OF SCIENCE IN MECHANICAL ENGINEERING

from the

NAVAL POSTGRADUATE SCHOOL
March 1980

ABSTRACT

Double-exposure specklegrams were made of aluminum 2024-T4 rectangular plates. The double-exposure speckle technique was applied to the aluminum plates to measure in-plane translation and rotation and out-of-plane tilt. Strain and vibrational analyses were also conducted. The vibrational results were compared with results previously obtained using double-exposure time average holography to ascertain their applicability to Naval Engineering.

Background in Fourier transforms, wave theory, Fraunhofer diffraction theory, and other areas of physical optics were investigated to enhance the development of speckle metrology techniques.

Results of the experiments indicate that speckle metrology used in conjunction with holography has significant potential for Naval Engineering applications. Further research is required to develop these techniques. These procedures currently are being utilized extensively in the aerospace industry and automotive research and development areas.

TABLE OF CONTENTS

LIST OF FIGURES

LIST OF TABLES

NOMENCLATURE

SYMBOL	DEFINITION	UNITS	EQUATION NUMBERS
A	Wave amplitude	meter	4, 84, 89, 90, 93, 94, 95, 97, 98, 100
A	Constant of integration	-	17, 18, 19, 24
A	Area of integration	meter squared	18, 19, 24, 32
a	Half length of rectangular aperture	meter	34, 35
a	Radius of circular aperture	meter	38, 40, 43, 44, 46
a	Portion in space	meter	47, 48, 56, 57, 58, 62
a	Length of rectangular aperture	meter	63, 64
a	Diameter of circular aperture	meter	66, 67
a	Amplitude of wave	meter	118, 119
B	Area of integration	meter squared	15
b	Half length of rectangular aperture	meter	33, 35
b	Length of rectangular aperture	meter	63, 64, 65
b_s	Speckle size	meter	124, 125, 126
C	Area of integration	meter squared	15
c	Constant of integration	-	33, 38, 40, 43, 44
c	Function of X	-	50

c	Constant	-	68, 73
d	Half length of aperture	meter	112, 144
d_o	Object distance from lens	meter	93
d	Object distance from Fourier plane	meter	94, 95
d_f	Fringe spacing	meter	128, 133, 135, 136, 138, 140
D	Lens diameter	meter	139
D_i	Image distance to lens	meter	139
D_o	Object distance to lens	meter	143
E	Electric field vector	meter	1, 4, 5, 44, 96, 97, 98
f	Focal length	meter	86, 87, 88, 89, 90, 92, 93, 94, 95, 122, 126, 127, 128, 135, 136, 137, 138, 139, 140
I	Irradiance or intensity	-	35, 44, 52, 53, 65, 75, 90, 96, 99, 100, 110, 114, 121, 123

J_n	Bessel function of nth order	-	40, 41, 42, 43, 44, 45, 67, 137
K	Wave number	1/meter	3, 4, 7, 9, 11, 12, 13, 17, 18, 19, 24, 33, 34, 35, 74, 75, 83, 86, 87, 88, 89, 92, 93, 94, 95, 97, 98, 101, 104, 109, 110, 129, 130, 131
L	Translation	meter	128, 129, 137, 138, 140
ℓ	Distance	meter	122, 123, 124, 128, 129
ℓ_i	Image distance to lens	meter	127
ℓ_o	Object distance to lens	meter	127
ℓ_o	Directional cosine	-	26, 27, 28, 30, 31
ℓ	Directional cosine	-	26, 27, 28, 30, 31
ℓ_s	Source distance to aperture	meter	112, 114
∇^2	Laplacian	-	8, 9
M	Lens magnification	-	128. 148
m_o	Directional cosine	-	26, 27, 28, 30, 31
m	Directional cosine	-	26, 27, 28, 30, 31

N	Integer	-	110
N	Fringe orders	-	146, 147
n	Axis direction	-	18
P	Axis direction	-	31, 32, 33, 34, 35
q	Axis direction	-	35, 37
r	Radial distance	meter	17, 18, 23
r'	Radial distance	meter	23, 24, 25, 26, 27, 28, 29, 30
R	Amplitude transmission function of x,y	-	68, 69, 70, 71, 73
R	Radial distance	meter	77, 78, 79, 80, 81, 82.
S	Surface area	meter squared	10, 11, 12, 13, 14, 18, 19
s	Distance from P to point (x,y,z)	meter	10, 11, 12, 13, 14, 18
s'	Distance from P to O	meter	12, 19, 23, 24, 25, 26, 27, 28, 29, 30
t	Time	seconds	6, 60, 61, 97, 98, 118, 119, 120
t_1	Phase transformation of the lens	-	83
t_o	Amplitude transmittance	-	84, 89, 90, 91, 93, 94, 95

U	Optical disturbance of light	meter	6, 7, 8, 9, 10, 11, 12, 13, 14, 15, 16, 17, 18, 19, 24, 32, 33, 35, 38, 40, 43, 44, 68, 74, 84, 87, 88, 89, 91, 92, 93, 94, 95, 118, 119, 120
u	Fourier transform function	-	55, 56, 57, 58, 60, 61, 62, 64, 65, 67, 73, 74, 144, 145, 147
u	x component of motion	meter	144, 145, 147
V	Monochromatic wave	meter	6
v	Volume	meter cubed	8
v	Fourier transform function	-	64, 65
v	y component of displacement	meter	145
w	z component of displacement	meter	144, 145
x	Function	meter	39, 41, 42, 45, 47, 48, 49, 50, 52, 53, 54, 55, 57, 58, 59, 60, 62, 63, 64, 66, 68, 69, 70, 71, 72, 73, 76, 77, 78, 79,

			80, 81, 83, 84, 85, 86, 87, 88, 89, 90, 91, 92, 93, 94, 95, 113, 137.
x	Rectangular coordinate axis	-	6, 20, 21, 22, 23, 24, 25, 26, 27, 102, 103, 108, 109, 119, 120, 130, 131.
δ_x	Distance of motion in image plane	meter	142, 144, 145, 147
δ'_x	Distance of motion in image plane	meter	142
X	Function	meter	50, 51
Δx	In-plane translation	meter	70, 71, 73, 74, 75
y	Function	meter	52, 53, 63, 64, 66, 68, 69, 71, 73, 76
y	Rectangular coordinate axis	meter	6, 20, 21, 22, 23, 24, 25, 26, 27, 112, 114, 115, 117, 119, 120, 130, 131, 132
y_s	Distance of source from y axis	meter	112, 114, 115, 117
z	Displacement	meter	1
z	Rectangular coordinate axis	-	6, 20, 21, 119, 120, 122, 123, 124, 125, 140.

NOMENCLATURE

SYMBOL	DEFINITION	UNITS	EQUATION NUMBERS
α	Angular measurement diverging core	degrees	139
α	Angle of prism wedge	degrees	141, 143
γ	Angle of tilt	degrees	128, 136, 137, 138
$\gamma_{x,y}$	Shear strain	-	145
δ	Delta function	-	47, 49, 50, 51, 52, 53, 56, 57, 58, 59, 60, 61, 62
δ	Angle between P_oP and normal to (See Fig. 4)	degrees	19, 24
δ	Phase difference between 2 waves	-	100, 101, 107
Δ	Phase difference	-	144, 145
Δ	Lens thickness	meter	76, 77, 78, 79, 81, 83
ε	Strain	-	145
ε	Electrical permittivity	-	5
ε	Radius of integration	meter	12
ζ	Rectangular coordinate	-	20, 22, 23, 24, 25, 27, 28, 29, 30, 32, 33, 34

ϕ	Phase angle	degrees	98, 101, 119, 120, 129, 132
η	Axis direction	-	20, 21, 22, 23, 24, 25, 26, 27, 28, 29, 30, 32, 33
λ	Wave length	meter	18, 19, 24, 29, 30, 32, 44, 59, 60, 61, 87, 88, 89, 90, 91, 92, 93, 94, 95, 110, 114, 122, 123, 124, 125, 126, 128, 129, 132, 136, 138, 140, 144
μ	Index of refraction of light	-	141, 143
ν	Temporal frequency	1/second	2, 59, 60, 61
ρ	Axis coordinate for polar coordinates	-	36, 38, 40
ω	Circular frequency	1/second	1, 2, 4, 72, 73, 118, 119, 120
ω	Circular coordinate axis	-	37, 38, 40, 43, 44
Ω	Element of solid angle	-	12

ACKNOWLEDGEMENTS

The author would like to acknowledge the support of the Naval Postgraduate School Foundation Research Program funded by the Office of Naval Research for providing the equipment necessary to conduct this research project.

Most of all, I would like to express my sincere appreciation to my Thesis Advisor, Dr. Allen E. Fuhs, Distinguished Professor of Aeronautics and Physics and Chemistry. Dr. Fuhs' technical guidance, unselfish sacrifice of his time and effort, patience and unparalleled ability to make difficult concepts seem simple were the guiding factors to the successful completion of the project. Also, I am very grateful to have had the distinct pleasure of having had the professional expertise of Professor David Salinas as a Second Reader.

I would like to thank Professors Charles M. Vest of Michigan State University and Yau Y. Hung of Oakland University and Mr. Gene E. Maddux for their technical support, unselfish donation of their time and patience, and vast depth of knowledge in the fields of holographic interferometry and speckle metrology which they so frequently shared during the discourse of this project.

Additionally, I would like to thank Mrs. Vicki Culley, Mrs. Carol Alejo, and Mrs. Kathy Bachelor for their logistic support without which much of this investigation would not have been completed. Also, I would like to thank Mrs. Elaine Reber and Mary Jane Ligairi for the numerous hours they spent

in helping prepare this project for presentation to the readers. I would like to thank Mr. Tom Kellog and Mr. Tom Christian for their technical support and Mr. Ken Mothersell and Mr. Bob Moeller for their expeditious and professional machine shop assistance, without whose ingenious equipment design several phases of this project would never have been started. The professional and unselfish aid of Mr. Howard Bench and Mr. Arthur Murray of the Educational Media Department Photo Lab was commendable and sincerely appreciated.

This thesis is dedicated to Dr. Allen E. Fuhs and Dr. J.E. Brock whose constant guidance and unending patience with my shortcomings as a student greatly enhanced the successful completion of this project.

I. INTRODUCTION

A. BACKGROUND

Laser Speckle, that granular, often annoying pattern produced upon laser illumination of a diffusely reflecting object, came into prominence as a holographer's nightmare. While continuing in that role, it is recognized that laser speckle, used in double-exposure form, is extremely useful for speckle photography. Laser speckle is perhaps the easiest form of laser metrology to exploit because in its simplest form, the equipment required for speckle image forming and processing requires only single beam, double-exposure, which eliminates the need for vibrational isolation. Techniques for reduction of the specklegram have been developed successfully and applied to the measurement of surface roughness [11, 18, 21], vibration [6, 20, 30, 51, 53] and deformation [12, 53], and displacement [4, 7, 10, 15, 38, 53] and strain [3, 4, 9, 15, 31-34, 40, 53]. A most convenient form of data reduction for speckle photographs is based upon Thomas Young's demonstration in the early 1800's of the interference of light emerging from a dual pinhole arrangement [13]. Thus a new field of speckle metrology evolved.

B. THESIS OBJECTIVE

The primary objectives of this thesis were to develop various techniques for measuring in-plane and out-of-plane

displacement and analysis of strain and vibrations using speckle metrology. The objective of using speckle techniques instead of holography procedures in Naval Engineering is to enhance the applicability of photographic metrology to the industrial environment [16, 21, 44, 55]. Holography, as a form of engineering stress, strain, and vibrational metrology, is excellent but requires highly sophisticated equipment, close tolerance set up requirements, and a vibrationless laboratory atmosphere for exact measurement [1, 8, 21, 44, 53]. With the development of speckle photography, a single beam, easy to setup, high tolerance system of engineering metrology is capable of being achieved in an industrial environment. [21, 44]

II. THEORY

A. INTRODUCTION TO SPECKLE METROLOGY

Speckle metrology spans a rather wide variety of techniques, all of which generally fall into one of two categories: direct laser (speckle) photography or speckle interferometry. [2, 21, 44] The distinction between the two is somewhat subtle since both involve photography and both involve interference. That is, speckle photography depends on the optical properties of the speckle which involves a condition of interference. After processing the speckle photograph, the analysis of the interference yields fringes. These fringes are directly correlated to the object motion. Therefore, there is no great difference between speckle photography and speckle interferometry. [21, 44] Hence, if there are regions in the two images where speckle patterns of each are well correlated, let the process be referred to as speckle photography. If, instead, the fringes form as a result of fluctuations in the correlation of the speckle patterns between two images, whether or not there is translation between the correlated portions of the pattern, let the process be called speckle interferometry.

B. ELECTROMAGNETIC WAVE THEORY

Light, being a form of electromagnetic radiation, is characterized by its amplitude, wave length (or frequency), phase, polarization, speed of propagation, and direction of

propagation. [13, 22, 43, 53] Light can be described by specifying the temporal and spatial dependence of its electric field vector, E. The simplest type of electromagnetic wave is the linearly polarized plane wave which has been assumed. If such a wave is polarized in the y direction and propagates in the z direction, the three components of E are:

$$\begin{aligned} E_x &= 0, \\ E_y &= A\cos(\omega t - kz), \\ E_z &= 0. \end{aligned} \tag{1}$$

where A is the amplitude of the wave. The circular frequency w and wave number K are given by

$$\omega = 2\pi\nu \tag{2}$$

$$k = \frac{2\pi}{\lambda}, \tag{3}$$

where ν is the temporal frequency and λ is the wave length. The frequency of light is on the order of 10^{15}HZ.

More generally, the direction light travels is described by its propagation vector $\vec{K}$ which has a magnitude $K = 2\pi/\lambda$ and points in the direction of propagation. A plane wave is a wave whose phase at any instant of time is constant at all points normal to K. If $\vec{r} = x\vec{i} + y\vec{j} + x\vec{k}$ is the position vector of any point in space, as shown in Fig. 1, the equation of a linearly polarized plane wave is:

$$\begin{aligned} E_{x'} &= 0, \\ E_{y'} &= A\cos(\omega t - \mathbf{k}\cdot\mathbf{r}), \\ E_{z'} &= 0. \end{aligned} \tag{4}$$

A surface over which phase is constant, in this case the planes $K \cdot r$ = CONSTANT, is called a wave front.

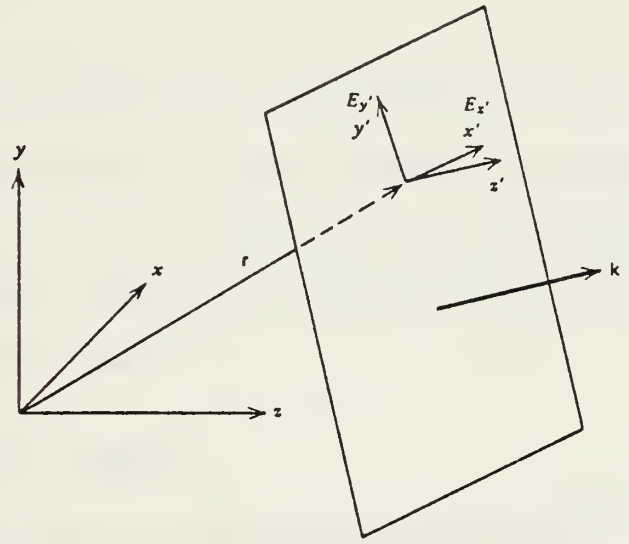

Figure 1. Plane wave of light propagating in the direction specified by the propagation vector K. From Vest [53]

Lasers emit narrow beams of monochromatic light with almost perfectly plane wave fronts. Most lasers emit linearly polarized light. Light from a typical He-Ne continuous wave (CW) laser has a wavelength, λ = 632.8 nm. The laser emits a beam of about 5 mm. in diameter. Laser light, as was mentioned previously, is highly coherent.

It was also noted previously that the frequency of light was on the order of 10^{15}Hz. Practical detectors, such as the eye and photographic film, are not capable of responding to such extremely rapid variations. Rather, they respond to irradiance I which is the time-average energy flux of the

light wave. Using electromagnetic wave theory, it can be shown that

$$I = \epsilon v \langle \mathbf{E}^2 \rangle, \tag{5}$$

where ε is the electrical permittivity of the medium in which light travels; ν is the speed of propagation. The key point is that the irradiance is proportional to the time average of the electrical intensity vector squared; the time average is indicated by <> .

C. DIFFRACTION THEORY

1. Derivation of the Fresnel-Kirchhoff Diffraction Formula

According to the HUYGEN-FRESNEL theory [13], the light disturbance at a point P arises from the superposition of secondary waves that proceed from a surface situated between this point and the light source.

Consider a strictly monochromatic wave

$$V(x,y,z,t) = U(x,y,z)\, e^{-iwt} \tag{6}$$

In a vacuum, the space-dependent part satisfies the time-independent (Homogeneous) wave equation.

$$(\nabla^2 + k^2)\, U = 0 \tag{7}$$

where $K = \omega/c$. This is known as the Helmholtz equation.

Let ν be the volume bounded by a closed surface S, and let P be any point within the surface; (see Fig. 2).

Assume that U possesses continuous first and second order partial derivatives within and on the surface. If U' is any other function which satisfies the same continuity requirements as U, then by Green's theorem

$$\iiint_v (U\nabla^2 U' - U'\nabla^2 U)dv = -\iint_S \left(U\frac{\partial U'}{\partial n} - U'\frac{\partial U}{\partial n}\right) dS, \tag{8}$$

where $\partial()/\partial n$ denotes differentiation along the inward normal to S. If U' also is a solution to the Helmholtz equation, i.e., if

$$(\nabla^2 + k^2)U' = 0, \tag{9}$$

then it follows that the integrand on the left of equation (8) vanishes at every point of v and consequently

$$\iint_S \left(U\frac{\partial U'}{\partial n} - U'\frac{\partial U}{\partial n}\right) dS = 0. \tag{10}$$

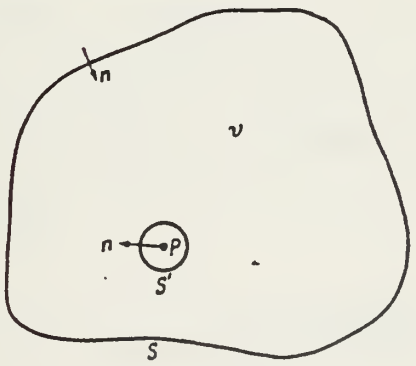

Figure 2. Derivation of the Helmholtz-Kirchhoff integral theorem: region of integration. From Born and Wolf [13]

Let $U'(x,y,z) = e^{iks}/s$, which is a spherical wave converging to the point P(s=0), where s denotes the distance from P to the point (x,y,z). This function has a singularity at s = 0; and since U' was assumed to be continuous and differentiable, P must be excluded from the domain of integration. Surrounding P with a small sphere of radius ε, the integration is expected throughout the volume between S and the surface S' of this sphere. In place of equation (10)

$$\iint_S + \iint_{S'} \left\{ U \frac{\partial}{\partial n}\left(\frac{e^{iks}}{s}\right) - \frac{e^{iks}}{s}\frac{\partial U}{\partial n} \right\} dS = 0, \tag{11}$$

whence

$$\begin{aligned} \iint_S \left\{ U \frac{\partial}{\partial n}\left(\frac{e^{iks}}{s}\right) - \frac{e^{iks}}{s}\frac{\partial U}{\partial n} \right\} dS &= -\iint_{S'} \left\{ U \frac{e^{iks}}{s}\left(ik - \frac{1}{s}\right) - \frac{e^{iks}}{s}\frac{\partial U}{\partial n} \right\} dS' \\ &= -\iint_{\Omega} \left\{ U \frac{e^{iks}}{\varepsilon}\left(ik - \frac{1}{\varepsilon}\right) - \frac{e^{iks}}{\varepsilon}\frac{\partial U}{\partial s} \right\} \varepsilon^2 d\Omega, \end{aligned} \tag{12}$$

where Ω denotes an element of the solid angle. Since the integral over S is independent of ε, the integral on the right-hand side may be replaced by its limiting value of $\varepsilon \to 0$. The first and third terms in the integral give no contribution in the limit, and the total contribution of the second term is

$$U(P) = \frac{1}{4\pi} \iint_S \left\{ U \frac{\partial}{\partial n}\left(\frac{e^{iks}}{s}\right) - \frac{e^{iks}}{s}\frac{\partial U}{\partial n} \right\} dS. \tag{13}$$

This equation is known as the Kirchhoff integral theorem. It relates the value of any scalar wave function

at any point P inside an arbitrary closed surface to the value of the wave function at the surface.

Note that as $K \to 0$, the time-independent wave equation (9) reduces to Laplace's equation $\nabla^2 U = 0$, and equation (13) goes into the formula of potential theory.

$$U(P) = \frac{1}{4\pi} \iint_S \left\{ U \frac{\partial}{\partial n} \left(\frac{1}{s} \right) - \frac{1}{s} \frac{\partial U}{\partial n} \right\} dS. \tag{14}$$

Only monochromatic waves will be analyzed, but a general form of Kirchhoff's theorem could be derived which applies to waves not necessarily monochromatic.

Consider a monochromatic wave from a point source P_o propagated through an opening in a plane opaque screen, and let P be the point at which the light disturbance is to be determined. It is assumed that the linear dimensions of the opening, while large compared to the wave length of light, are small compared to the distances of both P_o and P from the screen.

To find the disturbance at P, Kirchhoff's integral is taken over the surface S formed, as seen in Fig. 3, by: (1) the opening A, (2) a portion B of the non-illuminated side of the screen, and (3) a portion C of a large sphere of radius R, centered at P which, together with A and B, forms a closed surface.

Kirchhoff's theorem then gives

$$U(P) = \frac{1}{4\pi}\left[\iint_{\mathscr{A}} + \iint_{\mathscr{B}} + \iint_{\mathscr{C}}\right]\left\{U\frac{\partial}{\partial n}\left(\frac{e^{iks}}{s}\right) - \left(\frac{e^{iks}}{s}\right)\frac{\partial U}{\partial n}\right\} dS, \qquad (15)$$

where S is the distance of the element ds from P and denotes the differentiation along the inward normal to the surface of integration.

The values of U and $\partial U/\partial n$ on A, B, and C which should be substituted into equation (15) are never exactly known. However, it is assumed that everywhere on A, except in the neighborhood of the rim of the opening, U and $\partial U/\partial n$ will not appreciably differ from the values obtained in the absence of the screen and that on B these quantities will be equal to zero.

Then Kirchhoff set

$$\begin{aligned} &\text{on } \mathscr{A}: \quad U = U^{(i)}, \quad \frac{\partial U}{\partial n} = \frac{\partial U^{(i)}}{\partial n}, \\ &\text{on } \mathscr{B}: \quad U = 0 \qquad \frac{\partial U}{\partial n} = 0, \end{aligned} \qquad (16)$$

where

$$U^{(i)} = \frac{Ae^{ikr}}{r}, \qquad \frac{\partial U^{(i)}}{\partial n} = \frac{Ae^{ikr}}{r}\left[ik - \frac{1}{r}\right]\cos(n, r) \qquad (17)$$

are the values of U relating to the incident field (see Fig. 3b) and A is a constant. The approximations of equation (16) are called Kirchhoff's boundary conditions and

are the basis of Kirchhoff's diffraction theory.

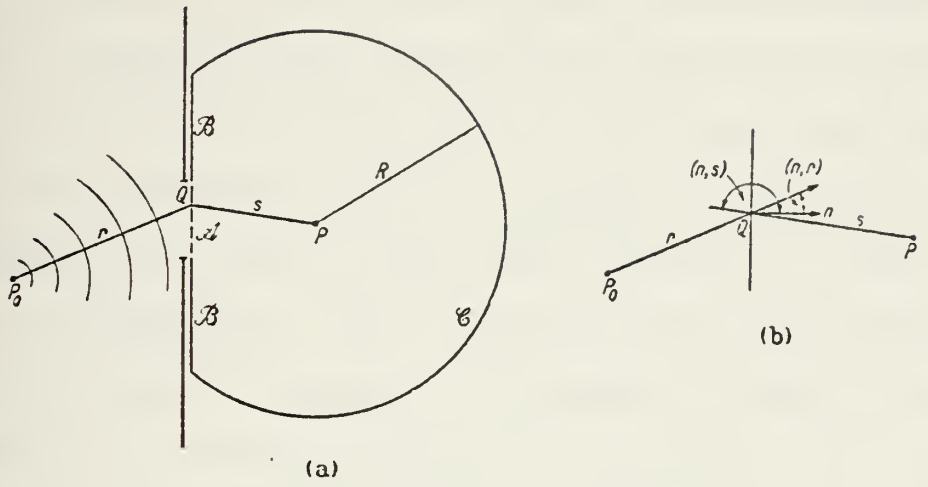

(a) Surface of integration (b) Definition of angles

Figure 3. Illustrating the derivation of the Fresnel-Kirchhoff diffraction formula. From Born and Wolf [13]

It remains to consider the contribution from the spherical portion C. If the radius R is sufficiently large so that at the time when the disturbance at P is considered no contributions from C could have reached P, then the integral over C will vanish. Neglecting the normal terms 1/r and 1/s in comparison to k, the Fresnel-Kirchhoff diffraction formula is obtained

$$U(P) = -\frac{iA}{2\lambda}\iint_{\mathcal{A}} \frac{e^{ik(r+s)}}{rs}[\cos(n,r) - \cos(n,s)]dS, \qquad (18)$$

Closer consideration of the Fresnel-Kirchhoff diffraction integral, equation (18), shows, as the element ds explores the domain of integration, (r + s) will in general change by many wave lengths, so that the factor

$e^{ik(r + s)}$ will oscillate rapidly. On the other hand, the distances of the points P_o and P from the screen are large compared to the linear dimensions of the aperture, and therefore the factor $[\cos(n,r) - \cos(n,s)]$ will not vary appreciably over the aperture. All angles are assumed to be small. The factor $[\cos(n,r) - \cos(n,s)]$ may be replaced by $\cos\delta$, where δ is the angle between the line P_oP and the normal to the screen (as seen in Fig. 4). Finally, the term 1/rs may be replaced by 1/r's', where r' and s' are the distances of P_o and P from the origin respectively. The Kirchhoff-Fresnel equation then reduces to

$$U(P) \sim -\frac{Ai}{\lambda}\frac{\cos\delta}{r's'}\iint_{\mathcal{A}} e^{ik(r+s)}\,dS. \tag{19}$$

Cartesian coordinates are used with the origin in the aperture at 0 and with the x and y axes in the plane of the aperture and the positive z direction to point into the half space that contains the point P of observation (see Fig. 4).

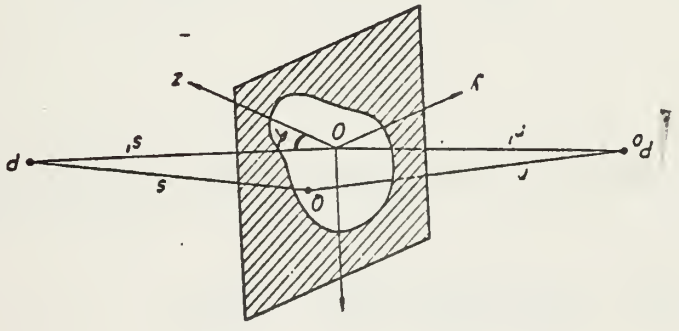

Figure 4. Diffraction at an aperture in a plane screen. Modified from Born and Wolf [13]

If $(x_o y_o z_o)$ and x,y,z) are the coordinates of P_o and P respectively, and (ξ,η) are the coordinates of a point Q in the aperture, then

$$\begin{aligned} r^2 &= (x_0 - \xi)^2 + (y_0 - \eta)^2 + z_0^2, \\ s^2 &= (x - \xi)^2 + (y - \eta)^2 + z^2, \end{aligned} \tag{20}$$

$$\begin{aligned} r'^2 &= x_0^2 + y_0^2 + z_0^2, \\ s'^2 &= x^2 + y^2 + z^2. \end{aligned} \tag{21}$$

$$\begin{aligned} r^2 &= r'^2 - 2(x_0\xi + y_0\eta) + \xi^2 + \eta^2, \\ s^2 &= s'^2 - 2(x\xi + y\eta) + \xi^2 + \eta^2. \end{aligned} \tag{22}$$

Since the linear dimensions of the aperture are small compared to both r' and s', r and s may be expanded as a power series in ξ/r', η/r', ξ/r', η/r'.

$$\begin{aligned} r &\sim r' - \frac{x_0\xi + y_0\eta}{r'} + \frac{\xi^2 + \eta^2}{2r'} - \frac{(x_0\xi + y_0\eta)^2}{2r'^3} - \cdots \\ s &\sim s' - \frac{x\xi + y\eta}{s'} + \frac{\xi^2 + \eta^2}{2s'} - \frac{(x\xi + y\eta)^2}{2s'^3} - \cdots \end{aligned} \tag{23}$$

Substituting from equation (23) into equation (19) gives

$$U(P) = -\frac{i\cos\delta}{\lambda}\frac{Ae^{ik(r'+s')}}{r's'}\int\int_{\mathscr{A}} e^{ikf(\xi,\eta)}\,d\xi d\eta, \tag{24}$$

where

$$f(\xi,\eta) = -\frac{x_0\xi + y_0\eta}{r'} - \frac{x\xi + y\eta}{s'} + \frac{\xi^2+\eta^2}{2r'} + \frac{\xi^2+\eta^2}{2s'} - \frac{(x_0\xi + y_0\eta)^2}{2r'^3} - \frac{(x\xi + y\eta)^2}{2s'^3} \cdots \qquad (25)$$

The first two directional cosines are (l_o , m_o) and (l,m)

$$l_0 = -\frac{x_0}{r'}, \qquad l = \frac{x}{s'},$$
$$m_0 = -\frac{y_0}{r'}, \qquad m = \frac{y}{s'}, \qquad (26)$$

and equation (27) may be written in the form

$$f(\xi,\eta) = (l_0 - l)\xi + (m_0 - m)\eta + \tfrac{1}{2}\left\{\left(\frac{1}{r'} + \frac{1}{s'}\right)(\xi^2+\eta^2) - \frac{(l_0\xi + m_0\eta)^2}{r'} - \frac{(l\xi + m\eta)^2}{s'}\right. \qquad (27)$$

The problem of determining the light disturbance at P has been reduced to the evaluation of the integral in equation (24). The evaluation can be simplified for two cases of particular interest. The quadratic and higher terms in ξ and η may be neglected in f for Fraunhofer diffraction; when the quadratic terms cannot be neglected, Fresnel diffraction is being represented. Fortunately, the simpler case of Fraunhofer diffraction is of much greater importance in optics. [13]

2. Fraunhofer Diffraction

Fraunhofer diffraction occurs when both the incident and diffracted waves are effectively plane. This will be the case when the distances from the source to the diffracting aperture and from the aperture to the receiving point are both large enough so that the curvatures of the incident and diffracted wave can be neglected (see Fig. 5a).

If either the source or the receiving point is close enough to the diffracting aperture so that the curvature of the wave is significant, then Fresnel diffraction occurs (see Fig. 5b).

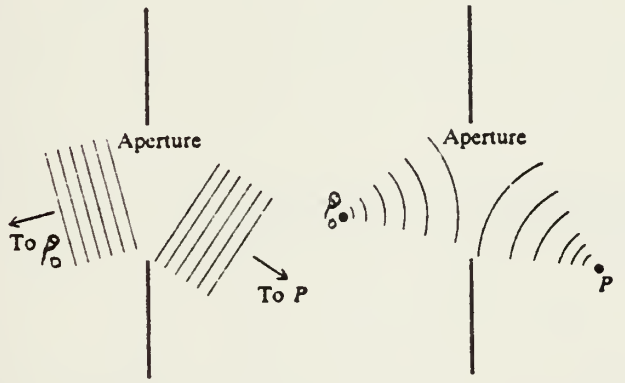

(a) Fraunhofer case (b) Fresnel case

Figure 5. Diffraction by an aperture. From Cowley [17]

The wave is effectively plane over the aperture if the second order and higher terms are negligible. Strictly speaking, these terms disappear only in the limiting case $r' \to \infty$, $s' \to \infty$, i.e., when both the source and the point of observation are at infinity. It is, however, evident that the second order terms do not contribute appreciably to the integral if

$$\tfrac{1}{2}k\left|\left(\frac{1}{r'}+\frac{1}{s'}\right)(\xi^2+\eta^2)-\frac{(l_0\xi+m_0\eta)^2}{r'}-\frac{(l\xi+m\eta)^2}{s'}\right|\ll 2\pi. \tag{28}$$

The conditions under which equation (28) will be satisfied exist when

$$|r'|\gg\frac{(\xi^2+\eta^2)_{\max}}{\lambda}\quad\text{and}\quad|s'|\gg\frac{(\xi^2+\eta^2)_{\max}}{\lambda}, \tag{29}$$

or if

$$\frac{1}{r'}+\frac{1}{s'}=0\quad\text{and}\quad l_0^2, m_0^2, l^2, m^2\ll\frac{|r'|\lambda}{(\xi^2+\eta^2)_{\max}}. \tag{30}$$

The conditions in equation (29) give estimates for r' and s' for which the Fraunhofer representation may be used.

In the case of Fraunhofer diffraction, the four quantities l_o, m_o, l, and m enter equation (27) only in the combinations

$$p=l-l_0,\qquad q=m-m_0. \tag{31}$$

The governing Fraunhofer diffraction integral may then be written

$$U(P) = C\int\int_{\mathscr{A}} e^{-ik(p\xi+q\eta)}\,d\xi d\eta,$$

$$\frac{1}{\lambda^2}E = |C|^2 D \qquad (32)$$

$$C = \frac{1}{\lambda}\sqrt{\frac{E}{D}}$$

where c is the constant term in front of the integral of equation (24).

Fraunhofer diffraction patterns for apertures of various forms (rectangle and circular, specifically) will be studied in detail.

a. Rectangular aperture

Consider first a rectangular aperture of sides 2a and 2b. With origin 0 at the center of the rectangle and with η and ξ axes parallel to the sides (see Fig. 6).

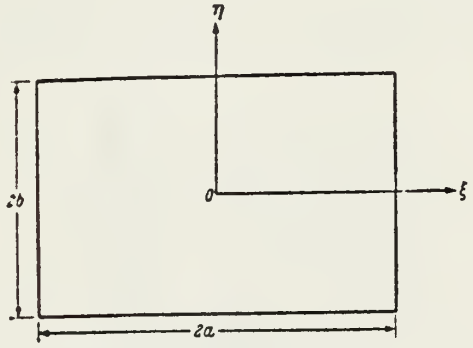

Figure 6. Rectangular aperture. From Born and Wolf [13]

The Fraunhofer diffraction integral then becomes

$$U(P) = C\int_{-a}^{a}\int_{-b}^{b} e^{-ik(p\xi+q\eta)}\,d\xi d\eta = C\int_{-a}^{a} e^{-ikp\xi}\,d\xi \int_{-b}^{b} e^{-ikq\eta}\,d\eta. \qquad (33)$$

Now

$$\int_{-a}^{a} e^{-ikp\xi}\, d\xi = -\frac{1}{ikp}\left[e^{-ikpa} - e^{ikpa}\right] = 2\,\frac{\sin kpa}{kp}, \qquad (34)$$

with a similar form for the integral of equation (33) taken with respect to dn from -b to b.

Hence the intensity is given by

$$I(P) = |U(P)|^2 = \left(\frac{\sin kpa}{kpa}\right)^2 \left(\frac{\sin kqb}{kqb}\right)^2 I_0, \qquad (35)$$

The function $y = (\sin x/x)^2$ is displayed in Fig. 7. It has a principal maximum of $y = 1$ at $x = 0$ and zero minima at $x = \pm\pi, \pm 2\pi, \pm 3\pi \ldots$ The roots asymptotically approach the values $x = (2m + 1)\,\pi/2$, m being an integer (see Table 1).

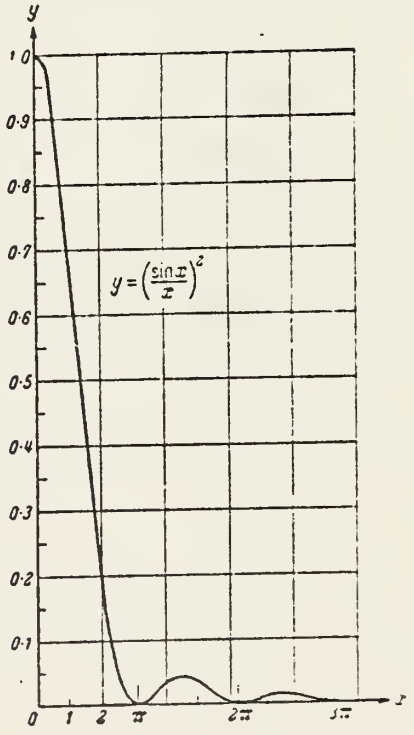

Figure 7. Fraunhofer diffraction at a rectangular aperture. $y = (\sin x/x)^2$

Within each rectangle formed by pairs of consecutive dark lines of the Fourier transform of the aperture the intensity rises to a maximum; all their maximums are, however, only a small fraction of the central maximum of the Fourier transform and decrease rapidly with increasing distance from the center (see Fig. 8). The larger the rectangular opening, the smaller the effective size of the diffraction pattern of the Fourier transform.

TABLE 1

The First Five Maxima Of The Function $y = (\sin x/x)^2$

x	$y = (\sin x/x)^2$
0	1
1.430 = 4.493	0.04718
2.459 = 7.725	0.01694
3.470 = 10.90	0.00834
4.479 = 14.07	0.00503

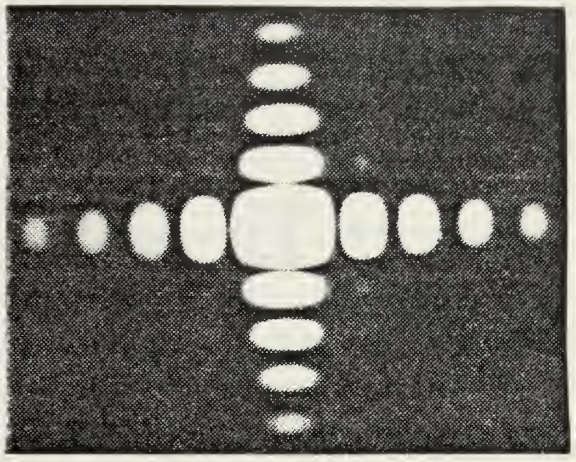

Figure 8. Fraunhofer diffraction pattern of a rectangular aperture

b. Circular Aperture

The Fraunhofer diffraction pattern for a circular aperture will be investigated. Using polar coordinates, let (ρ, θ) be the polar coordinates of a particular point in the aperture:

$$\rho \cos \theta = \xi, \qquad \rho \sin \theta = \eta; \tag{36}$$

and let (ω,ψ) be the coordinates of a point P in the diffraction pattern, referred to the geometrical image of the source:

$$w \cos \psi = p, \qquad w \sin \psi = q. \tag{37}$$

From the definition of p and q, it follows that $w = p^2 + q^2$ is the sine of the angle which the direction (p,q) makes with the central direction p = q = 0. The diffraction integral of equation (32) now becomes, if a is the radius of the circular aperture,

$$U(P) = C\int_0^a\int_0^{2\pi} e^{-ik\rho w\cos(\theta-\psi)}\rho d\rho d\theta. \tag{38}$$

Now using the integral representation of the Bessel function $J_n(z)$:

$$\frac{i^{-n}}{2\pi}\int_0^{2\pi} e^{ix\cos\alpha}e^{in\alpha}d\alpha = J_n(x). \tag{39}$$

Equation (38) therefore reduces to

$$U(P) = 2\pi C\int_0^a J_0(k\rho w)\rho d\rho. \tag{40}$$

Also, the recurrence relationship is

$$\frac{d}{dx}\{x^{n+1}J_{n+1}(x)\} = x^{n+1}J_n(x), \tag{41}$$

giving for n = 0, on integration

$$\int_0^x x'J_0(x')dx' = xJ_1(x). \tag{42}$$

From equations (40) and (42) it follows that

$$U(P) = CD\left[\frac{2J_1(kaw)}{kaw}\right], \tag{43}$$

where $D = \pi a^2$. Hence the intensity is given by

$$I(P) = |U(P)|^2 = \left[\frac{2J_1(kaw)}{kaw}\right]^2 I_0, \tag{44}$$

where

$$I_0 = C^2D^2 = \overline{ED}/\lambda^2.$$

Equation (44) is the formula derived by Airy in somewhat different form. [13]

The intensity distribution in the neighborhood of the geometrical image is characterized by the function $Y = (2J_1(x)/x)^2$ shown in Fig. 9a. This function y has its principle maximum y = 1 at x = 0, and with increasing x, it oscillates with gradually diminishing amplitude in a similar way to the function $(\sin x/x)^2$ which was discussed previously. The intensity is zero (minimum) for values of x given by $J_1(x) = 0$.

The minima are no longer equidistant (see Table 2). The positions of the secondary maxima are given by the values of x that satisfy the equation.

$$\frac{d}{dx}\left[J_1(x)/x\right] = 0$$

(a) The function $2J_1(x)/x)^2$

(b) Airy disk

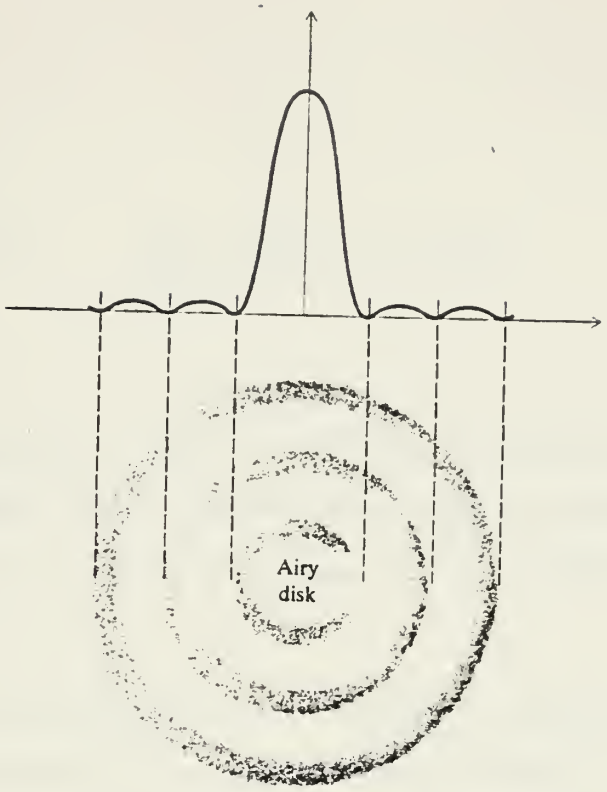

Figure 9. Fraunhofer diffraction pattern of a circular aperture. From Fowles [22]

TABLE 2

The First Few Maxima And Minima Of The Function

$y = (2J_1(x)/x)^2$

x		$(2J_1(x)/x)^2$	
0		1	Max.
1.220	= 3.833	0	Min.
1.635	= 5.136	0.0175	Max.
2.233	= 7.016	0	Min.
2.679	= 8.417	0.0042	Max.
3.238	= 10.174	0	Min.
3.699	= 11.620	0.0016	Max.

or using the equation $$\frac{d}{dx}\left[x^{-n} J_n(x)\right] = -x^{-n} J_{n+1}(x), \qquad (45)$$

by the roots of equations $J_2(x) = 0$ with increasing the separation between two successive minima or maxima approach the value of π as in the case of the rectangular aperture.

The results show that the pattern consists of a bright disk, centered on the geometrical image at $p = q = 0$ of the source and surrounded by concentric bright and dark rings (see Figs. 9b and 10).

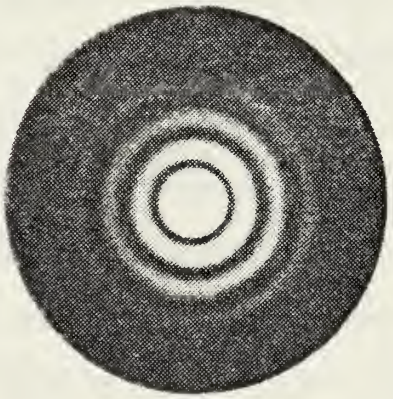

Figure 10. Fraunhofer diffraction pattern of a circular aperture (the Airy pattern) 6 mm in diameter, magnification 50X, mercury yellow light λ = 5790Å.

The intensity of the bright rings decreases rapidly with increasing radius; only the first or second rings are bright enough to be visible to the naked eye. The bright central area is known as the Airy disk (see Fig. 10). The Airy disk extends to the first dark ring whose size is given by the first zero of the Bessel function, namely $x = 3.833$. The angular radius of the first dark ring is thus given by

$$\sin\theta = \frac{1.22\lambda}{2a} \simeq \theta \qquad (46)$$

which is valid for small angles, θ. Here a is the radius of the aperture.

The image of a distant point source formed at the focal plane of a camera line is actually a Fraunhofer diffraction pattern for which the aperture of the lens is the opening. Thus the image of a composite source is a superposition of many Airy disks. The resolution of detail in the image, therefore, depends on the size of the individual Airy disks. If D is the diameter of the lens, then the angular radius of the Airy disk is approximately $1.22\lambda/D$. This is also the approximate minimum angular separation between two equal point sources such that they are just barely able to be resolved, because at this angular separation, the central maximum of the image of one source falls on the first minimum of the other (see Fig. 11). This condition for optical resolution is the Rayleigh criterion. The Rayleigh criterion

does not always give an absolute minimum separation for resolution, but it is almost always used because of its simplicity. [13, 17, 22, 53]

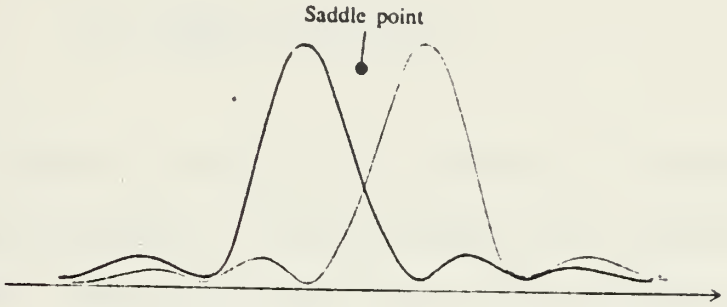

Figure 11. The Rayleigh criterion.

D. FOURIER TRANSFORMS

1. Convolutions

Most considerations of diffraction involve the use of the Fourier transform in one form or another. One of the most important properties of the Fourier transform involves the concept of a convolution, or convolution integral; and for both this and the Fourier transform, it is convenient to use delta-functions.

Consider a special delta function, the Dirac delta function. A Dirac delta function at $x = a$ is defined by

$$\delta(x-a) = \begin{cases} 0 & \text{for } x \neq a \\ \infty & \text{for } x = a \end{cases}$$

and (47)

$$\int_{-\infty}^{\infty} \delta(x-a)\,dx = 1 .$$

The delta function at $x = 0$, $\delta(x)$, can be considered as the limit of a set of real continuous functions,

such as Gaussians:

$$\delta(x) = \lim_{a\to\infty}\left[\frac{a}{\pi^{1/2}}\exp\{-a^2x^2\}\right]. \tag{48}$$

As a tends to infinity, the Gaussian function has a maximum value tending to infinity and a half-width (1/a) tending to zero, but the integral over the function is always unity. The delta function can be used as a convenient notation for any function of integral unity in the form of a sharp peak having a width so small it is not experimentally significant.

The definition of a delta function is

$$\delta(x) = \int_{-\infty}^{\infty}\exp\{2\pi ixy\}dy\,, \tag{49}$$

In one dimension, the convolution integral (or convolutions product) of two functions f(x) and g(x) is defined as

$$C(x) = f(x) * g(x) \equiv \int_{-\infty}^{\infty} f(X)g(x-X)dX\,. \tag{50}$$

By a simple change of variable.

$$f(x) * g(x) = \int_{-\infty}^{\infty} g(X)f(x-X)dX = g(x) * f(x)\,. \tag{51}$$

The identity operation is the convolution with the Dirac delta function:

$$f(x) * \delta(x) = f(x),$$
$$f(x) * \delta(x-a) = f(x-a). \qquad (51a)$$

For a general intensity distribution, I(x), each sharp spectral line or each part of a broader spectral line will be "spread out" by the "spread-function" g(x), so that the recorded intensity, I_{OBS} will be less sharply peaked or less well resolved than the original spectrum (see Fig. 12).

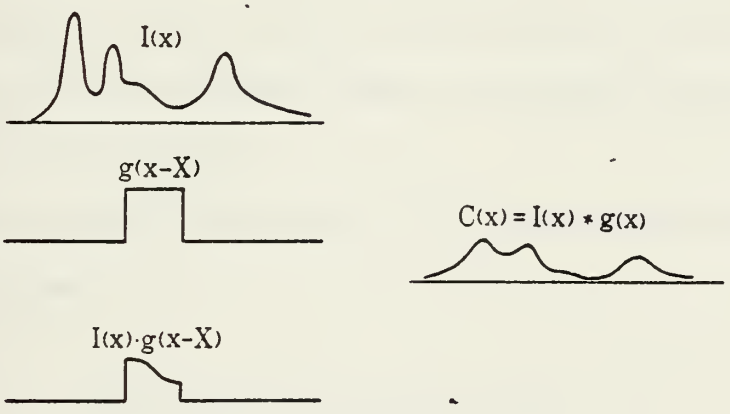

Figure 12. A convolution operation. An intensity function I(x) representing a spectral line is multiplied by the transmission function g(x-X) of a slit, centered at X=x; the product of these two functions is integrated to give the measured intensity $I_{OBS}(x)$.

Likewise, the blurring of an image due to the imperfections of a camera lens may be described in terms of convolution of the ideally perfect image intensity with some two dimensional function g(x,y). For a point source

of light, the ideal image would be a two dimensional function $\delta(x,y)$. The spreading gives

$$I_{obs} = g(x,y) * \delta(x,y) = g(x,y) . \tag{52}$$

For a general object, consisting of a large number of independently emitting point sources and having an ideal image, $I_o(x,y)$,

$$I_{OBS} = g(x,y) * I_o(x,y) \tag{53}$$

Thus each point of the original intensity distribution is spread into a disk of intensity of light and the overlapping of these disks gives a blurring and loss of resolution of the image.

The Fourier transform of a one-dimensional function f(x) is defined as

$$\mathcal{F}[f(x)] \equiv F(u) = \int_{-\infty}^{\infty} f(x) \exp\{2\pi i u x\} dx . \tag{54}$$

The inverse transform, F^{-1}, is defined so that

$$f(x) = \mathcal{F}^{-1}[\mathcal{F}\{f(x)\}] = \int_{-\infty}^{\infty} F(u) \exp\{-2\pi i u x\} du . \tag{55}$$

Here the convention of including 2π in the exponent is followed. This convention is commonly used in considerations of diffraction in order to avoid the necessity of adding a constant multiplier 2π in equations (54) or (55). [17]

2. Diffraction Analysis

The amplitude of scattering from an object in the Fraunhofer diffraction approximation, whether derived from the Kirchhoff formulation or from scattering theory, is described by a Fourier transform integral. Thus the diffraction amplitude may be described in terms of a distribution in Fourier transform space, often referred to as "reciprocal space."

The individual properties of Fourier transforms will not be expounded on here, as they are well documented in many references readily available. The remainder of this section will demonstrate the application of Fourier transforms and their relationship to diffraction.

The amplitude distribution of a very small source or the transmission through a very small aperture (or slit) in one dimension may be described as $\delta(x)$ or by $\delta(x-a)$ when it is not at the origin. The Fourier transform used to derive the Fraunhofer diffraction pattern is

$$\begin{aligned} \mathcal{F}\delta(x) &= 1, \\ \mathcal{F}\delta(x-a) &= \exp\{2\pi i u a\}. \end{aligned} \tag{56}$$

To illustrate the above, the following integral is written:

$$\int_{-\infty}^{\infty} \delta(x-a) \exp\{2\pi i u x\} dx . \qquad (57)$$

The integrand is zero except for x = a. Hence the integral may be written

$$\exp\{2\pi i u a\} \int_{-\infty}^{\infty} \delta(x-a) dx = \exp\{2\pi i u a\} . \qquad (58)$$

The amplitude of the diffraction pattern will be proportional to $F(u) = F\,\delta(x-a)$ where $u = 1/\lambda$. The intensity observed will be proportional to $F(u)^2 = 1$.

The Fourier transform of a plane wave with respect to t only, gives

$$\mathcal{F}_t \exp\{2\pi i(\nu_1 t - x/\lambda_1)\} = \delta(\nu+\nu_1) \exp\{-2\pi i x/\lambda_1\} , \qquad (59)$$

i.e., the delta function in frequency and a plane wave in real space. Fourier transform with respect to x gives

$$\mathcal{F}_x \exp\{2\pi i(\nu_1 t - x/\lambda_1)\} = \exp\{2\pi i \nu_1 t\} \delta(u - 1/\lambda_1) , \qquad (60)$$

i.e., a sinuisoidal variation in time and a delta function in reciprocal space. Transforming with respect to both variables gives

$$\mathcal{F}_{x,t} \exp\{2\pi i(\nu_1 t - x/\lambda_1)\} = \delta(\nu+\nu_1)\cdot\delta(u-1/\lambda_1)\,, \tag{61}$$

which is a delta function in both frequency and reciprocal space.

The Fourier transform of all possible waves which can exist in a given medium with respect to both x and t is a set of points defining the relationship between the frequency ν and λ^{-1} (or between the angular frequency ω and K) which is known as the dispersion relation for that type of wave and the particular medium.

For the translation of an object, the Fourier transform is written,

$$\mathcal{F} f(x-a) = \mathcal{F}[f(x) * \delta(x-a)] = F(u) \exp\{2\pi i u a\} \tag{62}$$

Thus the translation of the object in real space has the effect of multiplying the amplitude in reciprocal space by a complex exponential. The intensity distribution of the Fraunhofer diffraction pattern is given by $F(a)^2$, which is independent of translation.

a. Rectangular And Circular Apertures

The intensity distribution for both the rectangular and circular apertures is important when studying Fraunhofer diffraction. The transmission function of a rectangular aperture in two-dimensional form may be written

$$f(x,y) = \begin{cases} 1 & \text{if } |x| < a/2 \text{ and } |y| < b/2, \\ 0 & \end{cases} \tag{63}$$

Then

$$F(u,v) = \int_{-a/2}^{a/2} \exp\{2\pi i u x\}\,dx \int_{-b/2}^{b/2} \exp\{2\pi i v y\}\,dy = ab\,\frac{\sin(\pi a u)}{\pi a u}\,\frac{\sin(\pi b v)}{\pi b v}, \tag{64}$$

so that, for diffraction from a rectangular aperture, the intensity distribution is

$$I(u,v) = a^2 b^2\,\frac{\sin^2(\pi a u)}{(\pi a u)^2}\,\frac{\sin^2(\pi b v)}{(\pi b v)^2}. \tag{65}$$

The maximum intensity at u = ν = 0 is a^2b^2. Zeros occur at intervals of a^{-1} along the u direction, which is parallel to the x axis and at b^{-1} intervals along the ν direction (see Fig. 13).

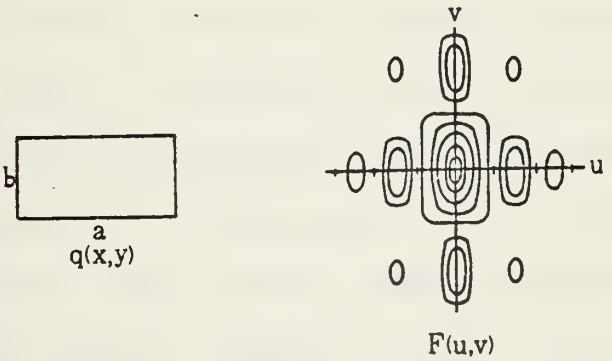

Figure 13. Diagram suggesting the form of the Fourier transform of a rectangular aperture. From Cowley [17]

Thus the intensity function falls off through decreasing oscillations in each direction. The dimensions of the distribution in reciprocal space are inversely proportional to the dimensions in real space.

The transmission function for a circular aperture is written

$$f(x,y) = \begin{cases} 1 & \text{if} \quad (x^2+y^2)^{1/2} < a/2\,, \\ 0 & \end{cases} \tag{66}$$

The Fourier transform is best carried out by writing the Fourier integral in plane polar coordinates. The result is:

$$F(u) = a\frac{J_1(\pi a u)}{\pi a u} \tag{67}$$

where u is the radial coordinate and $J_1(x)$ is the first order Bessel function. The function $J_1(x)/x$ is similar to the form $(\sin x)/x$ but has a somewhat broader central maximum with the first zero at $1.22a^{-1}$ instead of a^{-1}.

b. Single And Double Exposure Specklegrams

Before calculating the diffraction pattern from a double-exposure specklegram, first consider a single-exposure photographic transparency of an object illuminated by laser light. The recorded image is speckled. If a small diameter laser beam is passed through a portion of the transparency, the aperture w will be the amplitude transmission function R(x,y) inside the illuminated area. Thus

$$U_o = cF\{R(x,y) \tag{68}$$

and

$$I_o \alpha F\left[R(x,y)\right] * F\left[R(x,y)\right] \tag{69}$$

Now for a double exposure speckle photographic transparency where the object has suffered an in-plane displacement Δx in the x direction between exposures, the amplitude transmission function is

$$R_2(x,y) = R(x - \Delta x/2, y) + R(x + \Delta x/2, y) \tag{70}$$

A series expansion of equation (70) yields

$$R_2(x,y) = 2\left[R(x,y) + \frac{R''(x,y)}{2!}\left(\frac{\Delta x}{2}\right)^2 + \frac{R''''(x,y)}{4!}\left(\frac{\Delta x}{2}\right)^4 + \ldots\right] \tag{71}$$

where the prime indicates a differential with respect to the variable x. The linear properties of a Fourier transform provide that

$$F\left[g^n(x)\right] = (i\omega)^n F\left[g(x)\right] \tag{72}$$

where $g^n(x)$ is the n^{th} derivative of the function $g(x)$. Thus

$$\begin{aligned} U &= c\, F\left[R_2(x,y)\right] \\ U &= c\, F\left[R(x,y)\right] 2\left[1 - \frac{1}{2!}\, w, \frac{\Delta x}{2}^2 + \frac{1}{4!}\, w, \frac{\Delta x}{2}^4 + \ldots\right] \\ U &= c\, F\left[R(x,y)\right]\left[2\cos\left(w, \frac{\Delta x}{2}\right)\right] \end{aligned} \tag{73}$$

Using equations (72) and (73) and $w = K \sin\theta$

$$U = U_o \, 2 \cos\left(\frac{\Delta x}{2} \; K \sin\theta \right) \tag{74}$$

$$I = I_o \left[1 + \cos \left(K\Delta \; x \sin\theta \right) \right] \tag{75}$$

Thus the intensity distribution for a speckleqram is the diffraction halo from a single-exposure transparency modulated by Young's fringes. [3,4]

3. Two Dimensional Fourier Transforms

Two-dimensional Fourier transforms are fundamental to all image formation. The Fraunhofer diffraction pattern of an object is the Fourier transform of that object. An object of low spatial frequency, i.e., an object that has large details, and wide separation between details, will give a Fourier transform of small elements that are close together. An object of high spatial frequency will give maxima that are wide apart.

a. Thickness Function

To find the thickness $\Delta(x,y)$ of a lens at any point (x,y) we split the lens into two parts, as shown in Fig. 14, and write the total thickness function as the sum of the two individual thickness functions,

$$\Delta (x,y) = \Delta_1 (x,y) + \Delta_2 \; (x,y) \tag{76}$$

Referring to the geometry shown in Figure (14), the thickness $\Delta_1 (x,y)$ is given by

$$\Delta_1(x,y) = \Delta_{01} - (R_1 - \sqrt{R_1^2 - x^2 - y^2})$$
$$= \Delta_{01} - R_1\left(1 - \sqrt{1 - \frac{x^2 + y^2}{R_1^2}}\right) \tag{77}$$

Similarly,

$$\Delta_2(x,y) = \Delta_{02} - (-R_2 - \sqrt{R_2^2 - x^2 - y^2})$$
$$= \Delta_{02} + R_2\left(1 - \sqrt{1 - \frac{x^2 + y^2}{R_2^2}}\right) \tag{78}$$

where we have factored the positive number R_2 out of the square root. Combining equations (76), (77), and (78), the total thickness function is seen to be

$$\Delta(x,y) = \Delta_0 - R_1\left(1 - \sqrt{1 - \frac{x^2 + y^2}{R_1^2}}\right) + R_2\left(1 - \sqrt{1 - \frac{x^2 + y^2}{R_2^2}}\right) \tag{79}$$

where $\Delta_0 = \Delta_{01} + \Delta_{02}$.

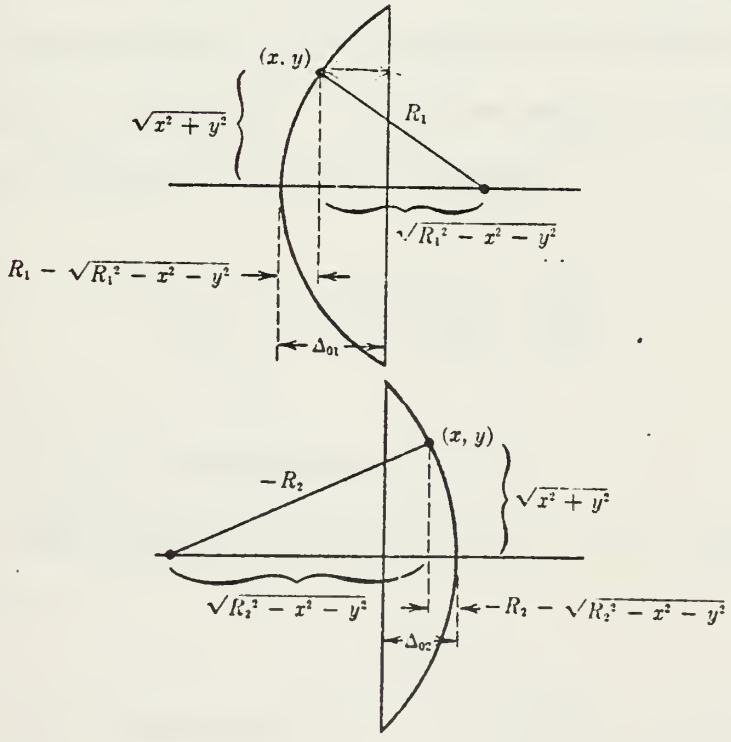

Figure 14. Calculation of the thickness function. From Goodman [25]

b. Paraxial Approximation

The expression for the thickness function can be substantially simplified if attention is restricted to portions of the wave front that lie near the lens axis, or equivalently, if only paraxial rays are considered. Thus we consider only values of x and y sufficiently small to allow the following approximations to be accurate:

$$\sqrt{1 - \frac{x^2 + y^2}{R_1^2}} \cong 1 - \frac{x^2 + y^2}{2R_1^2}$$
$$\sqrt{1 - \frac{x^2 + y^2}{R_2^2}} \cong 1 - \frac{x^2 + y^2}{2R_2^2} \qquad (80)$$

The resulting phase transformation will, of course, represent the lens accurately over only a limited area, but this limitation is no more restrictive than the usual paraxial approximation of geometric optics. Note that equation (80) amounts to approximation of the spherical surfaces of the lens by parabolic surfaces. With the help of these approximations, the thickness function becomes

$$\Delta(x,y) = \Delta_0 - \frac{x^2 + y^2}{2}\left(\frac{1}{R_1} - \frac{1}{R_2}\right) \qquad (81)$$

c. Phase transformation

The paraxial approximation to the lens transformation is:

$$t_l(x,y) = \exp\left[jkn\Delta_0\right] \exp\left[-jk(n-1)\frac{x^2 + y^2}{2}\left(\frac{1}{R_1} - \frac{1}{R_2}\right)\right]$$

where $t_\ell(x,y)$ is the lens transformation function. The physical properties of the lens (that is n, R_1, and R_2) can be combined in a single number f called the focal length; which is defined by

$$\frac{1}{f} \triangleq (n-1)\left(\frac{1}{R_1} - \frac{1}{R_2}\right) \tag{82}$$

Thus the phase transformation may be rewritten

$$t_\ell(x,y) = \exp\left[jkn\Delta_0\right] \exp\left[-j\frac{k}{2f}(x^2+y^2)\right] \tag{83}$$

This equation will serve as our basic representation of the effects of a lens on an incident disturbance.

One of the remarkable and useful properties of a converging lens is its inherent ability to perform two dimensional Fourier transformations.

d. Fourier Transform Configurations

Three separate configurations for performing the Fourier transform operation are considered (see Fig. 15).

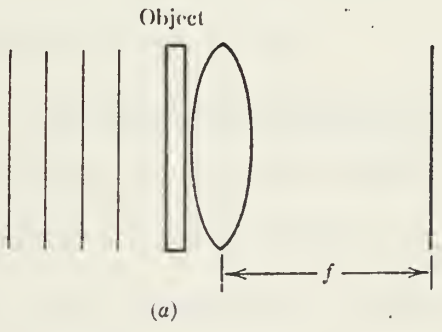

(a) Object placed against the lens.

Figure 15. Fourier Transforming Configurations.

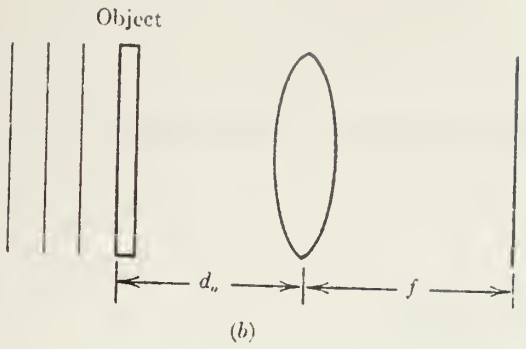

(b) Object placed in front of lens.

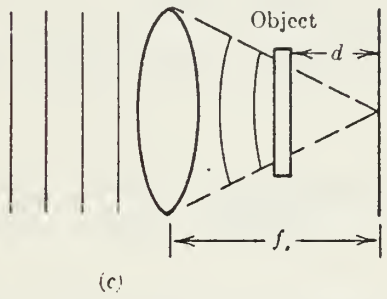

(c) Object placed behind lens.

Figure 15. (Continued).

In the material that follows, the illumination is assumed monochromatic and the distribution of light amplitude across the back focal plane of the lens is of concern. The front and back focal planes of a lens are defined as the planes normal to the lens axis situated at a distance f in front of and in back of the lens respectively. The front of the lens is the side of the lens the incoming beam strikes first.

(1) Object Placed Against The Lens. For the first case where the object is placed against the lens, let a plane object with amplitude transmittance $t_o(x,y)$ be placed immediately in front of a converging lens of focal length f, as shown in Fig. 15a. The object is assumed to be uniformly illuminated by a normally incident, monochromatic plane wave of

amplitude A, in which case the disturbance incident on the lens is

$$U_i(x,y) = At_o(x,y) \tag{84}$$

The finite extent of the lens aperture can be accounted for by associating with the lens a pupil function P(x,y) defined by

$$P(x,y) = \begin{cases} 1 & \text{inside the lens aperture} \\ 0 & \text{otherwise} \end{cases} \tag{85}$$

Thus the amplitude distribution behind the lens becomes, using equation (83),

$$U_i'(x,y) = U_i(x,y)P(x,y) \exp\left[-j\frac{k}{2f}(x^2 + y^2)\right] \tag{86}$$

The constant phase delay associated with the lens transformation has been omitted since it does not affect the result in any significant way.

To find the distribution $U_f(x_f y_f)$ of field amplitude across the back focal plane of the lens, the Fresnel diffraction formula is applied.

Thus, putting z = f,

$$U_f(x_f,y_f) = \frac{\exp\left[j\frac{k}{2f}(x_f^2 + y_f^2)\right]}{j\lambda f} \iint_{-\infty}^{\infty} U_i'(x,y) \exp\left[j\frac{k}{2f}(x^2 + y^2)\right] \exp\left[-j\frac{2\pi}{\lambda f}(xx_f + yy_f)\right] dx\,dy \tag{87}$$

where a constant phase factor has been dropped. Substituting equation (86) in equation (87), the quadratic phase factors within the integrand are seen to cancel, leaving

$$U_f(x_f,y_f) = \frac{\exp\left[j\frac{k}{2f}(x_f^2 + y_f^2)\right]}{j\lambda f} \iint_{-\infty}^{\infty} U_i(x,y)P(x,y)\exp\left[-j\frac{2\pi}{\lambda f}(xx_f + yy_f)\right]dx\,dy \tag{88}$$

Thus the field distribution U_f is proportional to the two-dimensional Fourier transform of that portion of the incident field subtended by the lens aperture. When the physical extent of the object is smaller than the lens aperture, the factor P(x,y) may be neglected, yielding

$$U_f(x_f,y_f) = \frac{A\exp\left[j\frac{k}{2f}(x_f^2 + y_f^2)\right]}{j\lambda f} \iint_{-\infty}^{\infty} t_o(x,y)\exp\left[-j\frac{2\pi}{\lambda f}(xx_f + yy_f)\right]dx\,dy \tag{89}$$

Evidently the amplitude and phase of the light at coordinates (x_f,y_f) are influenced by the amplitude and phase of the object Fourier component at spatial frequencies $(f_x = x_f/\lambda f \; f_y = y_f/\lambda f)$. Measurement of the intensity distribution yields knowledge of the power spectrum of the object; the phase distribution is of no consequence in such a measurement. Thus

$$I_f(x_f,y_f) = \frac{A^2}{\lambda^2 f^2}\left|\iint_{-\infty}^{\infty} t_o(x,y)\exp\left[-j\frac{2\pi}{\lambda f}(xx_f + yy_f)\right]dx\,dy\right|^2 \tag{90}$$

(2) Object In Front Of Lens. Consider next the more general geometry of Fig. 15b. The object, located

a distance d_o in front of the lens, is illuminated by a normally incident plane wave of amplitude A. The amplitude transmittance of the object is again represented by t_o. In addition, let $F_o(f_X, f_Y)$ represent the Fourier spectrum of the light transmitted by the object, and $F_\ell(f_X, f_Y)$ the Fourier spectrum of the light incident on the lens; that is,

$$F_o(f_X, f_Y) = \mathcal{F}\{At_o\} \text{ and } F_l(f_X, f_Y) = \mathcal{F}\{U_l\}$$
$$F_l(f_X, f_Y) = F_o(f_X, f_Y) \exp\left[-j\pi\lambda d_o(f_X^2 + f_Y^2)\right] \tag{91}$$

For the moment, the finite extent of the lens aperture will be neglected. Thus, letting P = 1, equation (88) can be rewritten

$$U_f(x_f, y_f) = \frac{\exp\left[j\frac{k}{2f}(x_f^2 + y_f^2)\right]}{j\lambda f} F_l\left(\frac{x_f}{\lambda f}, \frac{y_f}{\lambda f}\right) \tag{92}$$

Substitution of equation (91) in equation (92), gives

$$U_f(x_f, y_f) = \frac{\exp\left[j\frac{k}{2f}\left(1 - \frac{d_o}{f}\right)(x_f^2 + y_f^2)\right]}{j\lambda f} F_o\left(\frac{x_f}{\lambda f}, \frac{y_f}{\lambda f}\right)$$

$$U_f(x_f, y_f) = \frac{A \exp\left[j\frac{k}{2f}\left(1 - \frac{d_o}{f}\right)(x_f^2 + y_f^2)\right]}{j\lambda f} \iint t_o(x_o, y_o) \exp\left[-j\frac{2\pi}{\lambda f}(x_o x_f + y_o y_f)\right] dx_o\, dy_o \tag{93}$$

Thus the amplitude and phase of the light at coordinates (X_f, Y_f) are again related to the amplitude and phase of the object spectrum at frequencies $(x_f/\lambda f, y_f/\lambda f)$. Note that a phase factor again precedes the transform integral, but that it vanishes for the very special case $d_o = f$.

(3) Object Placed Behind The Lens. Finally, we consider the case of an object that is placed behind the

lens, as shown in Fig. 15c. The object again has transmittance t_o, but is now located a distance d from the focal plane of the lens. Let the lens be illuminated by a normally incident plane wave of amplitude A. Then incident on the object is a spherical wave converging toward the back focal point of the lens.

In the geometrical-optics approximation, the amplitude of the spherical wave impinging on the object is Af/d; the particular region of the object that is illuminated is determined by the intersection of the converging cone of rays with the object plane. If the lens is circular of diameter ℓ, then a circular region of diameter ℓ d/f is illuminated in the object space. The finite extent of this illuminating spot can be represented mathematically by projecting the pupil function of the lens along the cone of rays onto the object yielding an effective pupil function $P\left[x_o(f/d), y_o(f/d)\right]$ in the object plane. Note that the object transmittance t_o will have a finite aperture; the effective aperture in the object space is thus determined by the intersection of the true object aperture with the projected pupil function. If the object aperture is fully illuminated, then the projected pupil function may be ignored.

Using a paraxial approximation to the spherical wave that illuminates the object, the field amplitude transmitted by the object may be written

$$U_o(x_o,y_o) = \left\{\frac{Af}{d} P\left(x_o \frac{f}{d}, y_o \frac{f}{d}\right) \exp\left[-j \frac{k}{2d}(x_o^2 + y_o^2)\right]\right\} t_o(x_o,y_o) \qquad (94)$$

Assuming Fresnel diffraction from the object plane to the focal plane

$$U_f(x_f,y_f) = \frac{A \exp\left[j \frac{k}{2d}(x_f^2 + y_f^2)\right]}{j\lambda d} \frac{f}{d} \iint_{-\infty}^{\infty} t_o(x_o,y_o) P\left(x_o \frac{f}{d}, y_o \frac{f}{d}\right) \exp\left[-j \frac{2\pi}{\lambda d}(x_o x_f + y_o y_f)\right] dx_o\, dy_o \qquad (95)$$

Thus, up to a quadratic phase factor, the focal-plane amplitude distribution is the Fourier transform of that portion of the object subtended by the projected lens aperture.

The result represented by equation (95) is essentially the same result obtained previously when the object was placed directly against the lens itself. However, an extra flexibility has been obtained in the present configuration; namely, the scale of the Fourier transform is under the control of the experimenter. By increasing d, the spatial size of the transform is increased, at least until the transparency is directly against the lens (i.e., d = f). By decreasing d, the size of the transform is made smaller. /25/

E. INTERFERENCE

The phenomenon of interference is central to the subject matter presented within. To initiate consideration of interference, two different light waves, E_1 and E_2, of the same

frequency are superimposed. Since $E = E_1 + E_2$, the irradiance will be:

$$I = \langle E^2 \rangle = \langle E_1^2 \rangle + \langle E_2^2 \rangle + 2\langle E_1 \cdot E_2 \rangle. \tag{96}$$

where <> symbolizes the time average or mean. The proportionality constant εv of equation (5) will be neglected for the remainder of the discussion. From the previously stated assumption, both waves are linearly polarized in the same direction. Then

$$E_1 = A_1 \cos(\omega t - \mathbf{k}_1 \cdot \mathbf{r}) \tag{97}$$

$$E_2 = A_2 \cos(\omega t - \mathbf{k}_2 \cdot \mathbf{r} + \phi), \tag{98}$$

where θ is a constant relative phase between the two waves, and K_1 and K_2 are the wave propagation vectors for E_1 and E_2 respectively. Combining equations (96), (97), and (98) and carrying out the averaging, then

$$\overline{I = I_1 + I_2 + 2\sqrt{I_1 I_2}\cos\delta} \tag{99}$$

where $\text{where } I_1 = A_1^2, \overline{I_2 = A_2^2},$

(100)

and $\delta = \mathbf{k}_2 \cdot \mathbf{r} - \mathbf{k}_1 \cdot \mathbf{r} - \phi$

(101)

where α is the phase difference between the two waves at any location. The irradiance varies from a minimum value $I_{MIN} = I_1 + I_2 - 2(I_1 I_2)^{\frac{1}{2}}$ at points where $\delta = (2N + 1)$ to a maximum value $I_{MAX} = I_1 + I_2 + 2(I_1 I_2)^{\frac{1}{2}}$ at points where $\delta = 2N\pi$, where N is an integer. The irradiance pattern will be alternating light and dark fringes.

1. Interference From Two Point Sources Emitting Spherical Waves

A specific important example of interference is that of two spherical waves emanating from two point sources of light (see Fig. 16). Assume that light is radiated from points b and c in phase, that is $\theta = 0$. The irradiance at any point P_n in space is given by equation (99) with the phase difference being f.

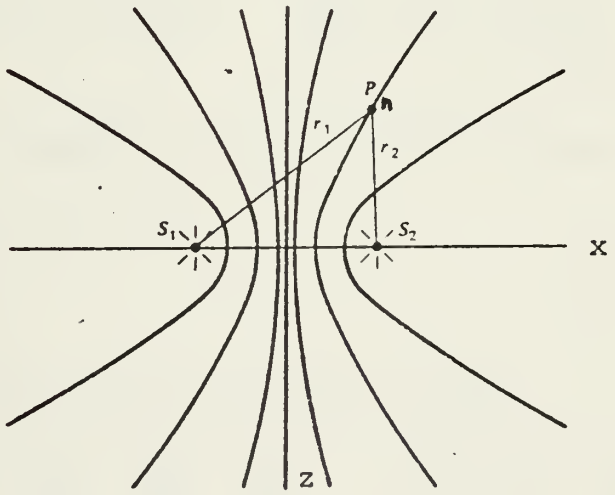

Figure 16. Interference of light emitted by two point sources, S_1 and S_2. Modified from Vest [53]

If ℓ is the perpendicular distance from the axis formed by S_1S_2 to the point P_n and $D = d/2$ is the distance S_1S_2, then

$$r_1 = \sqrt{\ell^2 + (d - x)^2} \tag{102}$$

$$r_2 = \sqrt{\ell^2 + (d + x)^2} \tag{103}$$

The phase at P_n due to S_1 and S_2 respectively is

$$Kr_1 = 2\pi r_1/\lambda \tag{104}$$

$$Kr_2 = 2\pi r_2/\lambda \tag{105}$$

where $K = 2\pi/\lambda$

The phase difference generated at the point P_n by S_1 and S_2 is then

$$\delta = K(r_1 - r_2) \tag{106}$$

Substituting the values for r_1 and r_2

$$\delta = K\left[\sqrt{\ell^2 + (d + x)^2} - \sqrt{\ell^2 + (d - x)^2}\right] \tag{107}$$

Assuming the following distance relationships

$$d/\ell << 1$$
$$x/\ell << 1 \tag{108}$$

Factoring ℓ out of equation (107) gives

$$\delta = K\ell\left[\sqrt{1 + \frac{d^2}{2} + \frac{2xd}{2} + \frac{x^2}{2}} - \sqrt{1 + \frac{d^2}{2} - \frac{2xd}{2} + \frac{x^2}{2}}\right]$$

using the power identity of

$$(1 + x)^n = 1 + nx + \frac{n(n-1)x^2}{2!} + \ldots \qquad (109)$$

and neglecting higher order terms

$$\delta = 2Kxd/\ell \qquad (110)$$

Then the locus of points forming a surface of maximum irradiance is determined by setting $\delta = 2\pi N$ where

$$r_1 - r_2 = \frac{2\pi N}{K} = N\lambda \; ; \; N = 0, 1, 2 \ldots \qquad (111)$$

This is the equation of a family of hyperboloids of revolution about the axis $\overline{S_1S_2}$ connecting the two point sources.

Two light waves which are capable of interfering are said to be coherent. Because of the coherence requirements, most interference experiments are conducted using two images of the same physical source.

2. Young's Fringes

A simple division of wave front interferometer is used to produce Young's fringes. This is shown in Fig. 17 . It is simply an opaque screen in which two holes separated by a distance D have been cut. This screen is illuminated by a point source located a distance ℓ_s from the screen and a distance y_s above the center line axis of symmetry of the screen. The light diffracted by the two holes forms an interference pattern which can be observed on a screen placed

some distance ℓ_o away. In practice, y_s, y, and D are much smaller than ℓ_s and ℓ_o.

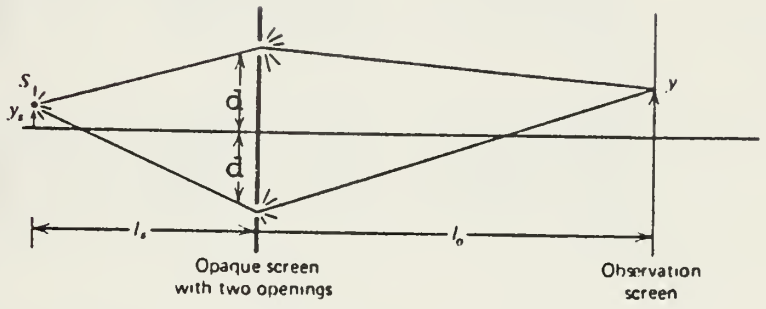

Figure 17. Interferometer to form Young's fringes.

The irradiance of each of the light waves at y therefore will be nearly equal $I_1 = I_2 = I_o$ so equation (99) becomes

$$I = 2I_o\ (1 + \cos\ \alpha)$$
$$I = 4I_o \cos^2\ (\alpha/2) \tag{112}$$

Here the phase difference is $\delta = K\Delta\ell$, where $\Delta\ell$ is the difference in the distance the light travels from the source S to the observation screen at y on the two paths.

$$\Delta\ell = \left\{ \left[\ell_s^2 + (d - y_s)^2\right]^{\frac{1}{2}} + \left[\ell_o^2 + (d - y)^2\right]^{\frac{1}{2}} - \left[\ell_s^2 + (d + y_s)^2\right]^{\frac{1}{2}} - \left[\ell_o^2 + (d + y)^2\right]^{\frac{1}{2}} \right\} \tag{113}$$

Dividing by ℓ_s and ℓ_o to set the equation up to utilize the identity of equation (109) and disregarding second order and higher terms gives

$$\Delta\ell = \ell_s' \left\{\left[1 + \frac{1}{2}\frac{(d-y_s)^2}{\ell_s^2}\right] - \left[1 - \frac{1}{2}\frac{(d+y_s)^2}{\ell_s^2}\right]\right\}$$

$$\left\{\left[1 + \frac{1}{2}\frac{(d-y)^2}{\ell_o^2}\right] - \left[1 - \frac{1}{2}\frac{(d+y)^2}{\ell_o^2}\right]\right\}$$

$$\Delta\ell = \ell_s \left[\frac{-2y_s d}{\ell_s^2}\right] + \ell_o \left[\frac{-2yd}{\ell_o^2}\right]$$

$$\Delta\ell = -\left(\frac{Dy_s}{\ell_s} + \frac{Dy}{\ell_o}\right) \tag{114}$$

Knowing that $\delta = K\Delta\ell$ gives

$$\delta = -K\left[\frac{Dy_s}{\ell_s} + \frac{Dy}{\ell_o}\right] \tag{115}$$

Where again $K = 2\pi/\lambda$ is the wave number. The irradiance is then equal to

$$I = 4I_o \cos^2\left(\frac{\delta}{2}\right) \tag{116}$$

Substituting for δ into equation (116) gives

$$I = 4I_o \cos^2 \left[\frac{\pi D}{\lambda} \left(\frac{y}{\ell_o} + \frac{y_s}{\ell_s} \right) \right] \qquad (117)$$

which represents parallel fringe spacing of $\lambda \ell_o / D$.

3. Scalar Wave Theory

Further consideration of the subject of diffraction, shows the representation of light waves may be modified. Seeing that the assumption of unidirectional polarized light has been made, only one vector component of E need be studied. In other words, E can be treated as a scalar instead of a vector. E is then replaced by the scalar quantity U(x,y,z,t), which is referred to as the optical disturbance. For example, a monochromatic plane wave is denoted by

$$U(x,y,z,t) = a(x,y,z) \cos(\omega t - K \cdot r) \qquad (118)$$

Similarly, the expression for any momochromatic wave can be written in the form

$$U(x,y,z,t) = a(x,y,z) \cos \left[\omega t - \theta (x,y,z) \right] \qquad (119)$$

where a(x,y,z) is the real amplitude of the light wave, and θ (x,y,z) is its phase. Of course, the plane wave is a special case for which θ (x,y,z) = K·r is constant. Equation (119) also can be written as

$$U(x,y,z,t) = \text{Re} \left\{ U(x,y,z) \exp (i\omega t) \right\} \qquad (120)$$

where

$$U(x,y,z) = a(x,y,z) \exp \left[-i \theta(x,y,z) \right]$$

is called the complex amplitude of the light. Because the temporal frequency of light is so high, there is no need to consider the time dependence ext(-iwt) explicitly. The complex amplitude U(x,y,z) contains all the information about the spatial structure of light waves essential to speckle photography.

The complex amplitude of light emitted from a rough surface received at a detector perpendicular to that surface is given by equation (120).

The irradiance of the light at the detector surface is a more important quantity because that is what is actually detected. The probability density function for the irradiance, $P_I(I)$, is

$$P_I(I) = \frac{1}{\langle I \rangle} \exp\left(\frac{-I}{\langle I \rangle}\right) \qquad (121)$$

The irradiance of the speckle pattern there obeys negative exponential statistics. A measure of the contrast of speckle is the ratio $C = \sigma_I / \langle I \rangle$, where I is the standard deviation of the irradiance, and I is its mean value. For the distribution given by equation (121), the speckle contract is unity. /26/

The most probable irradiance in a speckle pattern is seen to be zero, that is black (see Fig. 18).

F. SPECKLE THEORY

The speckle phenomenon has long been familiar, but only the introduction of lasers has brought a deeper understanding

and many new applications to this field. [21] Laser speckles appear whenever an optically rough surface is illuminated with highly coherent light. The microscopic, random height variation of roughness of the surface needs to be of the order of the wave length of light used to illuminate the object surface or coarser. This encompasses most surfaces except those highly polished. The optical wave originating from any moderately distant point consists of a series of coherent waves, each arising from a different rough element of the surface. The optical path difference of these various waves may be several wave lengths. These waves scattered from the optically rough surface have not only differing phases but also differing wave amplitudes. The interference of the dephased, but coherent, secondary waves results in a granular pattern of intensity called speckle.

1. Speckle Characteristics

Consider the factors which quantitatively determine the characteristics, size, shape, and intensity form of the speckle.

Figures (18 a -f) are photographs of a typical speckle pattern produced by scattering light from a rough surface.

The physical explanation of speckle is that each point on the surface scatters the incoming laser light in such a manner that the scattered light from one point interferes with that of another point. The randomness of the speckle pattern itself is generated by the surface roughness which generates phase differences in the reflected waves upon scattering.

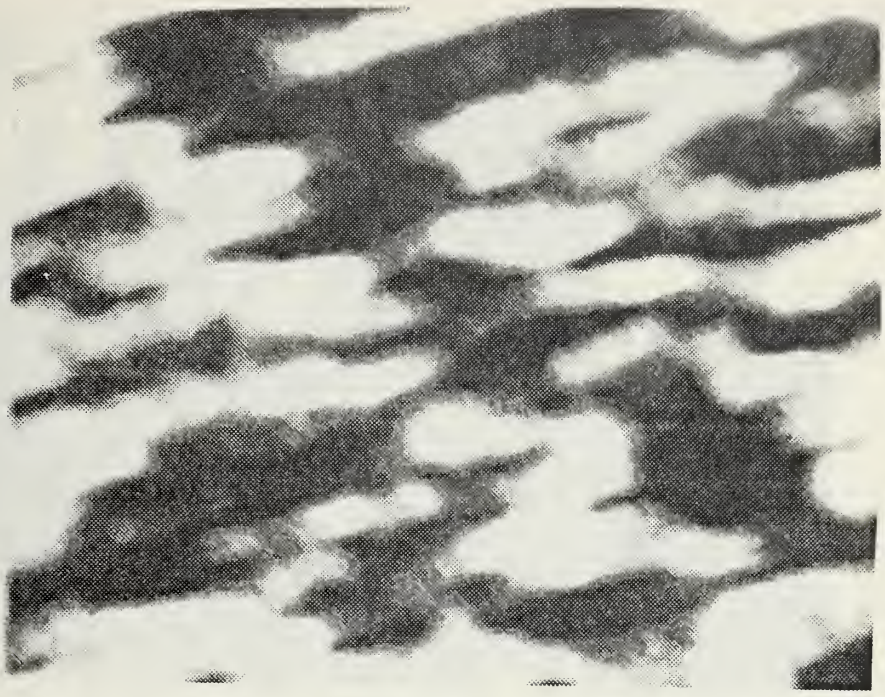

(a) Speckle size imaged by lens of f/2

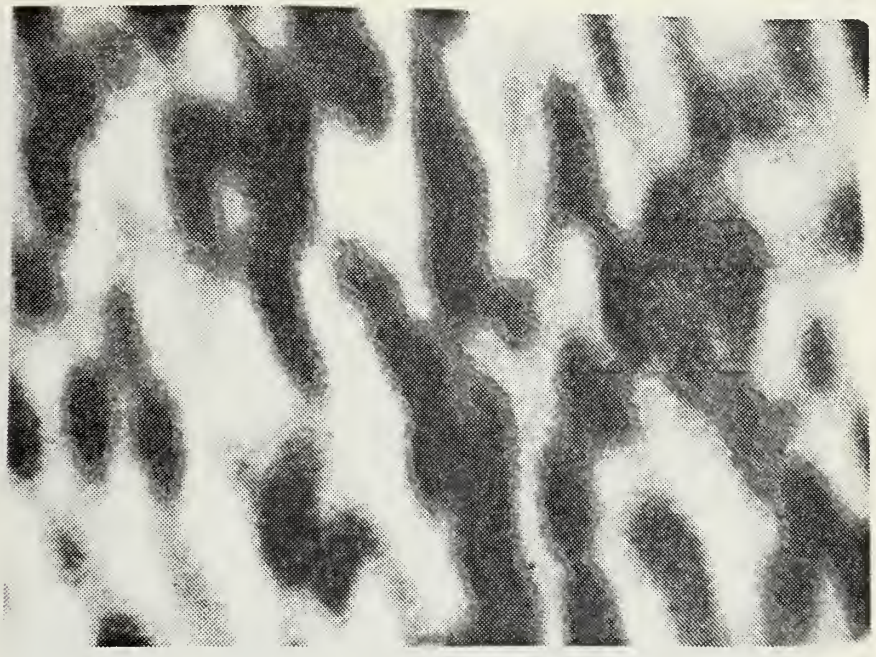

(b) Speckle size imaged by lens of f/2.8

Figure 18. Micrographs of speckle for various lens aperture settings, showing the speckle size dependence on imaging aperture. Image magnification equaled .137. Microscopic magnification 300X.

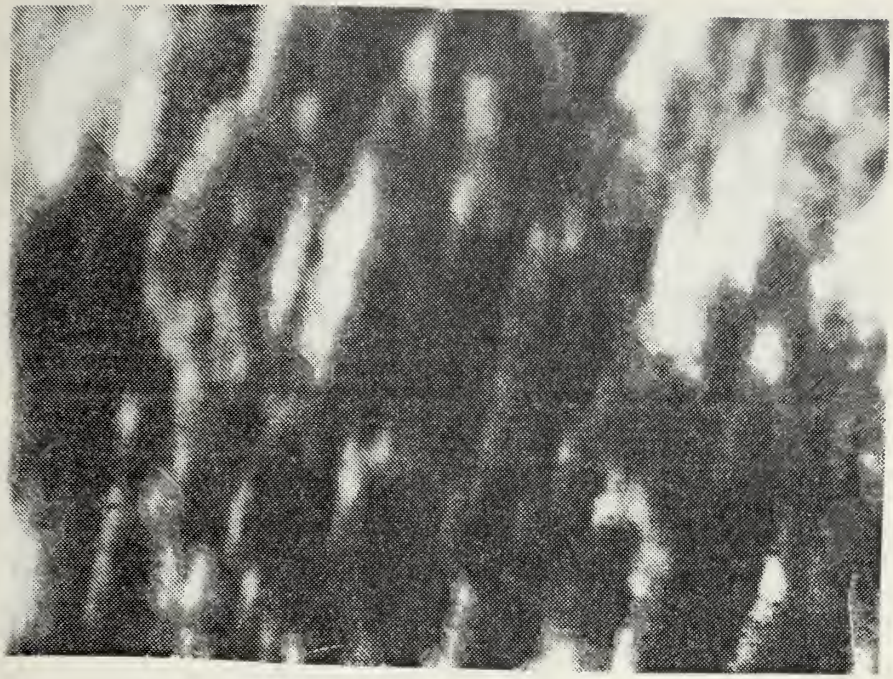

(c) Speckle size imaged by lens of f/4

(d) Speckle size imaged by lens of f/5.6

Figure 18. (Continued)

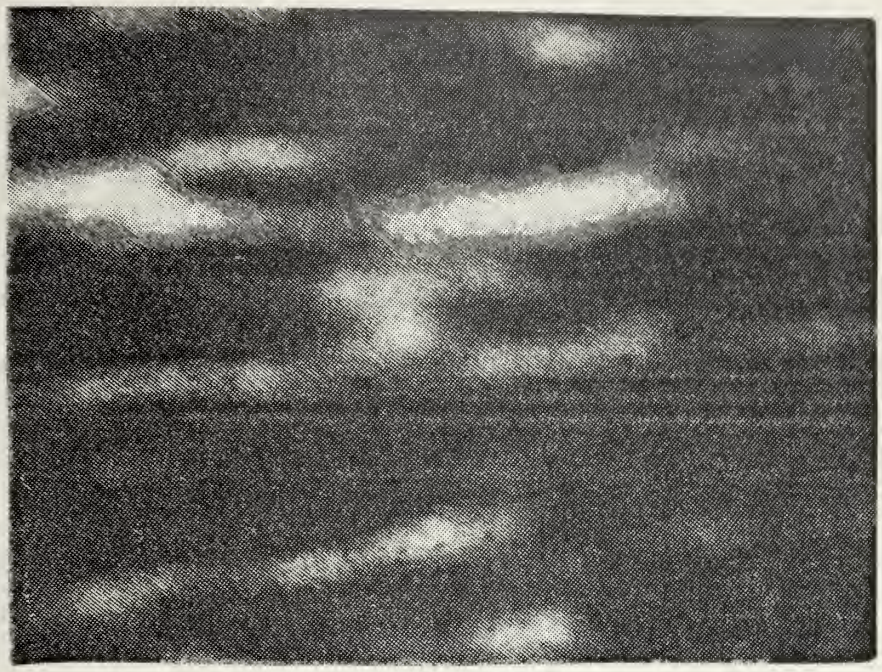

(e) Speckle size imaged by lens of f/8

(f) Speckle size imaged by lens of f/16.

Figure 18. (Continued)

To determine the statistical characteristics of the irradiance in the observation plane of the speckle, it is convenient to consider an ensemble average at a single detection point rather than the whole field of view. It is assumed that the incident light is monochromatic and linearly polarized, and that its polarization is not changed by the scattering.

The most important statistical characteristic of laser speckle is its size. From equation (117), it is seen that any two points on the object surface separated by a distance ℓ give rise to fringes of frequency, $f = \ell/\lambda z$. The average fringe frequency will be

$$f = \frac{1}{3} f_{MAX} = \frac{1}{3} (L/\lambda z) \tag{122}$$

where L is the length of the illuminated area in the y direction and z is the distance from the illuminated object to the image plane. Hence the irradiance distribution across a "typical speckle" will be

$$I(y) = 1 + \cos \left[2 \pi (Ly/3 \lambda z)\right] \tag{123}$$

where y is the vertical axis value.

The width of the speckle can be described as the distance between points where I drops off to one-half its maximum value. This width is $1.5 (\lambda z/\ell)$; then a typical speckle width b_s would be

$$b_s = 1.5 \left(\frac{\lambda z}{\ell}\right) \tag{124}$$

To estimate the speckle size in this case, treat the disk enclosed by the pupil of the lens as a uniformly illuminated diffuse surface. If the diameter of the lens is D and the image is formed a distance z from the lens, $b_s = 1.5 \frac{\lambda x}{D}$, as shown in equation (124), while a more rigorous analysis leads to a very similar expression

$$b_s \approx 1.22\left(\frac{\lambda z}{D}\right) \tag{125}$$

See Fig. (11) for the Rayleigh criterion analysis of resolution.

If the imaging system is focused on a relatively distant plane, z = f = focal length of the lens; therefore

$$b_s \approx 1.22\left(\frac{f}{D}\right) \tag{126}$$

where f/D is the F number of the lens; typical imagings systems vary from about f/1.4 to f/32. See equation (148) for a more exact equation for the speckle size.

The speckle pattern formed by an imaging scattered He Ne laser light (λ = 632.8 nm) produces the corresponding speckle size which varies from 1 to 24 micron. See Table 3. Figures 18(a - f) shows the correlation between F number and speckle size.

For the experimentation of this thesis, a diffusely reflecting object was viewed through a lens or imaging system, as indicated in Fig. 19a.

2. Speckle Photography

As was stated in the introduction to speckle metrology, whenever diffused laser light is passed through a finite

aperture, a speckle pattern is formed. For the science of holography, speckle is considered noise because of its limiting effect on fringe clarity. [1, 21]

In Fig. 19d, a double-exposure specklegram is seen at a magnification of 300X. Notice the speckle pairs. These speckle pairs developed due to the correlated motion of the actual speckle pattern during the double-exposure recording. Processing of this double-exposure specklegram produces a Young's fringe pattern from which in-plane translation and rotation, strain, and vibrational analysis can be analyzed.

There are two prominent advantages of the speckle process over holography. These advantages are simplicity of the optical system required for both recording and processing the image and the relative ease of interpreting the obtained results.

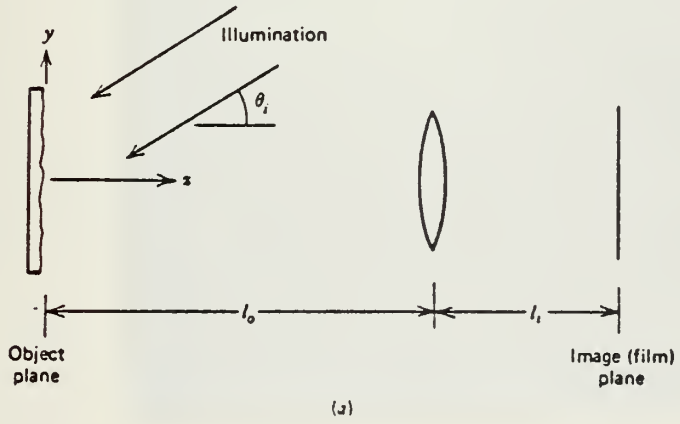

(a) Photographic plate imaging system

Figure 19. Two-exposure speckle photography for measurement of in-plane translation.

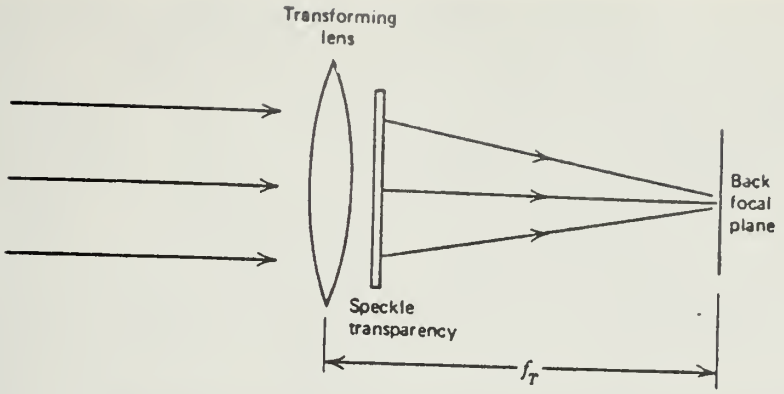

(b) Speckle transparency processing system

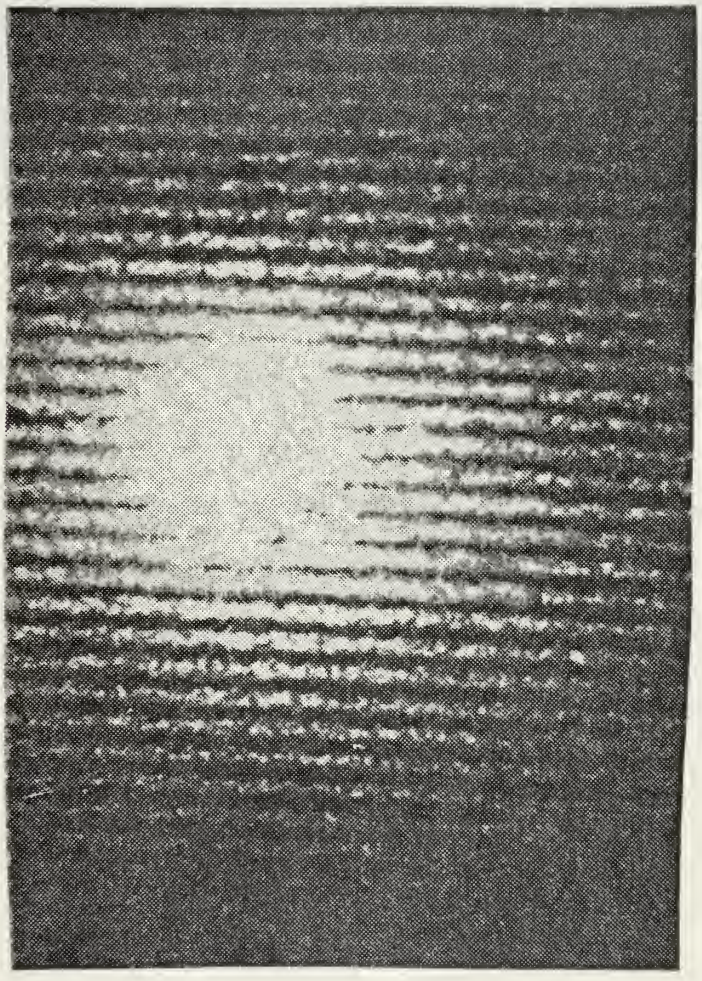

(c) Fringe pattern formed in the image plane of recording system. The object was translated in the x direction between exposures.

Figure 19. (Continued)

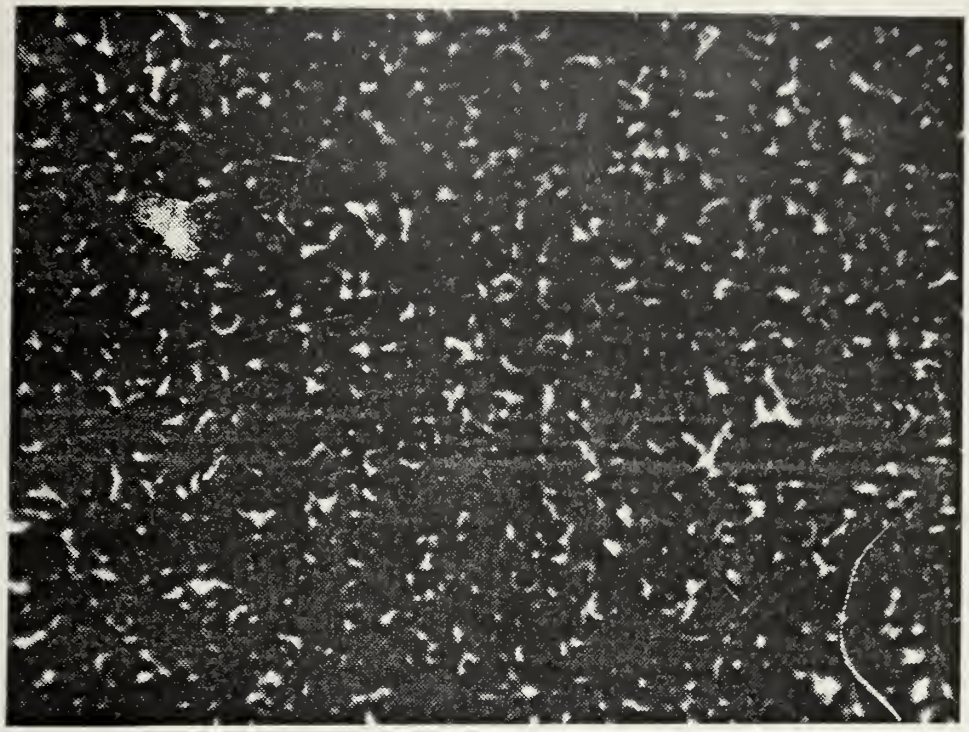

(d) Double-exposure specklegram magnified 300X.

Figure 19. (Continued)

In-plane displacement will be measured for both translation and rotation of a rigid, macroscopically-flat object using the experimental setup described by Figure 19a. An image of the object surface is formed in the film plane by a lens of focal length f and a diameter D. The object distance ℓ_o and the image distance ℓ_i are related by the thin lens imagery equation:

$$\frac{1}{l_o}+\frac{1}{l_i}=\frac{1}{f}, \tag{127}$$

This equation is approximately valid for real lenses and is quite accurate when an image is formed using only rays which are close to the optical axis.

Imagery systems or lenses are specified in terms of their relative aperture or F number. The F number is the ratio

of the focal length f to the diameter of the aperture D. If the same distant object is imaged by a lens of equal F number, the average irradiance in their image planes will be identical.

For an object illuminated by incoming laser light the image formed in the film plane will be modulated by a random speckle pattern having a characteristic size b_s determined by the aperture of the imaging lens, as is seen in equation (126).

3. In-plane Translation Measurements (x and y Translation and Rotation)

If an object translates horizontally by an amount L_x the relative phase of the light in each of the various rays that contributes to the formation of the speckle pattern will be unchanged. The entire speckle pattern will translate in the film plane of the imaging lens for small translations of the object to insure there is no decorrelation of the speckle pattern. The speckle pattern moves a distance ML_x in the image plane if the object is translated on amount L_x, where M is the magnification of the imaging lens. Similarly the speckle pattern in the object plane will translate an amount ML_y if the object is translated an amount L_y.

The amount of speckle motion is independent of the angle of illumination for in-plane translation.

To measure in-plane translation a double exposure is made. The film is exposed once prior to the object motion and once after the object motion. If the translation is greater than the speckle size b_s then the resultant negative

of the image plane will contain pairs of identical speckle patterns as is seen in Fig. 19d. The speckle pairs will be separated by a distance ML. The separation ML of the speckle pair can be measured directly by microscopic examination of the film. Alternatively, the translation can be measured by the optical system seen in Fig. 19a. For this Fourier transforming system the beam is first collimated. It is then sent through the transforming lens. The specklegram is then placed behind the Fourier transforming lens. The collimated beam then passes through the transforming lens and the specklegram and the speckle pairs recorded on the specklegram form Young's fringes in the back focal plane of the transforming lens as is seen if Fig. 19c. The bright central spot seen in Fig. 19c is formed by undiffracted light transmitted by the specklegram. Each pair of the corresponding speckles act as a pair of identical sources of coherent light which form Young's fringes. Since all speckle pairs are separated by the same distance ML, all of the Young's fringes overlay to form the pattern shown in Fig. 19c.

Interpretation of the fringes is straight forward. As in a Fourier transform, the fringe orientation is normal to the in-plane translation L. The magnitude L of the translation can be determined by applying equation (117). The speckles on the transparency are separated by a distance d_s; the fringes will have a spacing $d_f = \frac{\lambda f_T}{d_s}$. The in-plane translation of the object is given therefore by

$$L = \frac{\lambda f_T}{M d_f} \tag{128}$$

where λ is the wave length of the laser light used to form the fringes, f_T is the focal length of the tranforming lens, M is the magnification of the imaging system used to record the specklegram, and d_f is the fringe spacing.

In-plane rotation is the clockwise or counter-clockwise rotation of a rigid body. The recording or imaging system for in-plane rotation is identical to that for in-plane translation. Another type of optical processing system must be utilized. Due to the nature of rotational rigid body motion every point on the body will undergo a differing amount of translation. Therefore, the specklegram must be analyzed in a point-by-point fashion. The optical processing system for in-plane rotation is seen in Fig. 22a. Figure 22b shows the different fringe patterns that are obtained from a counter-closkwise rotation about the plates center. The fringe spacing is again inversly proportional to the point motion while the fringes are 90^{o} to the direction of the relative motion of the body.

4. Out-Of-Plane Rotation Measurement (TILT) [52, 53]

Tilt is out-of-plane rotation. Tilt will be measured using a two-exposure speckle photograph. The experimental setup is identical to that seen in Fig. 19a utilized for in-plane translation with a slight modification. Instead of focusing the imaging system on the image, the focus will be

placed in the back focal plane or at infinity. Again, a speckle pattern with characteristic size $b_s = 1.22\lambda F$ will be formed in this plane.

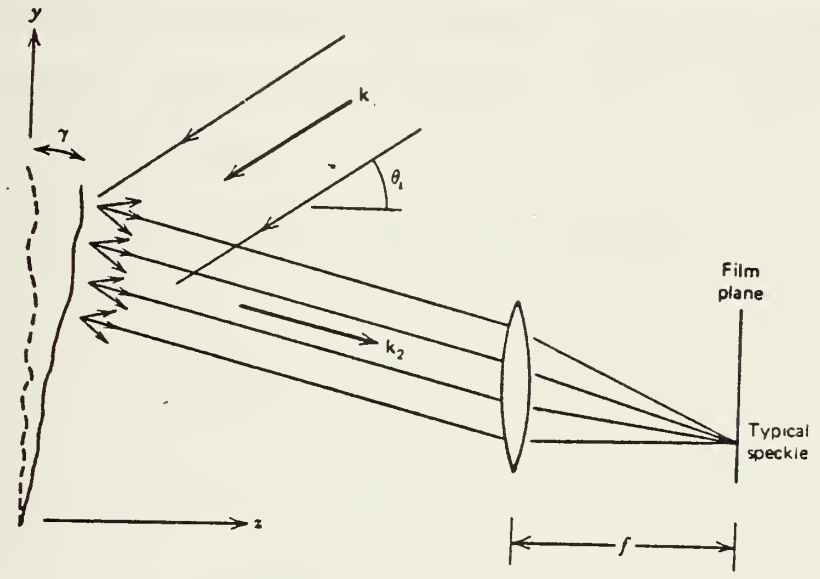

Figure 20. Two-exposure speckle photography for measurement of tilt. Light rays contributing to the formation of one speckle are shown. From Vest [53]

Each speckle is formed by all light scattered in a particular direction, as is indicated in Fig. 20. If the object is translated in its own plane $L = L_x\vec{i} + L_y\vec{j}$, the speckle pattern remains stationary; however if the object tilts by an angle γ, as in Fig. 20, the speckle pattern in the back focal plane will translate. Each ray contributing to the formation of a single speckle leaves the object surface at a different location y, but all travel in nearly the identical direction. When the object is tilted by an amount γ, there is a systematic change of relative phase among these

rays. The phase shift can be written

$$\Delta\phi = \frac{2\pi}{\lambda}(\hat{k}_2 - \hat{k}_1)\cdot \mathbf{L}, \tag{129}$$

where K_1 is the unit direction vector of the illumination, and K_2 is the unit direction vector of the rays contributing to the speckle under consideration. For the configuration of Fig. 20, $L = -\gamma y \vec{K}$ and

$$k_{1x} = 0, \quad k_{1y} = -\sin\theta, \quad k_{1z} = -\cos\theta_i, \tag{130}$$

and

$$k_{2x} = 0, \quad k_{2y} \cong 0, \quad k_{2z} \cong 1; \tag{131}$$

therefore

$$\Delta\phi = \frac{2\pi}{\lambda}(1+\cos\theta_i)\gamma y. \tag{132}$$

Equation (132) describes a linear variation of phase with y, so the effect is as if all the rays contributing to a single speckle tilted by a small angle, $(1 + \cos\theta_i)\gamma$. The corresponding displacement in the focal plane can be calculated using equation (133).

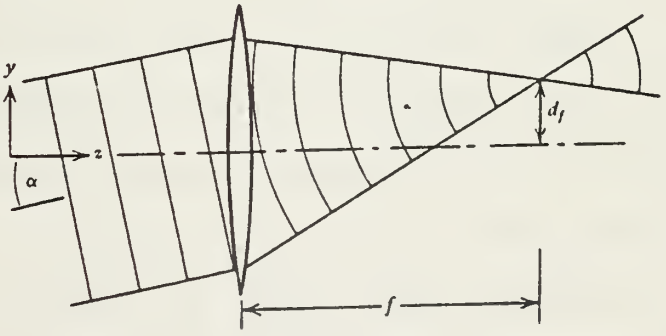

Figure 21. Spatial filtering light of an off axis plane wave focused to an off axis spot by a thin lens. From Vest [53]

Figure 21 shows what can be considered to be a plane wave indicent from an off-axis object point located a large distance away, that is, $\ell_o \to \infty$. This light will be focused to an off-axis spot in the back focal plane. If the plane wave propagates at an angle with respect to the optical axis, it will focus to a point a distance d_f from the axis, where

$$d_f = f \tan\alpha \tag{133}$$

We are concerned primarily with the paraxial case; hence α will be small, and

$$\tan \alpha = \sin \alpha = \alpha \tag{134}$$

Then the translation of the speckle in the back focal plane, d_s, will be

$$d_s = f(1 + \cos \theta_i)\gamma \tag{135}$$

where f_T is the focal length of the transforming lens. If the angular aperture of the lens is not too large, the translation of the entire speckle pattern will be given by equation (135).

To measure tilt, the film is placed in the back focal plane of the lens. If a 35 mm. camera is used, the camera is focused at infinity instead of on the object. A double-exposure speckle photograph is then taken of the object in the infinite focus position. The object is exposed once before tilting the object and once after the object is tilted. The transparency formed by developing the film is

then illuminated by a converging spherical wave formed by a lens of focal length f_T, as in Figure 19b. This will form a speckle pattern modulated by cosinusoidal fringes of spacing $d_f = \lambda f_T/d_s$, so the tilt of the object is given by

$$\gamma = \frac{\lambda f_T}{f(1+\cos\theta_i)d_f}. \tag{136}$$

Several extensions and applications of the previously discussed concepts of speckle photography exist for the analysis of vibration and strain. Theory for each of these two areas will be discussed here briefly.

5. Vibrational Analysis [6, 20, 30, 51, 53]

In-plane vibrations can be measured by time-average speckle photography. [6, 20] If the object of Fig. 19a vibrates harmonically as a rigid body, $L(t) = (Lx_i + Ly_j)\cos\omega t$. Where $L = (Lx_i^2 + Ly_j^2)^{\frac{1}{2}}$ is the amplitude of the vibration. A time-average exposure will record speckle streaks of length 2ML. The speckles spend most of their vibrational period near two ends of the streaks; therefore, if the film is processed using the system of Figure 20b, the fringes observed in the back focal plane will be similar to those caused by an object translation of 2L. Specifically, the form of the fringes that modulate the speckle pattern in the back focal plane is described by the square of the zero order Bessel Function

$$J_0^2\left[\left(\frac{2\pi ML}{\lambda f_T}\right)x'\right], \tag{137}$$

where x' is the coordinate parallel to the direction of motion. The amplitide of the vibration is determined by measuring the distance d_f between the dark fringes to the left and those to the right of the bright spot. The fringes occur where the argument of J_o equals ± 2.4, so

$$L = 0.76\left(\frac{\lambda f_T}{M d_f}\right), \tag{138}$$

where λ is the wave length of the laser light used to form the fringes, f_T is the focal length of the fringe imaging lens (transforming lens), and M is the magnification of the imaging system used to record the speckle photograph.

6. Strain Analysis [3, 4, 9, 15, 31-34, 40, 53]

If the object under study is now strained during the experiment, displacement varies from point to point on the object surface. Hence a different method of analyzing the speckle photographs must be devised.

Using the system of Fig. 22, the speckle photograph can be examined one region at a time by illuminating it with a small beam such as an unexpanded He-Ne laser bean as shown in Fig. 22a. The speckle pattern on the transparency will diffract this beam into a diverging cone of angular extent

$$\alpha \cong \left(\frac{f}{D}\right)^{-1}, \tag{139}$$

where f/D is the F number of the lens used to record the speckle photograph.

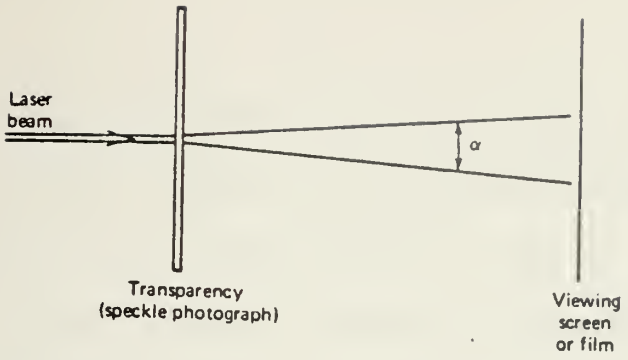

(a) Specklegram processing system

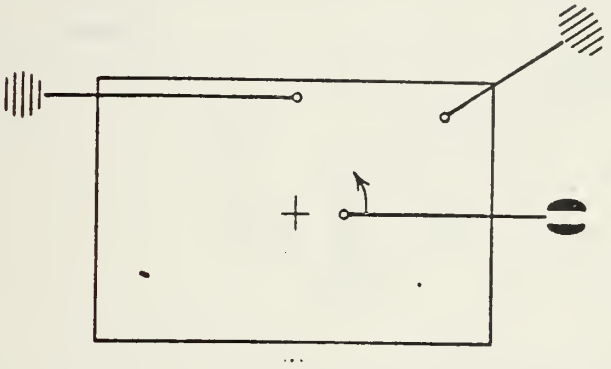

(b) Appearance of fringes at various locations on the specklegram of a rigid plate that was rotated about a normal axis through the center 0.

Figure 22. Formation of fringes by illuminating a double exposure photograph with a thin laser beam. From Vest [53]

If the small illuminated region contains pairs of identical speckles displaced by a distance d_s, the light in the resulting pairs of diffraction cones will interfere to form a diffraction pattern modulated by Young's fringes. [3, 4, 53] If the fringes are viewed from the photograph at a distance Z from the transparency, their spacing will be $d_f = \frac{\lambda Z}{d_s}$. Since $d_s = ML$, where M is the lateral magnification of the optical imaging system used to record the speckle photograph and L is the unknown displacement,

$$L = \frac{\lambda z_f}{M d_f}. \qquad (140)$$

Equation (140) gives the displacement of points in a single small region of the object surface. The fringes are normal to the local in-plane motion.

An alternative method of analyzing strain was discovered by Professor Y. Y. Hung. It is the Speckle Shearing Camera [32]. This method utilizes an image shearing interferometer camera.

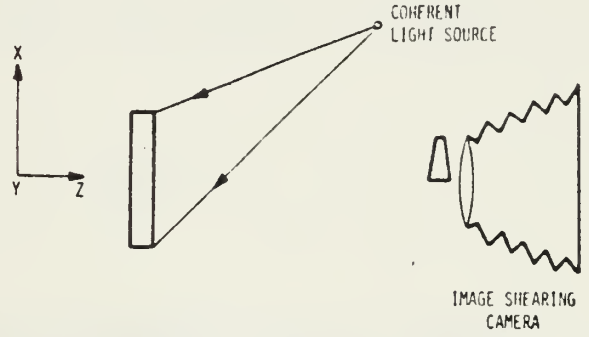

(a) Schematic diagram of optical setup of an image shearing camera.

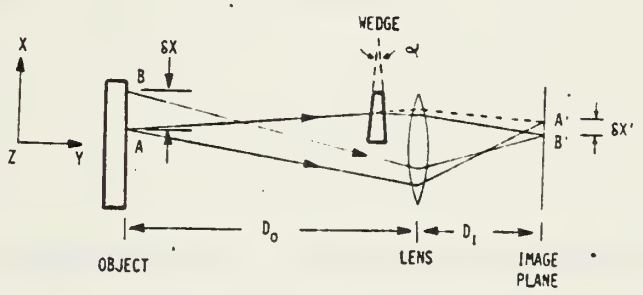

(b) Imaging detail of the image shearing camera.

Figure 23. Two exposure speckle photography using image shearing camera for strain and vibrational measurements. From Hung [32]

The image shearing camera of Fig. 23a has its lens divided into two parts by a thin glass wedge. The lens images the object, which is illuminated by a diverging beam,

inclined at an angle θ_i to the viewing direction. Since the rays passing through the glass wedge are deviated, the two images, (one focused by each half the lens) are laterally sheared with respect to each other as is seen in Fig. 23b.

Let the plane containing the prism angle be parallel to the x-z plane. Rays passing through the wedge are laterally shifted in the x-direction. Assuming that the wedge is placed very close to the lens, the amount of shift dx' in the image plane is

$$\delta x' = D_i(\mu - 1)\alpha, \tag{141}$$

Where D_i is the image distance from the lens, μ is the refractive index of the prism, and α is the prism angle. The equivalent shift δx on the object is

$$\delta x = (\delta x')/M, \tag{142}$$

Where M is the magnification, which is the ratio of the image distance D_i to the object distance D_o from the lens. Thus,

$$\delta_x = \delta_{x'} (D_o/D_i) = D_o(\gamma - 1)\ \alpha \tag{143}$$

The image shearing camera brings the rays from point P(x,y) on the object to meet with that from the neighboring point P(x + dx,y) in the image plane. Since the object is

coherently illuminated, the rays from the two points interfere with each other in the film plane.

The image shearing camera focuses two laterally-sheared coherent images in the film plane which interfere with each other. The direction of shearing depends on the orientation of the plane containing the wedge angle. Thus, by rotating the wedge on the wedge-lens assembly about the axis parallel to the viewing direction, the direction of shearing can be varied. The amount of shearing can be adjusted, as indicated in equation (143), by varying the wedge angle α as well as the object distance D_o. When the object is deformed, a relative displacement between two points produces a relative optical phase change Δ given by:

$$\Delta = \frac{2\pi}{\lambda} \left\{ \begin{array}{l} (1 + \cos\theta)\left[w(x+dx,y) - w(x,y)\right] \\ \sin\theta\left[u(x+dx,y) - u(x,y)\right] \end{array} \right\} + \qquad (144)$$

where u and w are the displacement components in the x and z directions, respectively. If the shear dx is small, the relative displacemnts may be approximated by the displacement derivatives and thus equation (144) becomes

$$\Delta = \frac{2\pi}{\lambda} \left\{ (1 + \cos\theta)\left(\frac{\partial w}{\partial x}\right) + \sin\theta \frac{\partial u}{\partial x} \right\} (\delta x) \qquad (145)$$

where the strains are given by

$$\varepsilon_x = \frac{\partial u}{\partial x} \quad \varepsilon_y = \frac{\partial v}{\partial y} \quad \gamma_{xy} = \frac{\partial u}{\partial y} + \frac{\partial v}{\partial x}$$

The term δx is equivalent to the gage length. Should the shear be in the y direction, the derivatives in equation (145) would be with respect to y. This is achieved by rotating the camera lens 90°. If the object is rotated 90° about the z axis, u is replaced by v, the displacement component in the y direction.

By taking a double-exposure recording with the object being strained between exposures, a speckle fringe pattern depicting Δ will be generated. Dark fringes occur when

$$\Delta = N\pi \qquad (146)$$

where $N = 1, 3, 5, 7 \ldots$

To measure $\frac{\partial w}{\partial x}$ this derivative may be isolated using normal illumination ($\theta = 0$).

However, it is impossible to isolate $\partial u/\partial x$. To achieve this $\frac{\partial u}{\partial x}$ isolation requires recording two fringe patterns using two different illumination angles; then $\frac{\partial u}{\partial x}$ can be separated from $\frac{\partial w}{\partial x}$ on a point by point basis using the following equation:

$$\frac{\partial u}{\partial x} = \frac{\lambda}{2\delta x}\left[\frac{N_1(1 + \cos\theta_2) - N_2(1 + \cos\theta_1)}{\sin\theta_1\ (1 + \cos\theta_2) - \sin\theta_2\ (1 + \cos\theta_1)}\right] \qquad (147)$$

where N_1 and N_2 are fringe orders corresponding to illumination angles θ_1 and θ_2 respectively.

G. FILM THEORY

1. Film And Optical Requirements

The sensitivity measurement by speckle photography is limited by the requirement that speckle motion in the film plane must exceed the characteristic speckle size, $b_s = 1.22 \frac{\lambda f}{D}$. If f/2.8 is used as a camera aperture, then $b_s = 2.16\mu m$ and a film resolution of about 462 lines/mm is required. A high resolution film is necessary for speckle photography. S0253 film was used for all speckle experimentation. This film has a resolution of 2500 lines/mm. The maximum frequency of the speckle pattern is $f_{MAX} = \left(\frac{f}{D}\right)^{-1} = 564$. Since film speed varies inversely with resolution, relatively long exposure times were required.

2. Measurement Limitations

The upper limit to measurable displacements or tilts is set by the decorrelation of the two speckle patterns. This is evident because processing of speckle photographs requires formation of Young's fringes by diffraction of light by pairs of identical speckles. A loss of correlation will be caused if strains are large enough to alter the microscopic structure of the opaque surface under study. Loss of correlation also occurs when motions are sufficiently large that the aperture of the object forming lens samples an appreciably different portion of the wave front scattered by the object during the two-exposures. When this occurs, only a fraction of the speckle pattern recorded on the photograph consists of pairs of identical speckles, so the fringes they generate are washed

out by the light diffracted by the rest of the speckle. A rough estimate of the sensitivity range of speckle photography, based on experiments reported, is that motions resulting in speckle translations of the order of 15-200 μm in the film plane can be measured. [6, 20, 53] In the upper limit, the object translation equals about ten percent of the diameter of the entrance pupil of a typical camera lens at f/4.

The practical sensitivity range in terms of actual object translation or tilt depends on object size, magnification, and required depth of focus. [21, 44] In general, the range extends to motions as large as about 1.5 mm. Above this limit, direct measure by ordinary double-exposure photography is more practical. The lower limit of the range is about 5 μm , but depth of focus requirements usually raise this limit to about 100 μm or higher. Hence, in practice there is a large gap between the maximum displacement measurable by holographic interferometry and the smallest displacement measurable by speckle photography. [44]

III. EXPERIMENTAL ANALYSIS AND PROCEDURES

A. FILM

Two types of film were used during this thesis experimentation. During the Fourier transform, speckle microphotography, and basic Fraunhofer diffraction studies, Polaroid positive negative 4x5 land film with an ASA (55) was used. An f/16 aperture and an exposure time of between 1/250 sec. and 1/125 sec. were used for optimim results. A Kodak special order (S0253) film was used for all speckle photography. A Pentax 35 mm camera was used with either a 55 or 85 mm focal length lens. For object speckle photography using the 85 mm lens with an M = .11 and an F = 2.8 for optimum results an exposure time of .5 sec. was used. For object speckle photography using the 55 mm lens with an M = .137 and an F = 4 and an object distance of 450 mm an exposure time of 2 seconds was used for optimum results. For fringe photography only the 55 mm lens was used with an F = 2.0 with an object distance of five feet giving exposure times of 5-7 min. depending on the fringe spacing.

The resolution of the S0253 film is very high (on the order of 2500 lines/mm). The higher resolution demanded longer exposure times, but this higher resolution was needed as will be seen during the discussion of speckle size.

Lastly, the film developing was done in Kodak D-19 developer 70^{o}F for 5½ minutes with constant agitation. Then

using Kodak rapid fixer, the film was fixed for 3 minutes. A film bath followed which usually required 30-40 minutes of constant water flow due to the heavy blue tint of the S0253 film.

B. SPECKLE SIZE

As was seen in the theory section under speckle size from the governing equation (126) speckle size is a function of the wave length of light and the F number of the imaging lens. Table 3 tests the various F numbers and their corresponding speckle size, b_s, when using a He-Ne gas laser as was used in the experimentation for this thesis. The wave length of a He-Ne gas laser is $\lambda = .6328.10^{-3}$mm.

TABLE 3

Speckle Size Versus Lens F Number And Film Resolution

F	1.9	2	2.8	4	5.6	8	11	16	32
$D_s x(10^{-3}$mm)	1.4668	1.544	2.16	3.088	4.323	6.176	8.492	12.352	24.704
resolution (lines/mm)	681	647	462	323	231	161	117	80	

Looking at the optical system used to record the speckle, lens magnification should be included in the speckle calculation. [3, 4] Fig. 24 shows the object-to-image position which relates the lens equation to the magnification.

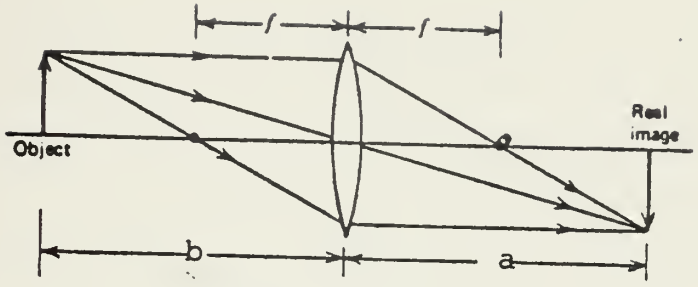

Figure 24. Formation of a real image with a thin, spherical lens.

Assuming the size of the speckle dot to be equal to the Airy disk in the image plane

$$b_s = \frac{1.22\lambda a}{D} \quad \frac{b}{b} \qquad \text{from equation (125).}$$

where a = z in this case. From the lens equation (127)

$$\frac{1}{f} = \frac{1}{a} + \frac{1}{b}$$

$$f = \frac{ab}{(a+b)} \quad \text{or} \quad f(a + b) = ab$$

which relates the speckle size to the image magnification, M. It is seen that

$$b_s = \frac{1.22\lambda f}{D} \quad \frac{(a + b)}{b} = \frac{1.22\lambda f}{D} \quad \left(1 + \frac{a}{b}\right) \qquad (148)$$

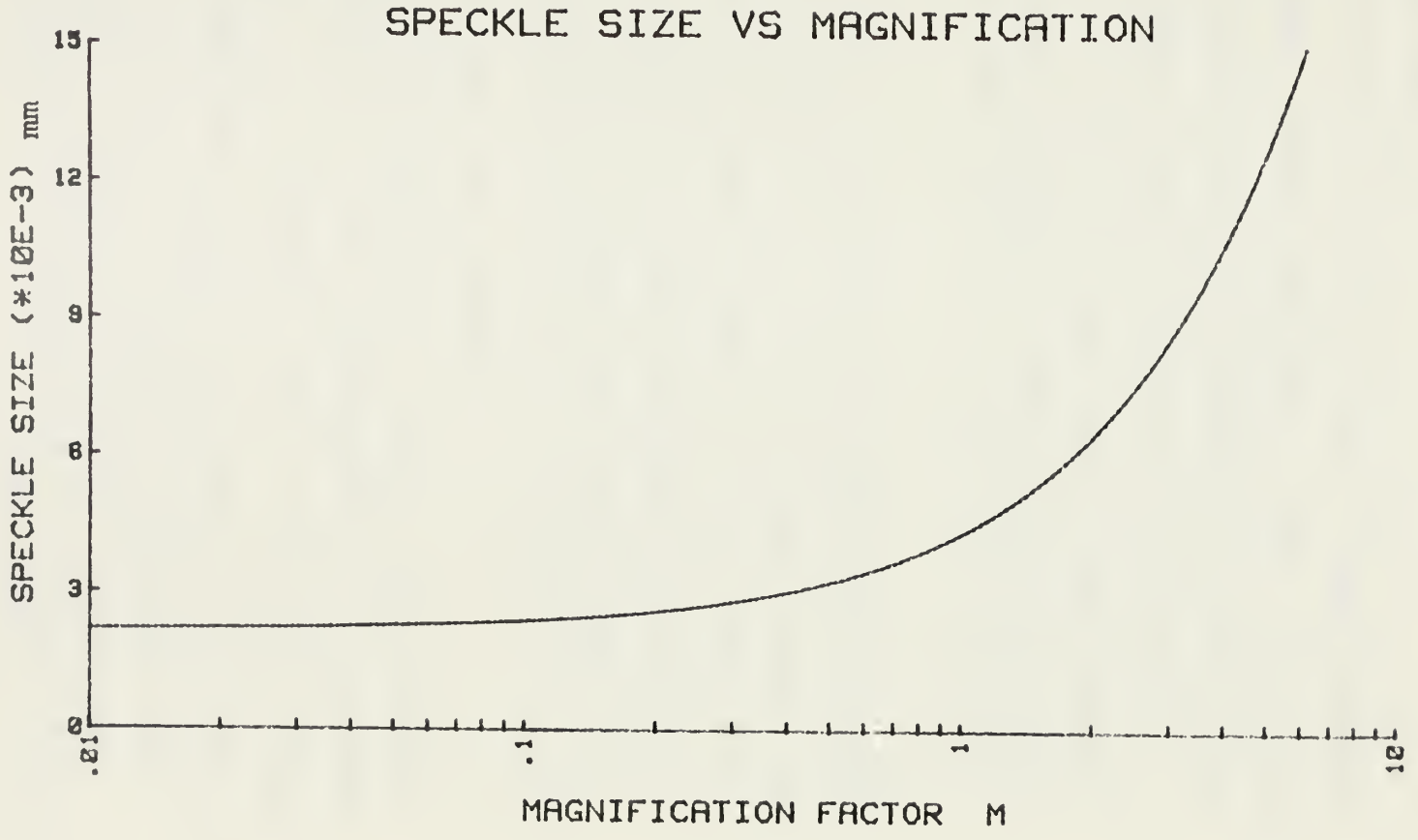
SPECKLE SIZE VS MAGNIFICATION
SPECKLE SIZE (*10E-3) mm
15
12
9
6
3
0
.01
.1
1
10
MAGNIFICATION FACTOR M

Figure 25

where

$M = \frac{a}{b}$ is the magnification of the imaging system.

Fig. 25 shows the relationship between the magnification M and the speckle size b_s.

Another area of concern is the effect of magnification change during laser speckle photography. [45] An assumption is made that during the speckle photograph no magnification change occurs, where in fact a change does take place.

For example, in the plane stress case, a magnification change arises from the Poisson's effect whereby the plane model undergoes lateral thickness changes when loaded in its plane.

In the tilt case, a magnification change occurs due to the out-of-plane motion toward the camera thus changing the object distance and the magnification M. This effect of change of magnification is examined in detail by Archbold and Ennos [5, 7, 10] and Dedretti and Chiang [45] The problem of magnification change can be minimized by using imaging lenses of long focal lengths.

The Airy disk size limitation on speckle size considerations for resolution is a good approximation, but subpeckle size measurements can be effected. [54] This lower measurement range can easily be reduced to one order of magnitude of the usual Airy disk limit. The method of subspeckle size speckle photography measurement is discussed in detail by Vikram and Vedam [54]. It requires a known lateral movement

being measured. The orientation of the Young's fringes gives the unknown deformation.

There are two other fundamental limitations in the recording methods of this thesis. First, laser speckles are three dimensional. Speckle patterns decorrelate in a distance which is small compared to conventional depth of field for an imaging lens system [3, 4]. Decorrelation is particularly severe with lens apertures wider than about f/4. Most speckle photography of this project was done with a lens aperture of f/2.8 therefore decorrelation of speckle was a problem. An increased image magnification would reduce the problem of the lens aperture effect, but again a low magnification was used for most experimentation (M = .11). Second, speckle photography is significantly vulnerable to lens aberrations. Ennos recognized this effect and published some data with regard to in plane rotation. [5, 10]. A more indepth study of the problem is given by Stetson [46]. Stetson's figures showing a comparison of Young's fringes achieved by a well-corrected copy lens at unity magnification and speckle halos from a normal camera at the same magnification vividly illustrate the loss of fringe visibility due to lens aberations.

C. FOURIER TRANSFORMS

In order to better understand diffraction, lens resolution, spatial filtering and other areas of optical physics, a preliminary study of Fourier transforms was conducted.

The first experiment that was conducted consisted of comparing differing rectangular aperture spacing. Fourier transforms were achieved using Ronchi ruling combinations of 100-300 lines/mm and 100-450 lines/mm. The results of the 100-300 lines/mm Ronchi ruling is seen in Fig. 26.

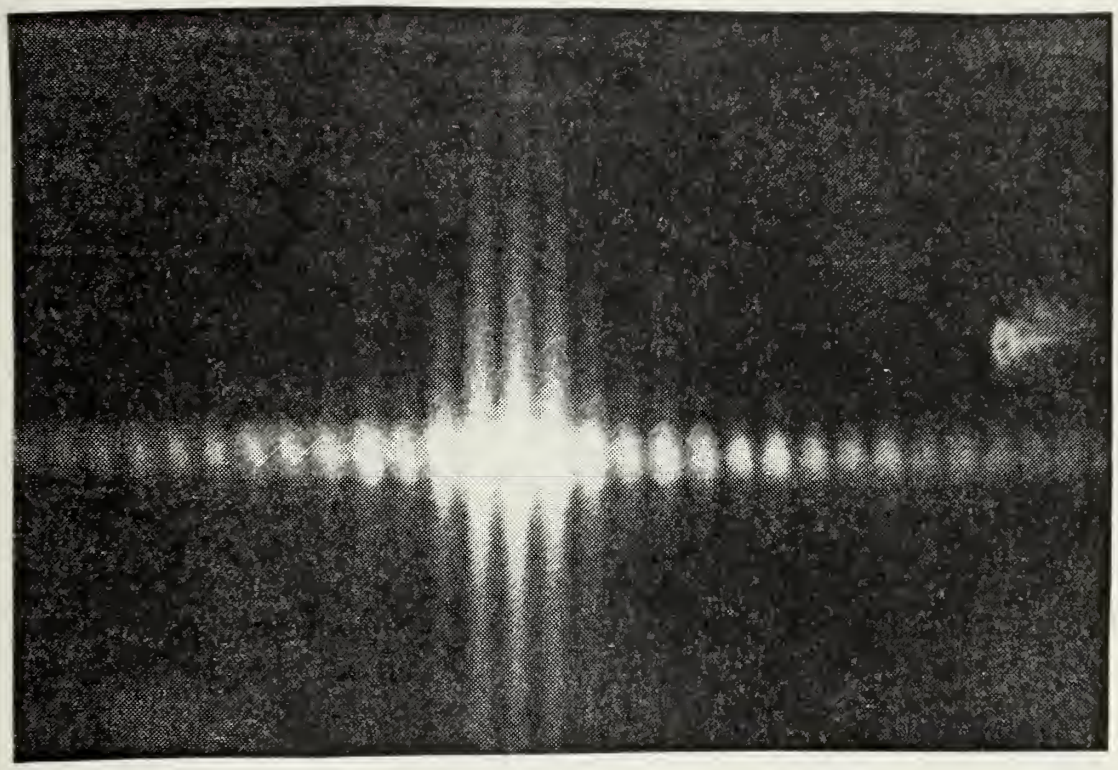

Figure 26. Fourier transform of a 100 and 300 lines/mm Ronchi ruling combination.

Three types of filtering were conducted. Using two Ronchi rulings of 300 lines/mm, a rectangular aperture grid was setup. First, the center of the Fourier transform of the rectangular aperture was filtered, which eliminated all lines from the reproduced grid pattern as seen in Fig. 27a. Second, the horizontal lines were filtered out of the

Fourier transform of the rectangular aperture, which eliminated all horizontal lines from the reproduced grid pattern. Last, the vertical lines were filtered out of the Fourier transform of the rectangulary aperture, which eliminated the vertical lines from the grid pattern as is shown in Fig. 27b.

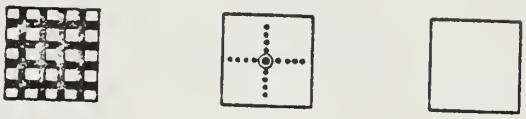

(a) Image pattern as a result of filtering the center of the Fourier transform.

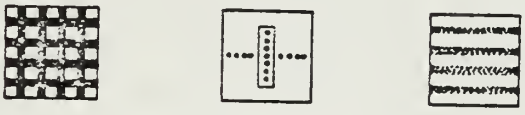

(b) Image pattern as a result of filtering the vertical lines of the Fourier transform.

Figure 27. Fourier transform filtering using a rectangular grid.

Figure 28 shows the lab setup for all Fourier transform experimental analysis. A 1.5 milliwatt He-Ne gas laser with a λ = 632.8 nm was used to produce the monochromatic wave. A combination 10X microscope objective combined with a 25 μm spatial filter were used to expand the beam. All lenses in this Fourier transform arrangement were spherical double convex lenses with a focal length f_T of 177.8 mm. Another lens collimated the beam. The grid was then placed in the optical system followed by the transforming lens. The grid pattern was then reproduced after passing through the beam filter.

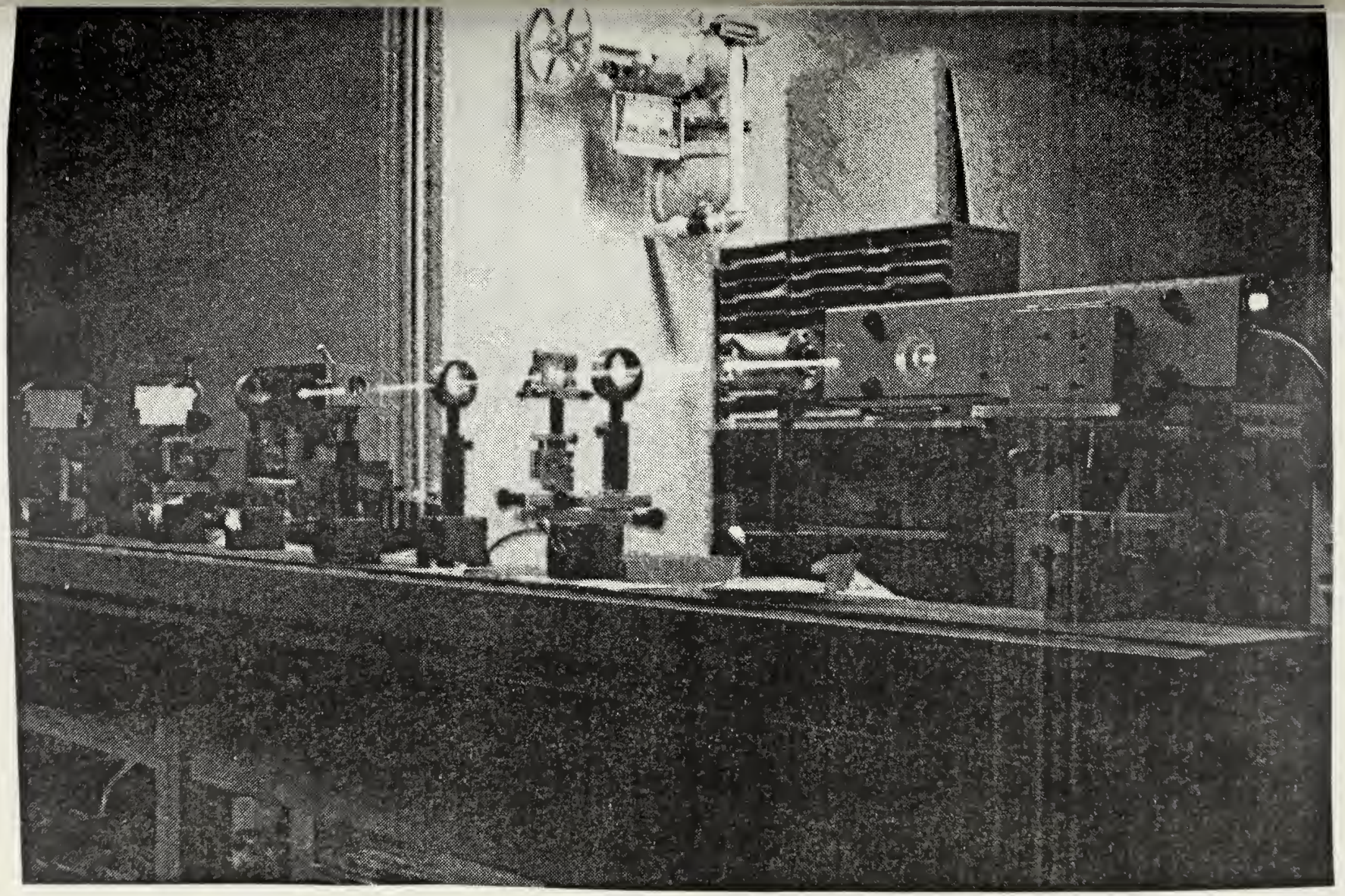

Figure 28. Equipment arrangement for conducting Fourier transform experimentation.

A 10X microscope lens was used to expand the beam onto a mirror which then reflected the reproduced grid image on a frosted glass screen. A magnifying eyepiece enabled the observer to view the image grid.

In order to process the double-exposure specklegram, the Fourier transform system of Fig. 28 was utilized. This system of fringe analysis was done using either the film prior to or after the transforming lens as is seen in Fig. 15 b & c and described in detail in the Fourier transform section of this thesis.

D. IN-PLANE TRANSLATION AND ROTATION

Figure 29 shows the lab setup for in-plane translation and rotation. A 1.5 milliwatt He-Ne gas laser was used to produce a monochromatic wave.

A double shutter was used to facilitate the double-exposure speckle photographing system. A 40X lens with a 25 μm spatial filter was used to expand the beam. A 5" x 7" 2024-T4 Aluminum plate was used for the object. A Pentax 35 mm camera with an 85 mm lens was used to record the image at an object distance of 850 mm. Optimum exposure times for this setup were ½ second for an F = 2.8.

For in plane translation, a micrometric holder which read in 1/10,000 in. and 1 turn = 1/40 in. was used while for in-plane rotation a micrometer holder which read in .01 degrees and 1 turn = 0.1 degrees was used.

Translation of .003 in. to .070 in. were measured. A plot of actual translation versus fringe calculated

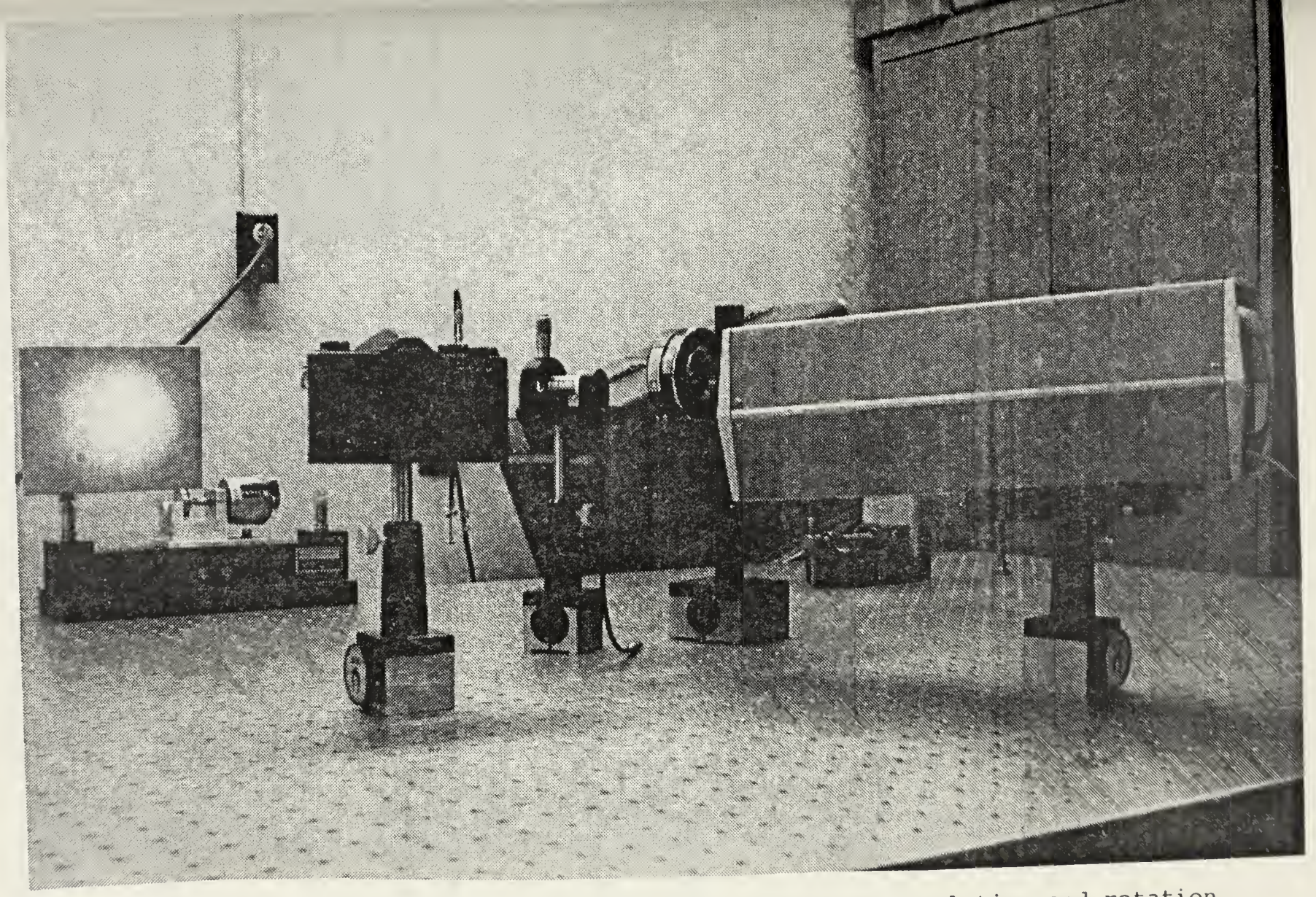

Figure 29. Laboratory arrangement for recording in-plane translation and rotation.

translation can be seen in Fig. 30, while Table 4 shows calculation of fringe spacing and fringe density for each translation.

The average error for the overall translation data was calculated to be one percent. Both Fig. 30 and the calculated error show that there was excellent correlation between the actual and calculated translation. Fig. 31 (a-f) show fringe spacing for various translations. As in the Fourier transform experimentation done previously, it can be seen that for small translations, speckle pair spacing is small, the aperture of diffraction on the specklegram is small and the resultant Young's fringe spacings are large, and conversely for large translation motion, the speckle pair spacing is large on the specklegram, therefore a large diffraction aperture resulting in Young's fringes which are closely spaced together.

Figure 33 shows fringes produced from specklegrams of various rotations. Seeing that each point in the specklegram field is rotated a different amount, individual points on the specklegram were inspected.

As seen in Fig. 32-33, fringes showing almost pure translation in both the x and y direction were observed at the four quarters of the specklegram. At the center of the specklegram no relative displacement occurs, therefore Young's fringes are not visible. At the outer edge between the quarter points of the specklegram, diagonal fringes show the existence of both x and y components of the rotation. Moving

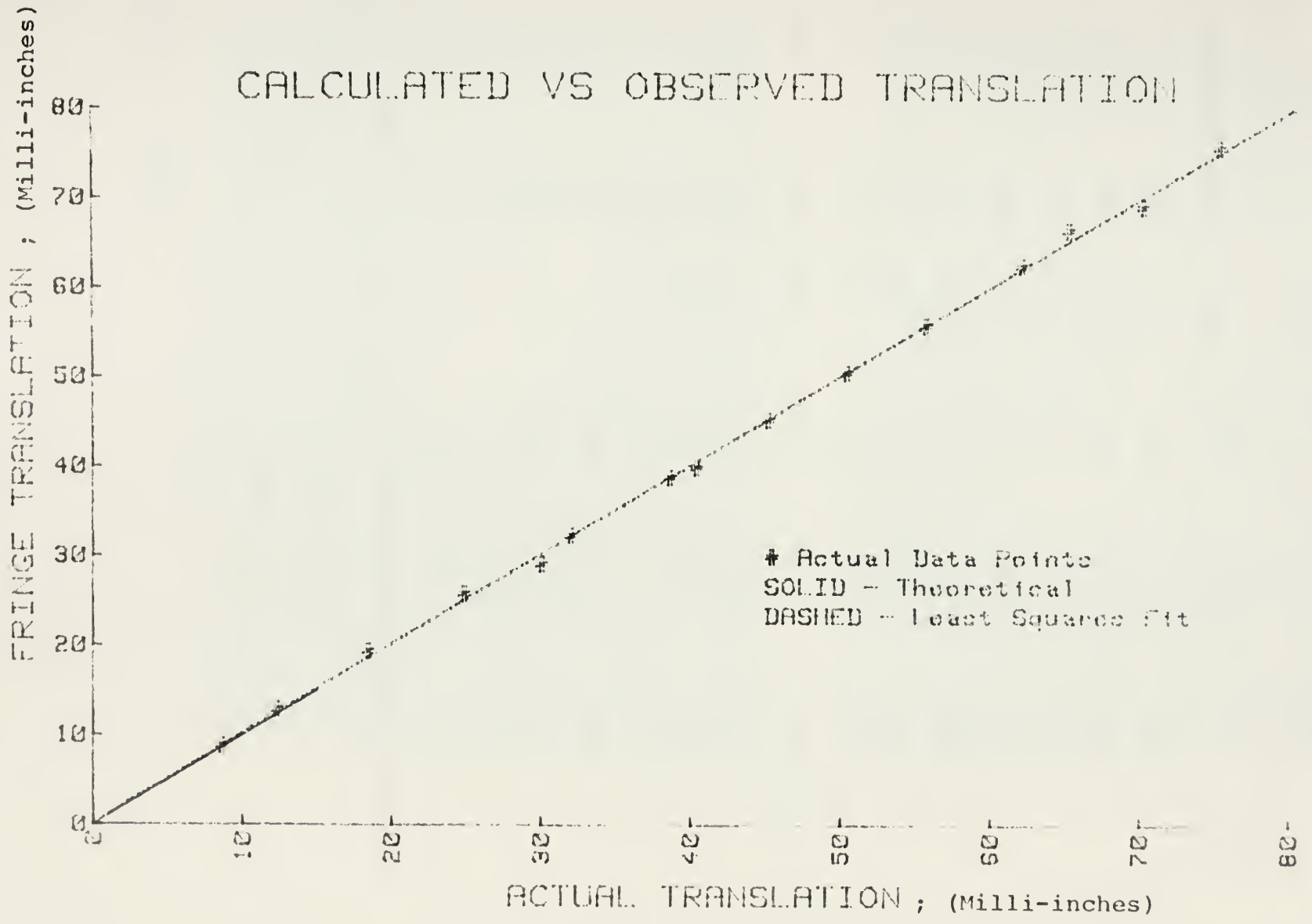
CALCULATED VS OBSERVED TRANSLATION
FRINGE TRANSLATION ; (Milli-inches)
ACTUAL TRANSLATION ; (Milli-inches)
0
10
20
30
40
50
60
70
80
* Actual Data Points
SOLID - Theoretical
DASHED - Least Square Fit

Figure 30.

TABLE 4

Calculation Of Fringe Spacing For Various Translations

Δ actual X0.001 (in.)	lines per area	area (mm)	d_f (mm)	$L_{(mm)}$ exp.	L(in.) X0.001 in. exp	Error x $\frac{1}{100}$
8.61	5.5	600	109.09	.2259	8.89	.0325
12.31	8	600	75.0	.3286	12.9	.0479
18.45	12	600	50.0	.493	19.4	.0515
24.87	16	600	37.5	.656	25.8	.0374
30.06	18	600	33.33	.7395	29.1	.0319
31.98	20	600	30	.8215	32.3	.010
38.58	24	600	25	.986	38.81	.0059
40.37	15	365	24.33	1.013	39.88	.0121
45.12	17	365	21.47	1.148	45.20	.0177
50.32	19	365	19.21	1.283	50.5	.0357
55.51	21	365	17.380	1.4182	55.8	.0413
61.95	23.5	365	15.332	1.587	62.48	.0855
65.05	25	365	14.6	1.688	66.47	.0218
70	26	365	14.03	1.755	69.12	.0126
75	28.5	365	12.807	1.9247	75.77	.0103

$L_{exp} = \lambda Z_f / M d_{f_{OBS}}$

$\lambda = .6328 \cdot 10^{-3}$ mm

$Z_f = 3896.2$ mm

$M = .11$

Mean Error = 3.057%

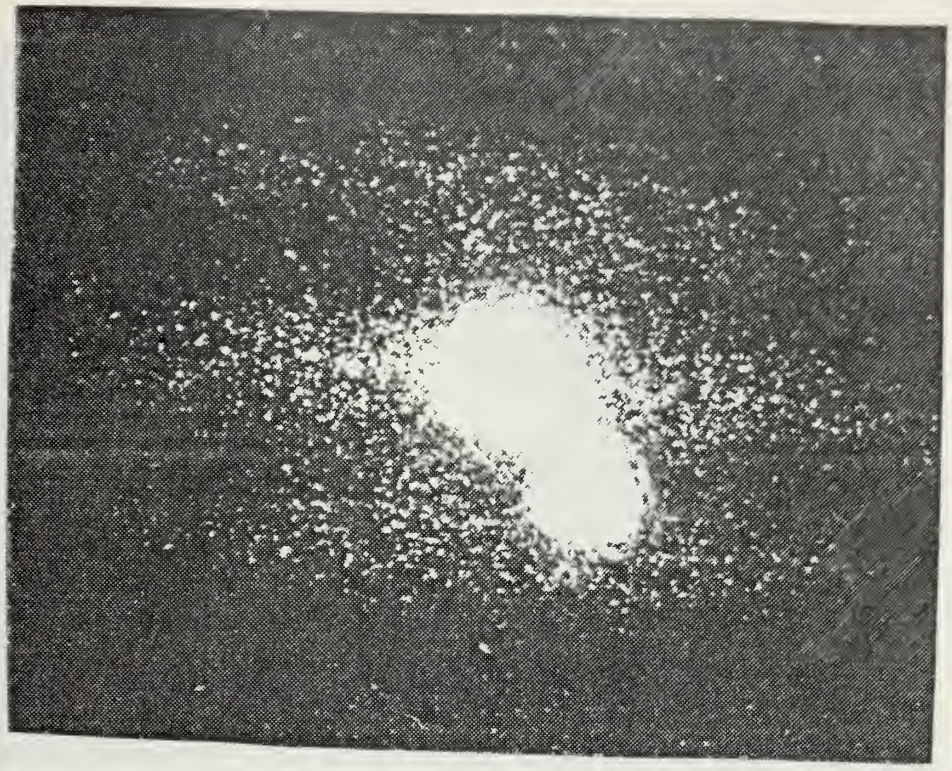

(a) Fringes generated due to 0.005 inch translation.

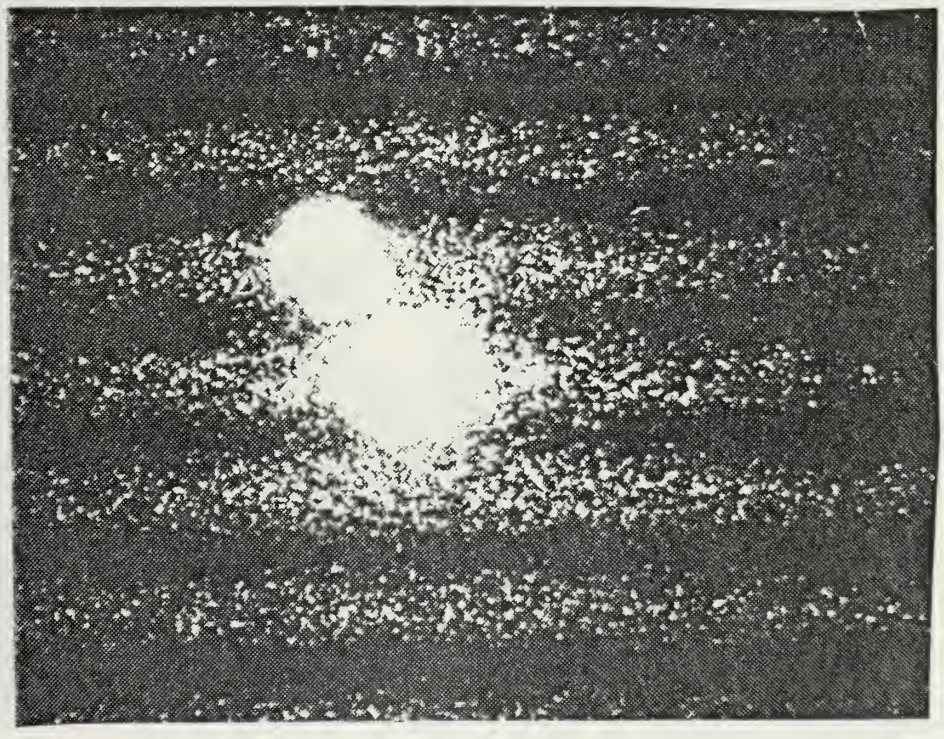

(b) Fringes generated due to 0.010 inch translation.

Figure 31. Fringe spacing for various in-plane translations.

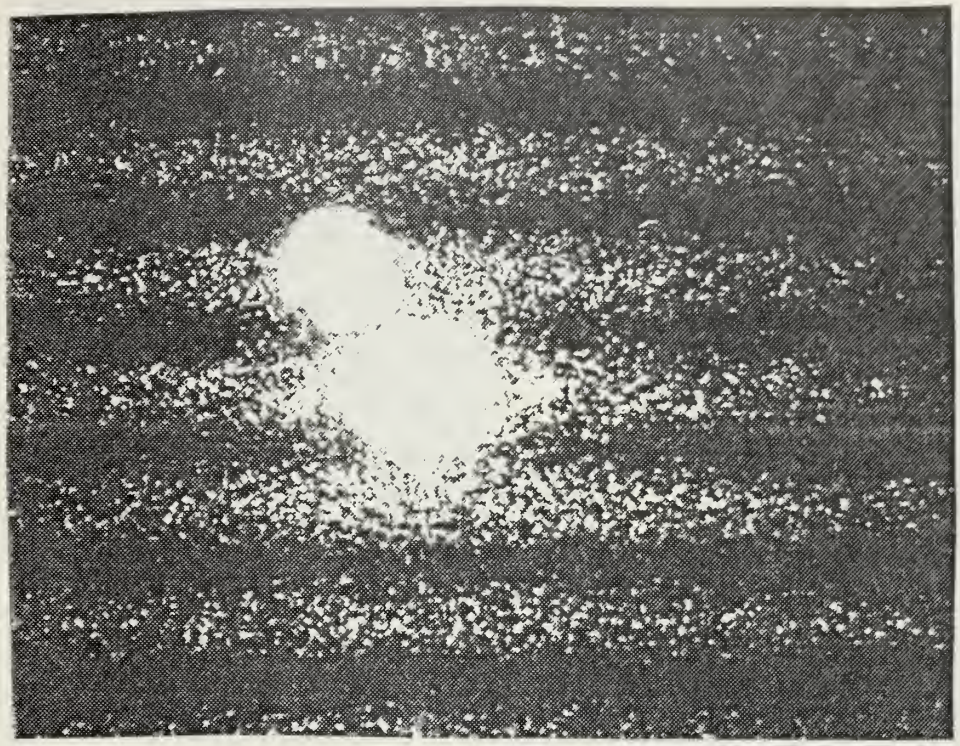

(c) Fringes generated due to 0.020 inch translation.

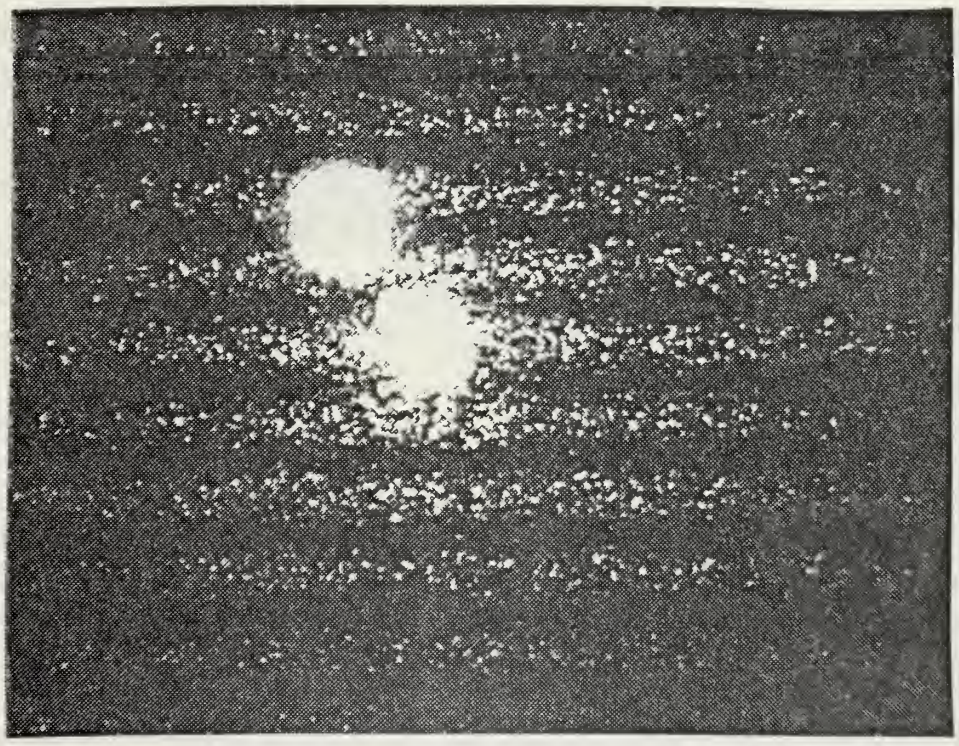

(d) Fringes generated due to 0.030 inch translation.

Figure 31 (Continued)

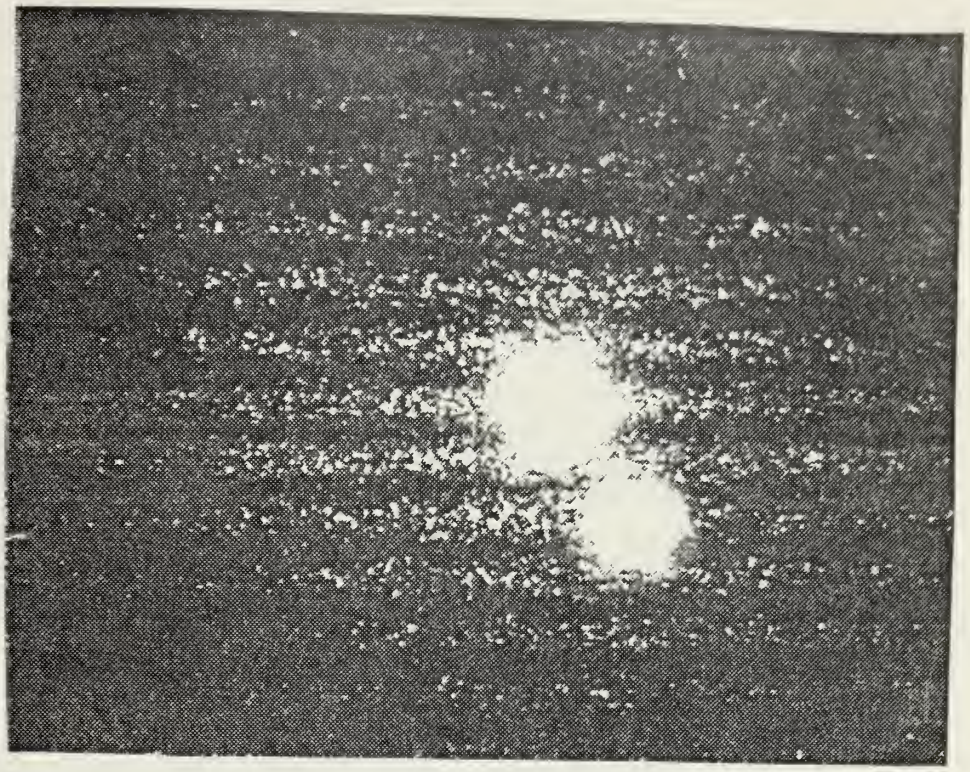

(e) Fringes generated due to 0.040 inch translation.

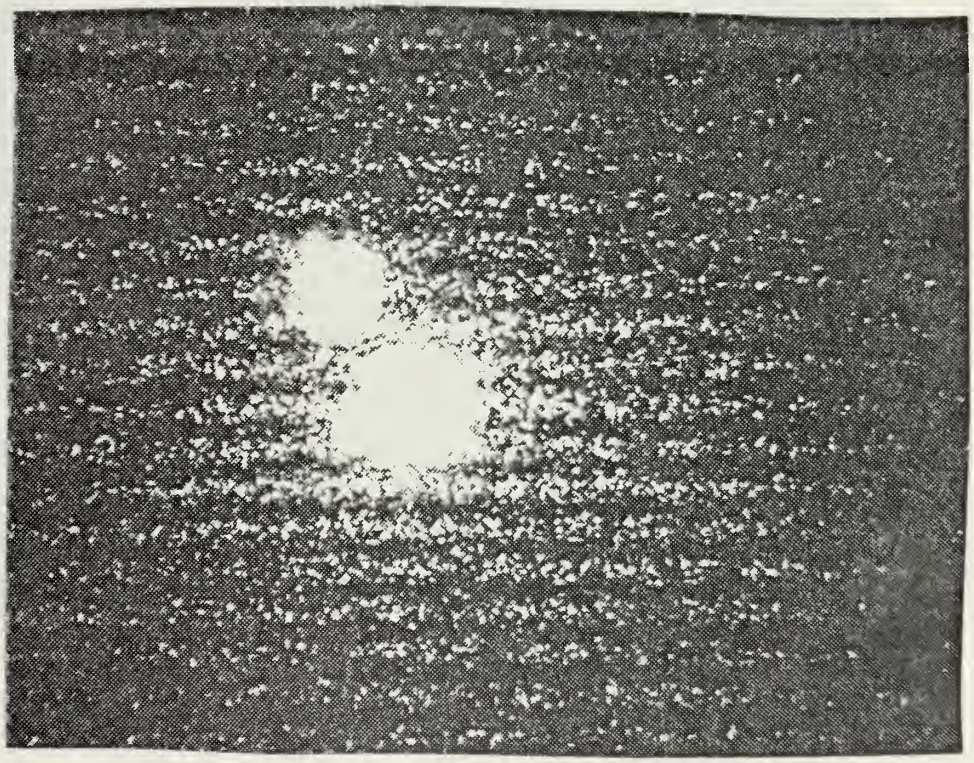

(f) Fringes generated due to 0.050 inch translation.

Figure 31 (Continued)

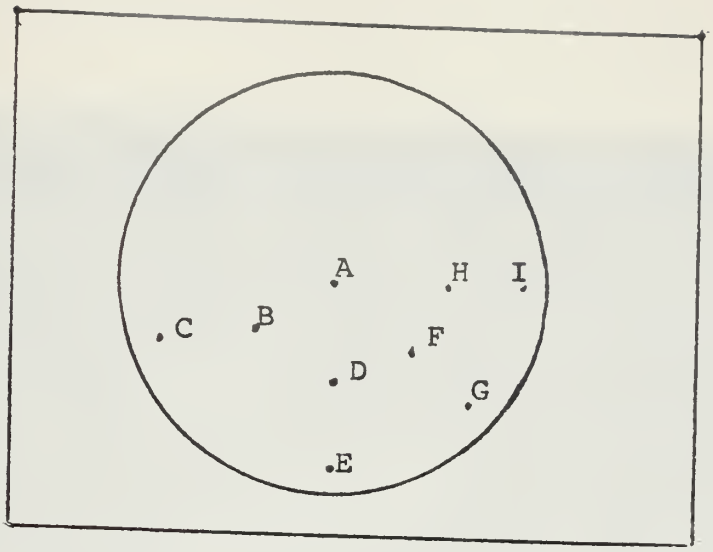

Figure 32. Double exposure rotation specklegram showing location of various fringe observation points.

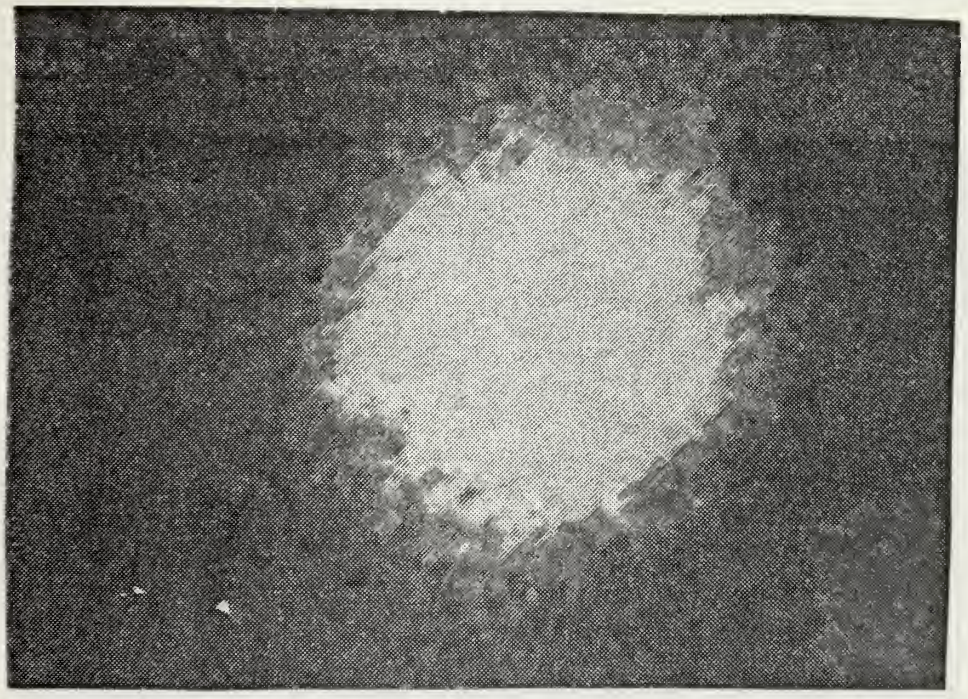

(a) Lack of fringes observed at Point A.

Figure 33. Young's fringes produced from various points of observation on a rotation specklegram as indicated in Figure 32.

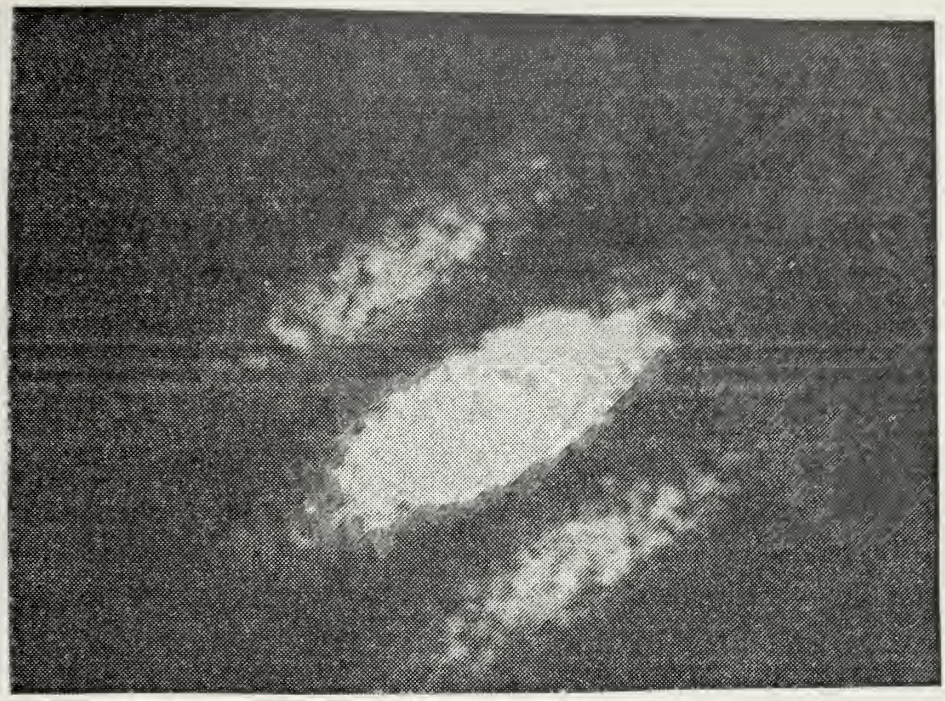

(b) Rotation fringes observed at Point B on the specklegram.

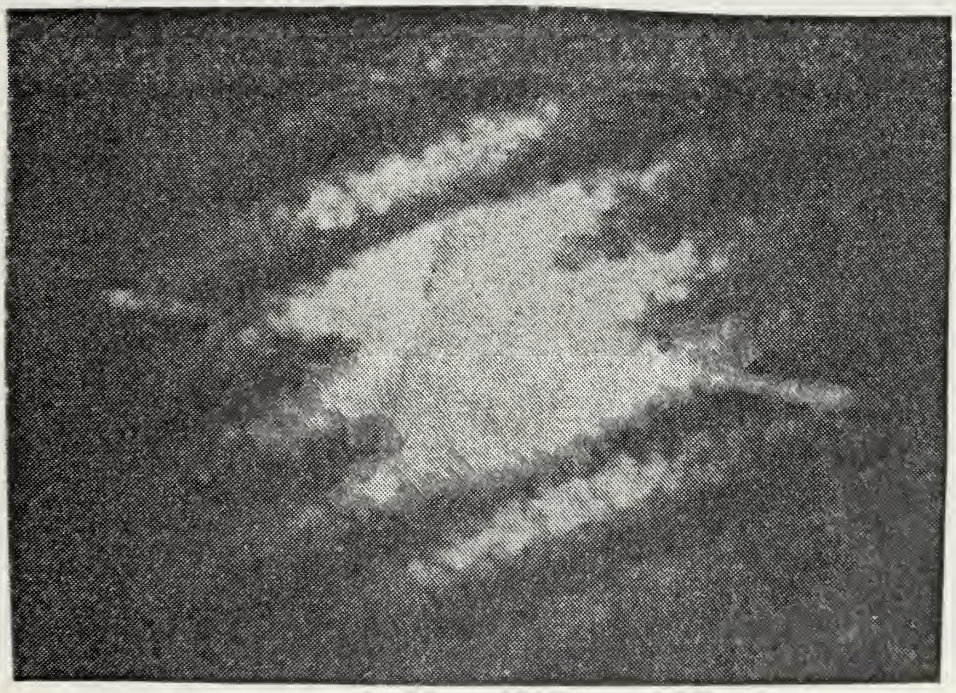

(c) Rotation fringes observed at Point C on the specklegram.

Figure 33 (Continued)

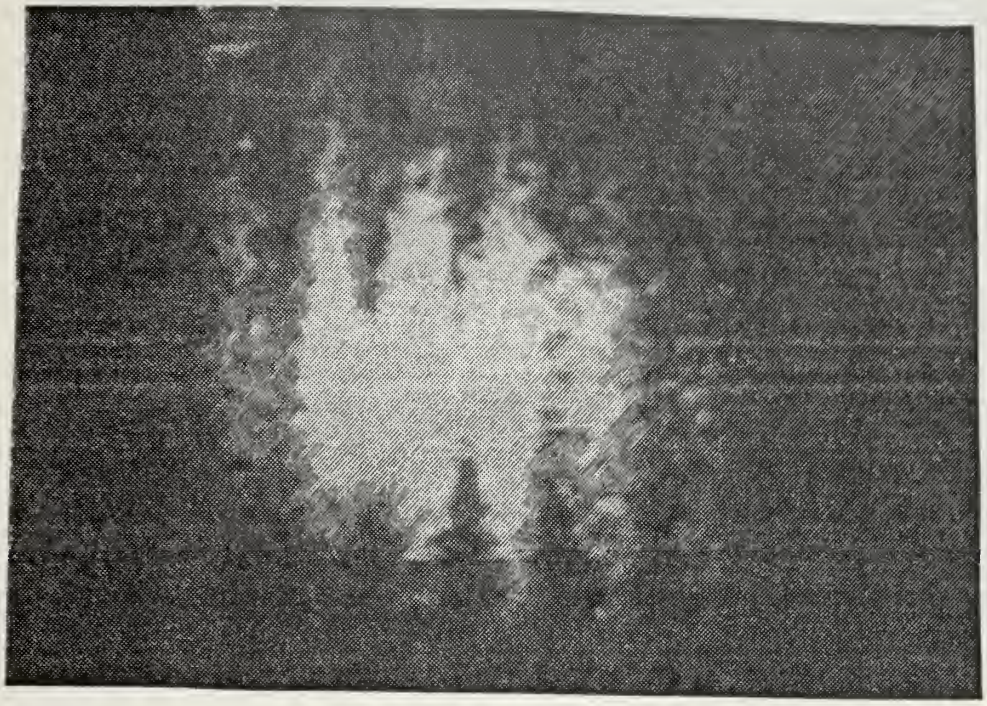

(d) Rotation fringes observed at Point D on the specklegram.

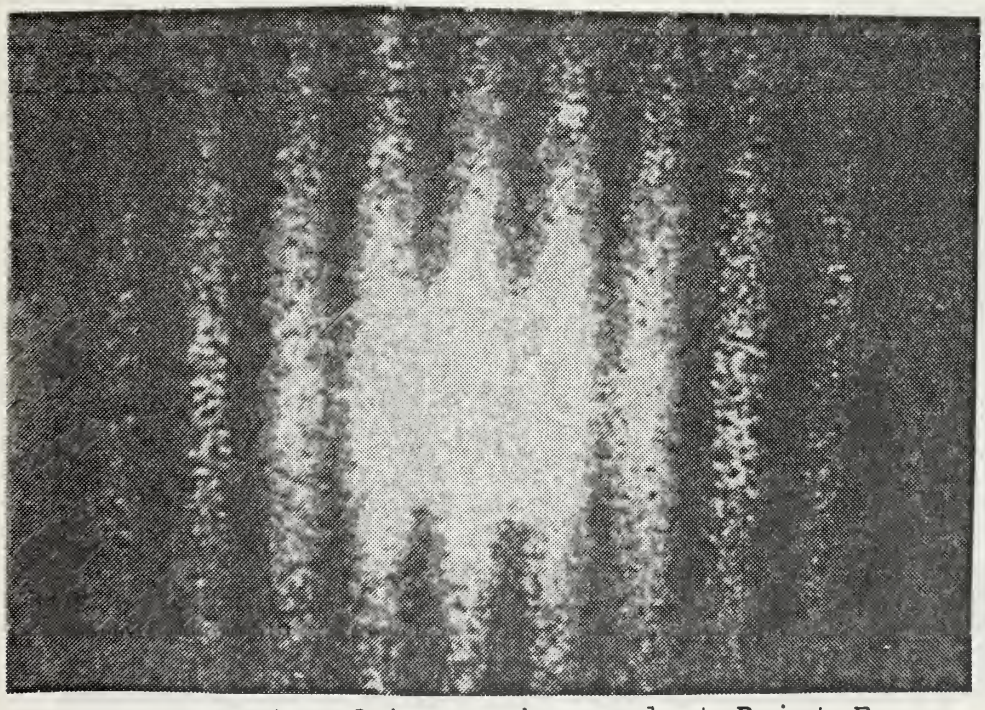

(e) Rotation fringes observed at Point E on the specklegram.

Figure 33 (Continued)

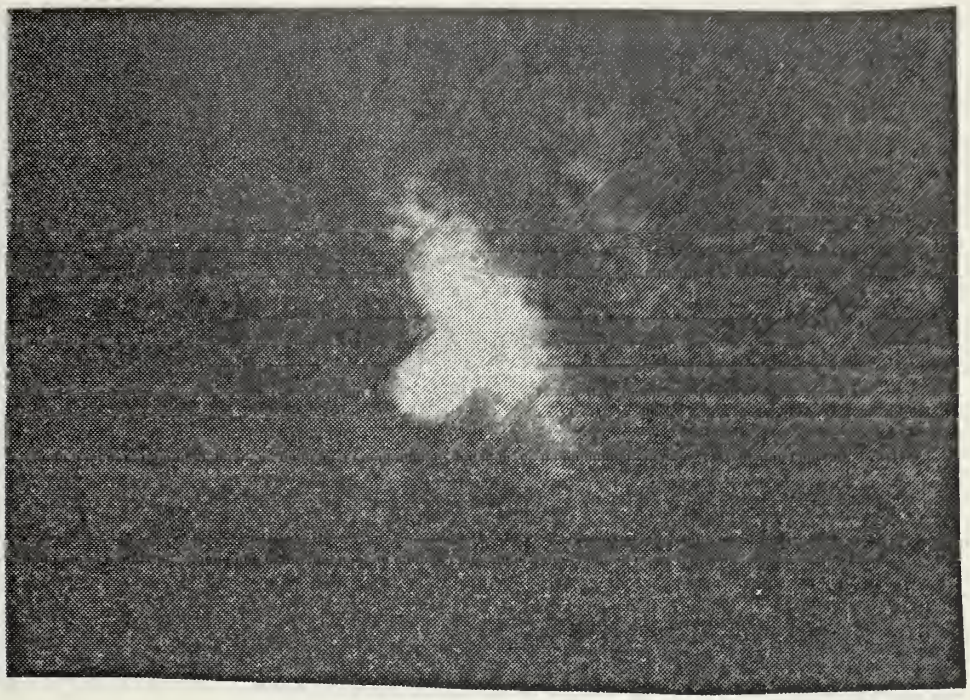

(f) Rotation fringes observed at Point F on the specklegram.

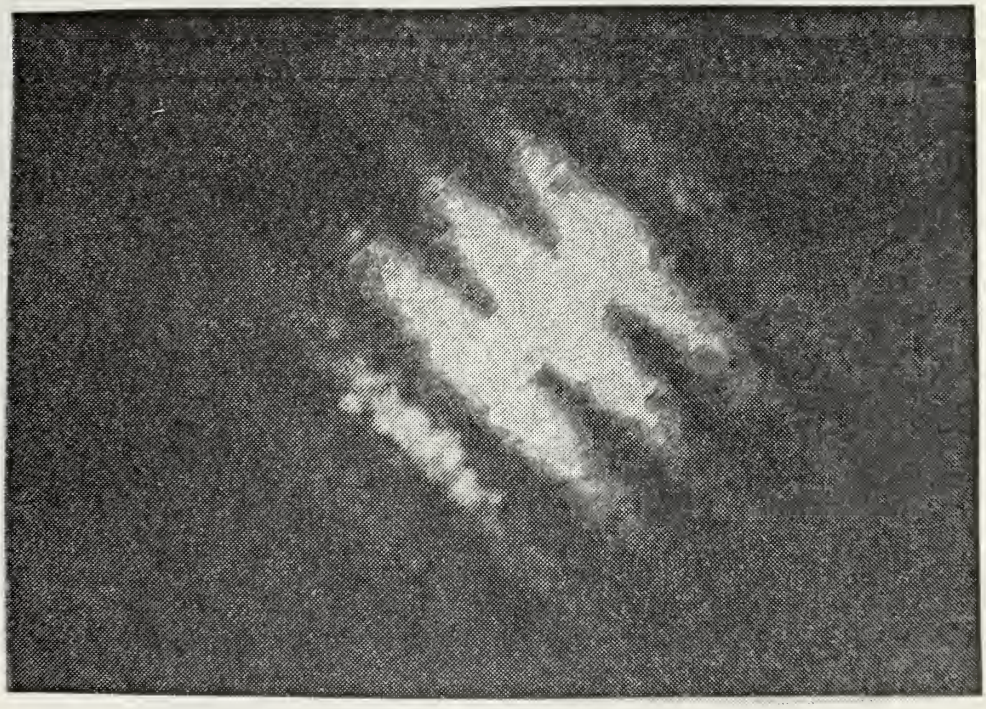

(g) Rotation fringes observed at Point G on the specklegram.

Figure 33 (Continued)

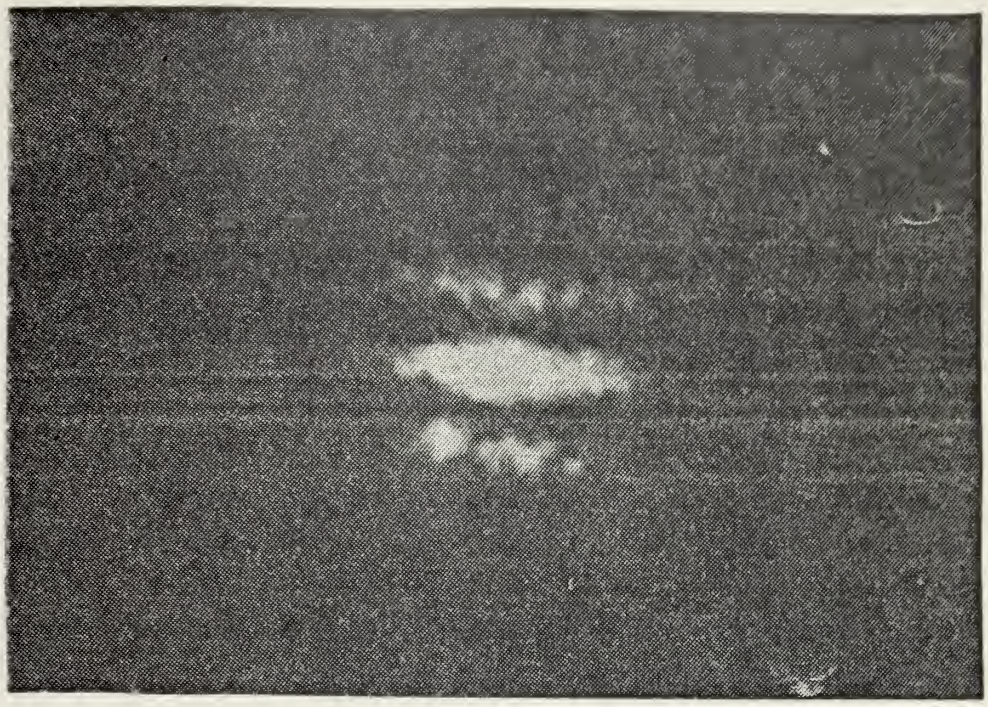

(h) Rotation fringes observed at Point H on the specklegram.

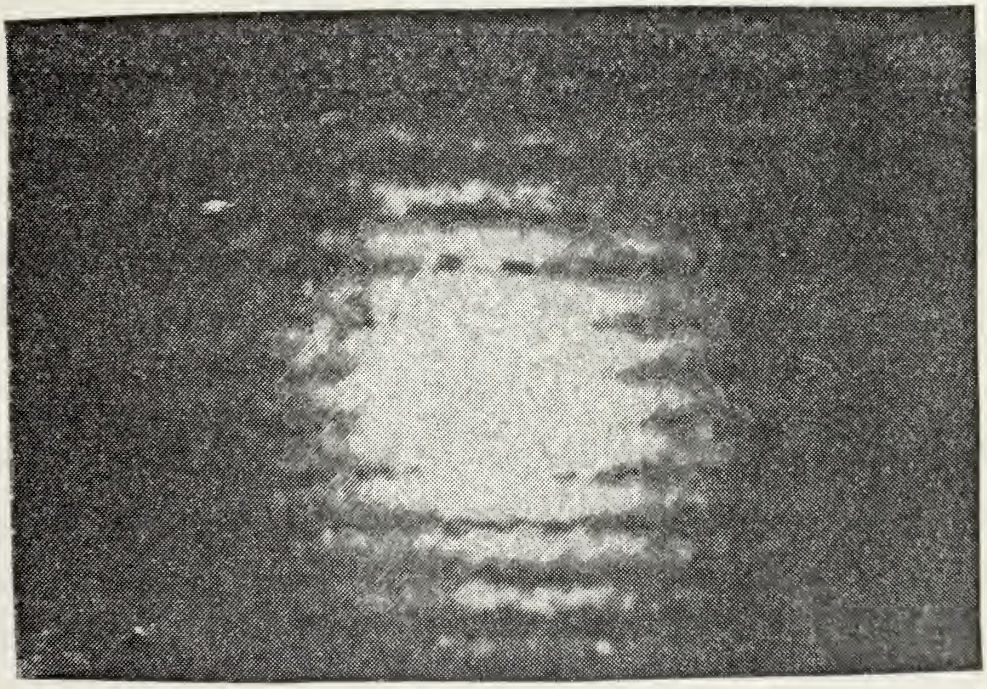

(i) Rotation fringes observed at Point I on the specklegram.

Figure 33 (Continued)

inward from each of these points toward the center of the specklegram, the relative displacement is less, as would be expected, the Young's fringe spacing increases.

E. OUT-OF-PLANE ROTATION - (TILT)

Figure 34 shows the laboratory arrangement of equipment for imaging tilt double-exposure specklegrams.

The laboratory setup is identical to the one used for recording translation and rotation with two differences. First, after the beam is expanded, it is collimated prior to illuminating the object. This collimation process is necessary for recording all out-of-plane motion using this type recording system. Second, instead of recording the image in the image plane, the camera is focused at infinity, placing the image in the back focal plane of the camera. An F number of 2 was used at an object distance of 450 mm with an exposure time of 3 seconds per exposure for optimim results. A tilt range of 1.5" - 15" was tested producing fringes as seen in Figures 35 a and b.

Calculations were made of fringe spacing, tilt, and tilt angle and compared with the actual tilt observed during experimentation. Results of these calculations are tabulated in Table 5.

A graphical comparison of calculated tilt angle versus calculated fringe is observed in Fig. 36.

Both the graph, the tabular results, and the mean error analysis confirm that there is excellent correlation between

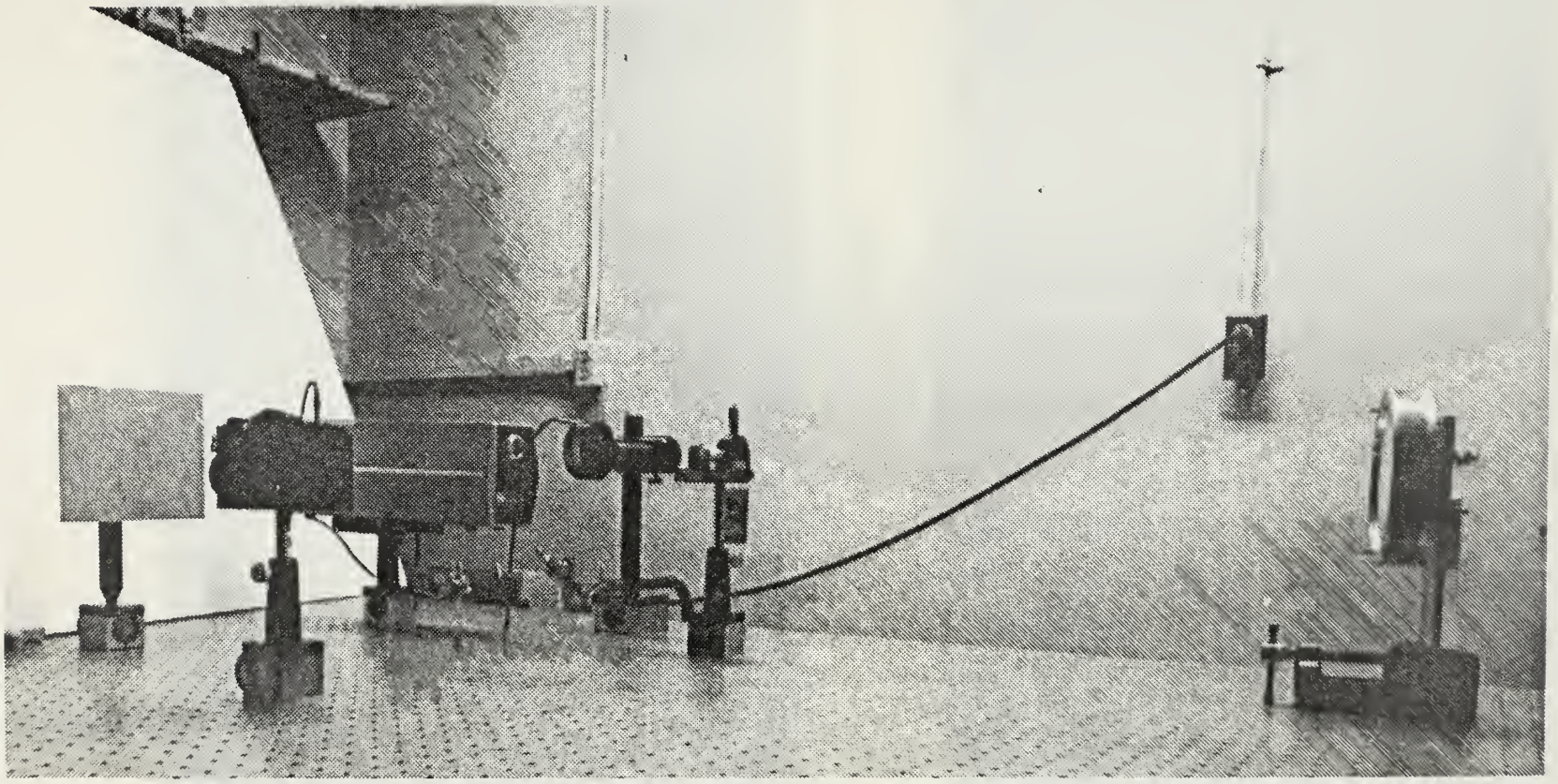

Figure 34. Laboratory equipment arrangement for imaging tilt double-exposure specklegrams.

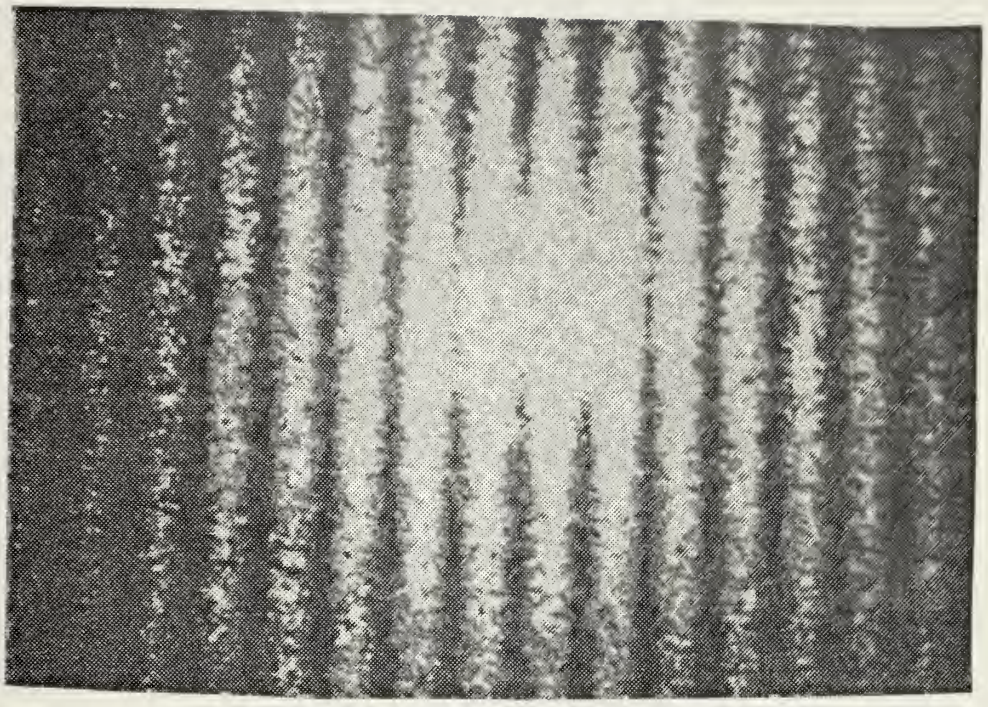

(a) Fringes observed due to a tilt of 3" (double primes denote seconds of arc).

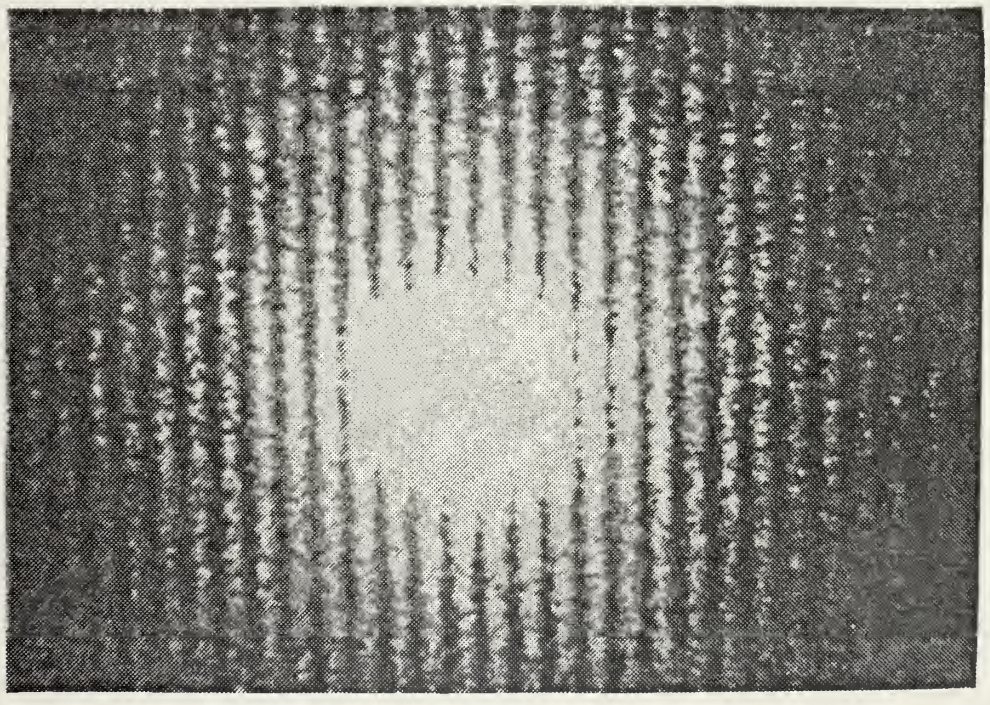

(b) Fringes observed due to a tilt of 10".

Figure 35. Young's fringes produced from various angles of out of plane rotation (tilt).

TABLE 5

Tilt Calculations

γ actual (sec)	d_f (mm)	γ calc. (sec)	Error
15	6	14.414	.039
10	8	10.810	.081
5	18	4.804	.039
4	22	3.931	.017
3	27	3.203	.067
2	37	2.337	.168
1.5	51	1.695	.13

Mean Error = 7.70%

Tilt calculation governing equation and parameters

$$\gamma = \lambda Z/f(1 + \cos\theta_i)d_f \quad \text{(in degrees)}$$

where

$\lambda = .6328 \cdot 10^{-3}$ mm

$Z = 3896.2$ mm

$f = 55$ mm

$\theta_i = 30^{\circ}$

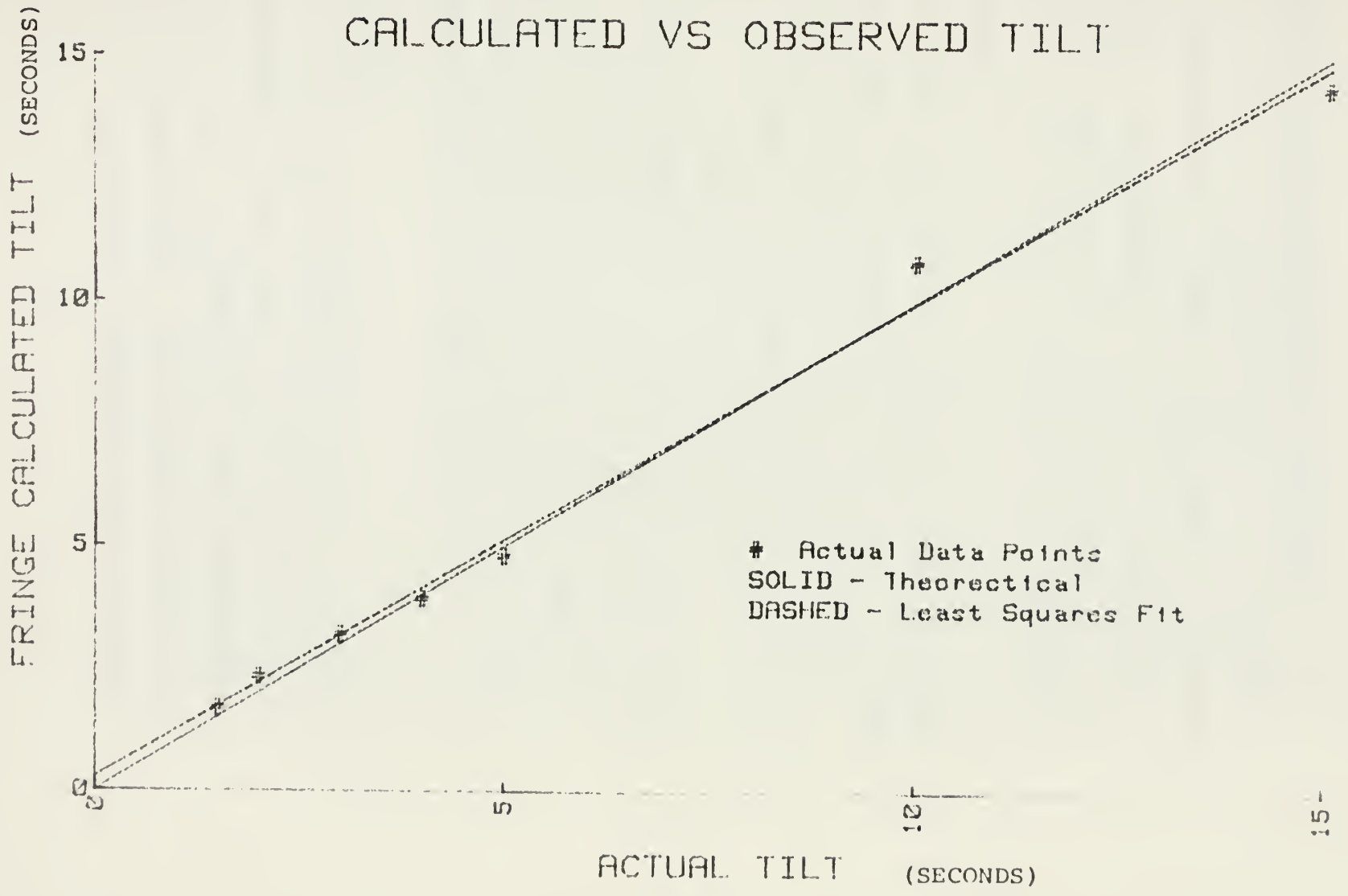
CALCULATED VS OBSERVED TILT
FRINGE CALCULATED TILT (SECONDS)
15
10
5
0
0
5
12
15
ACTUAL TILT (SECONDS)
Actual Data Points
SOLID - Theoretical
DASHED - Least Squares Fit

Figure 36

the actual tilt angle observed during experimentation and the fringe calculated tilt angle.

F. MEASUREMENT OF DISPLACEMENTS DUE TO VIBRATION

Figure 37 shows the laboratory setup for the in-plane vibrational experimentation that was conducted in conjuction with this thesis. The equipment required for vibrational analysis was the same as for tilt experimentation with the exception of the plate holders, excitor, power transformer and oscilliscope.

The plate holder was modified to enable small amplitude in-plane vibrations to be transmitted to the 5 x 7 aluminum plate. A piezoelectric excitor linked in series with a spring having a large spring constant enabled vibrational amplitudes of .1 - 2 mm range to be transmitted.

The image was recorded with a 35mm Pentax camera using the double-exposure speckle technique described previously. An F = 2.8 with an 85mm lens using an exposure time of 2 seconds per exposure were used to record the image at an image distance of 850 mm and a magnification of .11.

G. STRAIN ANALYSIS

Figure 38 shows the experimental setup for the strain analysis conducted in this thesis. With the exception of the plate holder and a modification to the imaging camera, which will be discussed later, the equipment setup is identical to the tilt experimental equipment system discussed previously.

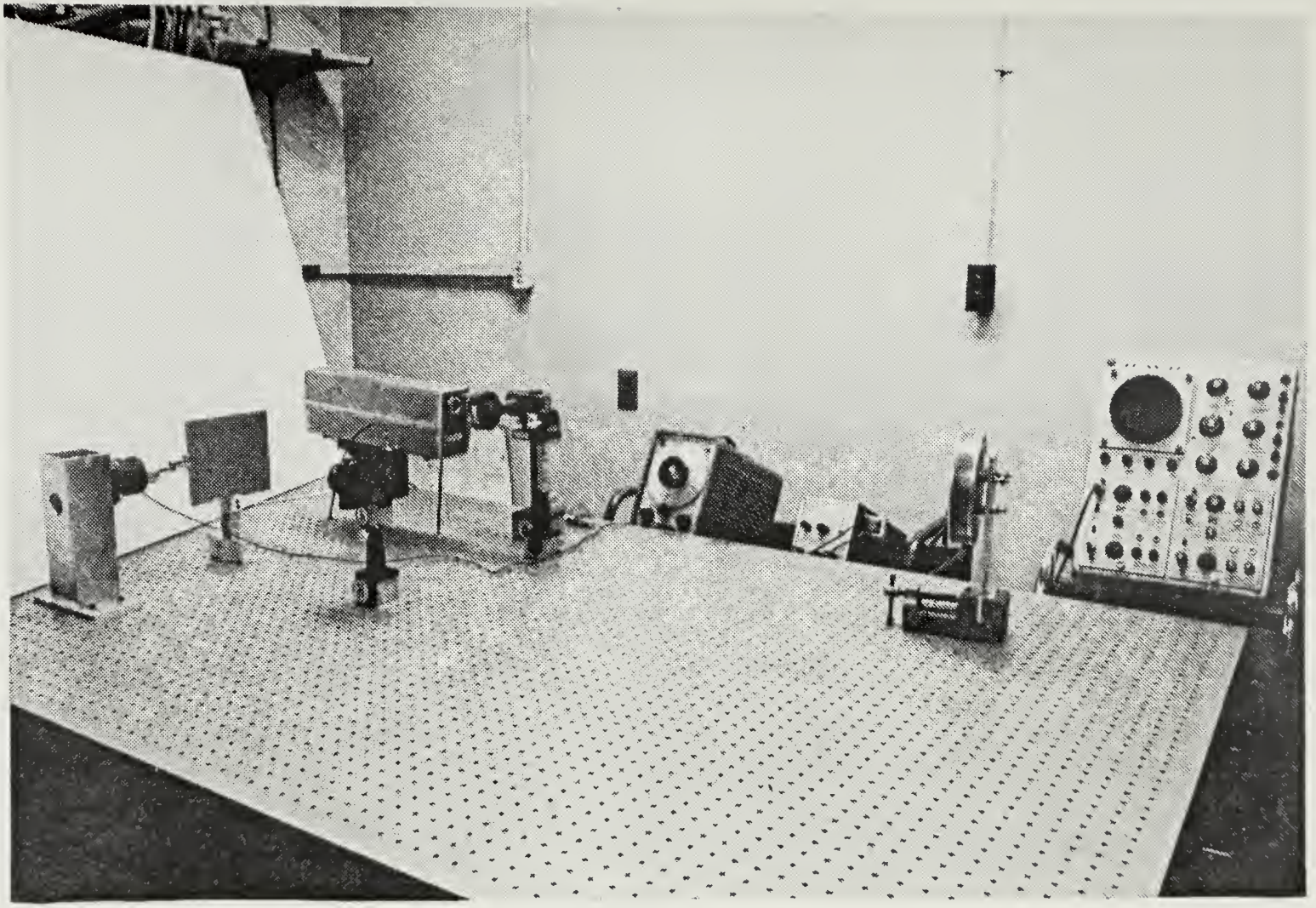

Figure 37. Laboratory equipment arrangement for vibrational analysis.

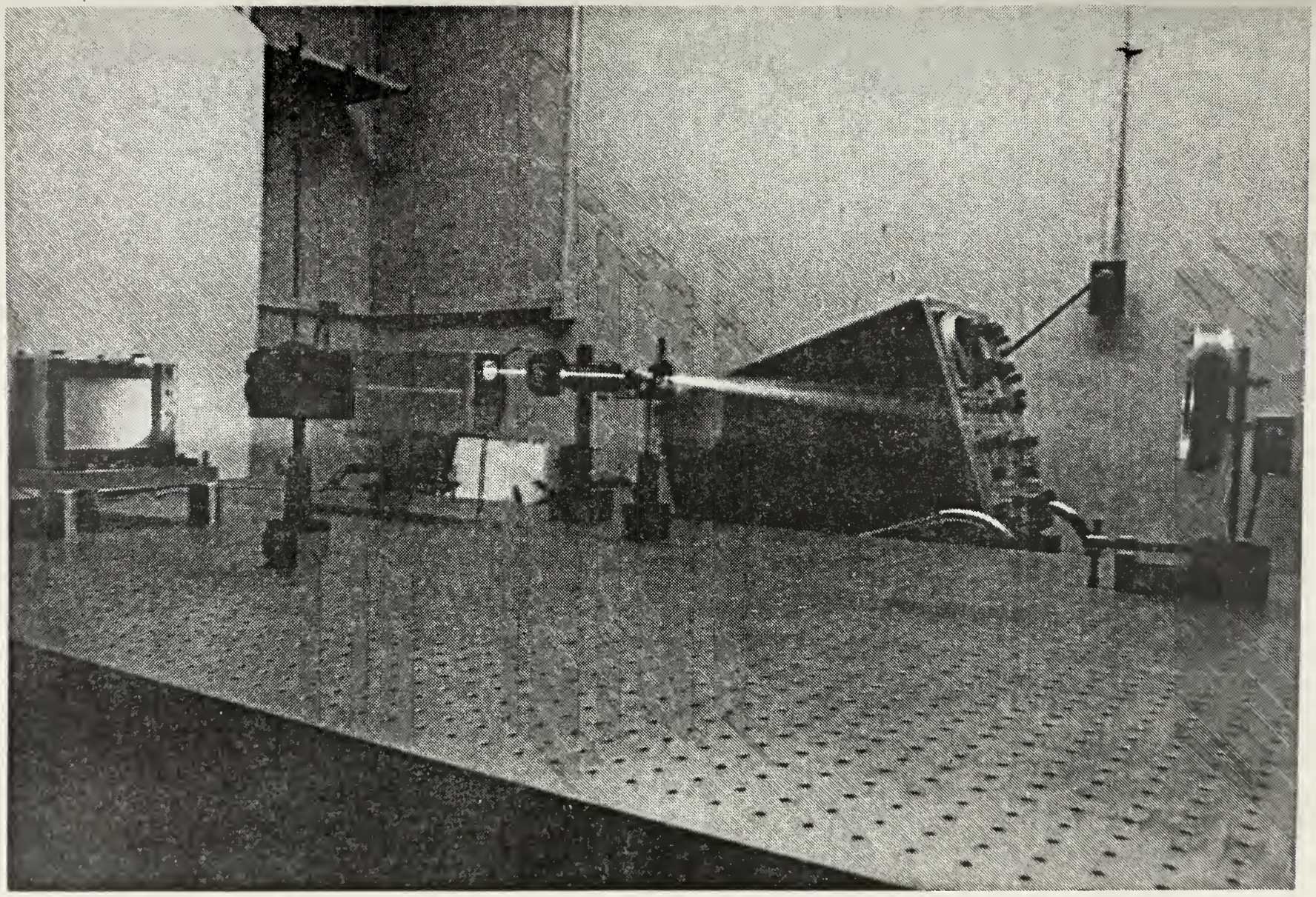

Figure 38. Laboratory equipment arrangement for strain analysis.

The image shearing camera was used to record the double exposure specklegram. In the theory section, the image shearing camera was described in general. Both a 55mm and 85mm lens were used with the Pentax 35mm camera. The shearing prism was a 1^{o} glass wedge with an index of refraction of 1.57. With the 55mm lens an image distance of 450mm and an F of 2.0 with an exposure time of 3 seconds per exposure was used, while with the 85mm lens an image distance of 850mm and an F of 2.8 with an exposure time of 2 seconds per exposure was used. The image shearing camera gives a double-exposure specklegram which is processed using the system seen in Fig. 39.

Figure 40 shows the fringe pattern obtained from the processed image shearing specklegram. This specklegram can be processed in white light without a lens if the shearing is adequate.

To produce the fringes of Fig. 40, a 6 in. x 8 in. rectangular aluminum plate with its surface sprayed flat red was used. The plate was securely clamped along its four boundaries. With collimated illumination with a He-Ne laser a double exposure of the image was photographed. The plate was displaced at the center 0.0005 between exposures.

A no fringe area was seen during experimentation in areas of plastic deformation. During plastic deformation there is no motion of that area of the body, therefore there are no local fringes developed in any area where plastic deformation is experienced.

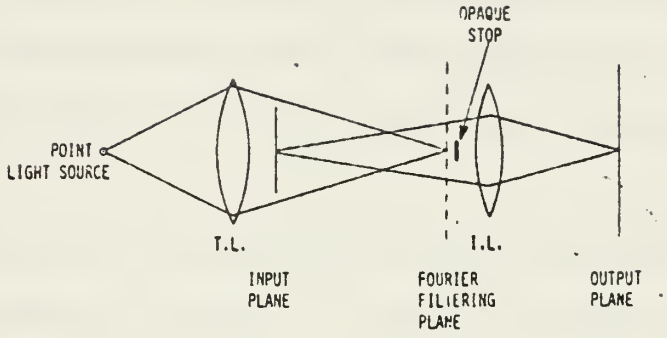

Figure 39. Double-exposure specklegram optical processing system used to analyze strain fringes. From Hung [32]

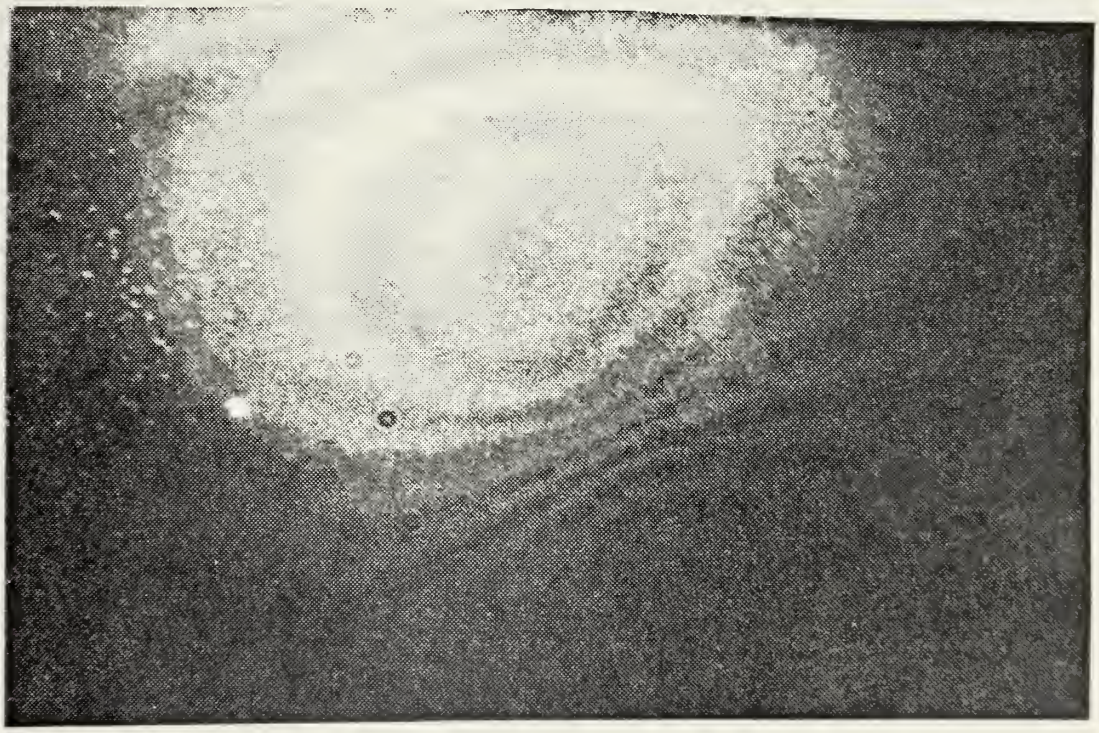

Figure 40. Fringe pattern obtained from the double-exposure specklegram for a displacement at the center of the plate of 0.0005 inches.

Compared with other methods of speckle photography and interferometry, the image shearing camera was found to produce superior fringes. Besides the improved quality of fringes there are several other areas where the speckle image shearing camera improves over conventional speckle methods or holography.

First, the setup is relatively simple and does not require precision alignment of optics. Second, it does not require the special vibrational isolation that accompanies holographic measurements. Third, the need of coherence in the illuminating light source is minimized. Although a collimated beam was utilized, it was not required. Fourth, it provides a wider and more controllable range of sensitivity. The sensitivity can be changed by either changing the illumination angle θ_i or the amount of shearing. Fifth, the strain is measured directly by the image shearing camera.

While this technique works well for small shearing effects, like other speckle techniques the image shearing method is highly susceptible to decorrelation when the object undergoes large, tilt, translation, or strains. This decorrelation deteriorates the fringe visibility.

IV. CONCLUSIONS AND RECOMMENDATIONS

A. CONCLUSIONS

The following conclusions have been drawn from the research conducted during the course of this project.

A comparison of holographic interferometry to speckle metrology shows that both systems of measurement have favorable points which support further research in each area.

The simplicity of equipment arrangement for speckle metrology requires no precision alignment of optics as is required in holographic measurements [7]. Speckle metrology requires no vibrational isolation system. The use of multinode lasers is possible because speckle metrology minimizes the coherent length of the light source required for accurate measurements. There is a wider range of sensitivity and an ease of sensitivity variation in speckle metrology that is not found in holography [34, 35, 53]. Speckle metrology requires a much lower film resolution. Decorrelation of the speckle pattern due to large tilt, translation, or strains deteriorates the fringe visibility. Speckle produced fringes are highly susceptible to lens aberration. Even at best, speckle produced fringes are of poorer quality than holographic fringes. Holographic interferometry presents a much broader band of measurement [53]. Three dimensional motion can be studied using holography much more readily than can be achieved by speckle metrology [53].

From the previously listed conclusions, it is seen that holographic interferometry used in conjunction with speckle

metrology can provide accurate, wide range, highly sensitive, means of metrology to Naval Engineering in general and Naval shipyards specifically.

Specific conclusions derived by actual experimentation are as follows:

Measurements of in-plane translations were measured for a range of 0.001 inches to 0.07 inches with a mean error of less than four percent.

Actual measurements of in-plane rotation were not made, but rather a comparison of relative fringe spacing from individual point inspection of the specklegram was performed. Direction of rotation and relative size of point displacement could be determined from the resultant fringe patterns.

Measurements of out-of-plane rotation (tilt) were made. The range of experimantation of 1.5" to 15" was too small and too few points were sampled to effectively conclude that the accuracy of measurement was as precise as experimentation indicates. Also a more effective method of measuring actual tilt should be used to insure the actual tilt measurements are exact.

Vibrational analysis of both in-plane amplitude measurements and modal shape studies were conducted with limited success. The fringes produced from in-plane vibrations gave good results, but too small an amplitude range and too few points were sampled to make any conclusions concerning the effectiveness of this system.

Strain analysis using the image shearing camera produced fringes which showed the strain field over the entire plate due to a center displacement of approximately 0.0005 inches. Object and image distances can be varied to increase the range of shear observation; but this was not done. Therefore, the effectiveness of the image shearing camera for a wide range of measurements can not be stated. Good fringes were achieved using this system for a limited range of shear.

Each area of study, i.e., translation both in-plane and out-of-plane, vibrations, and strain, is a broad enough field sufficient to support thesis investigation.

B. RECOMMENDATIONS

The field of speckle metrology is in its embryo stage of development. New techniques and methods of analysis and measurement are being discovered continually. The only restriction placed on this field is the imagination of the experimenter.

It is recommended that several of the other methods of speckle metrology be investigated. Experimentation in two and four aperture Fourier filtering analysis of two and possibly three dimensions is being conducted with considerable success [5, 7, 9, 21, 53]. Dual beam speckle interferometry for strain component isolation and vibrational analyses is achieving results comparable to that of holography [15, 30, 37, 40, 51, 53].

In the area of in-plane rotation, it is recommended that x and y component isolation be conducted to measure both direction and relative amount of translation using fringe spacing and orientation.

The system of experimentation used to measure tilt was found to be highly effective and accurate. Two improvements could be made in this area. First, a more accurate method is needed for measuring the actual out-of-plane the tilt which has occurred. This would validate the error analysis conducted in this project. Second, an increased range of measurement could be achieved by varying the object and image distances.

The surface of vibrational and strain analyses were barely scratched during the course of this project. In conjunction with these areas of study, it is recommended that speckle metrology be utilized for beam analysis. Deflection, slope, and moment measurements could easily be effected using the dual beam [5,6,10,21], Fourier filtering [21,53], or shear camera [31-33] methods discussed previously. Vibrational analysis should be conducted, and the results compared with those achieved using holography.

The area of heat transfer is relatively untouched by the literature in conjunction with the rise of speckle metrology. It is felt that transient, two-dimensional, heat transfer problems could be analyzed using speckle metrology methods.

Analyses of transient and real time phenomena using television speckle recordings have been conducted with

relative success by both Maddux [1] and German Da Costa of Simon Bolivar University [21]. This area of study could be undertaken for less than $5,000, greatly expanding the field of speckle metrology for the Naval Postgraduate School.

Currently in industry speckle metrology is being utilized for crack detection and non-destructive testing [21], pressure vessel inspection [21], and stress concentration analysis [21]. The applicability of speckle metrology to Naval Engineering should be highly evident by the remarks entertained in these recommendations and conclusions. Again, as mentioned previously, this is a relatively new science; the potential for growth is constrained by the intensity of the analysts' inquisitiveness. Further studies are considered a must, and they are assumed to be very enlightening and positive contributors to modern science and Naval Engineering.

APPENDIX A

Notes Added During Proof

After the thesis was approved, the author continued research because of extreme interest in the development of speckle metrology. The image shearing camera described in the Strain Analysis section of this thesis was used to obtain slopes of modal amplitudes at various frequencies and compare these results with those achieved by Fahey [A-1].

I. VIBRATION THEORY

The specimen of Fig. 41 undergoes a steady state sinusoidal oscillation represented by:

$$w(x,y,t) = A(x,y) \cos(\omega t + \theta)$$

where $w(x,y,t)$ = normal displacement of a point $P(x,y)$ at a time t.

$A(x,y)$ = modal amplitude function

ω = circular frequency

θ = arbitrary phase

and if normal incidence of light is employed, then Δ is a function of time given by:

$$\Delta(x,y,t) = \frac{4\pi}{\lambda} \delta x \frac{\partial w(x,y,t)}{\partial x}$$

Thus $I_2(x,y)$ is a time dependent function given by,

$$I_2(x',y',t) = 2A^2 \left[1 + \cos^2 \frac{\pi}{\lambda} \left[2\beta x' + f_1(x',y') - f_2(x',y') + \Delta(x',y',t)\right]\right]$$

where I_2 is the intensity distribution received by the photographic plate. If the film is exposed to $I_2(x',y',t)$ for a time T which is large compared to the period of vibration, the recorded intensity is an integration of $I_2(x',y',t)$ over the time T given by:

$$I_i(x',y') = \int_0^T I_2(x',y',t)dt$$

where $I_i(x',y')$ is the integrated intensity. The above integration yields:

$$I_i(x',y') = T\left[1 + \cos\frac{2\pi}{\lambda} 2\beta x' + f_1(x',y') - f_2(x',y')\right]$$
$$J_0\left[\frac{\partial\pi}{\lambda} \quad \delta x \frac{\partial A(x,y)}{\partial x}\right]$$

This is a case where a high frequency term is amplitude modulated by a zero order Bessel function.

Thus Moire fringes will be formed when:

$$J_0\left[\frac{2\pi}{\lambda} \delta x \frac{\partial A(x,y)}{\partial x}\right] = 0$$

Again, the carrier fringes are not visible by the eye. Therefore Fourier filtering is required to make the fringes visible. See Fig. 39.

Figure 41 shows the laboratory equipment arrangement for imaging the slopes of the modal amplitudes. The equipment arrangement is identical to the setup of Fig. 38 for strain analysis with one exception. A piezoelectric excitor was placed behind the plate and excited the center of the plate at various frequencies and amplitudes using the oscillator and transformer described previously in the vibrational section of this thesis.

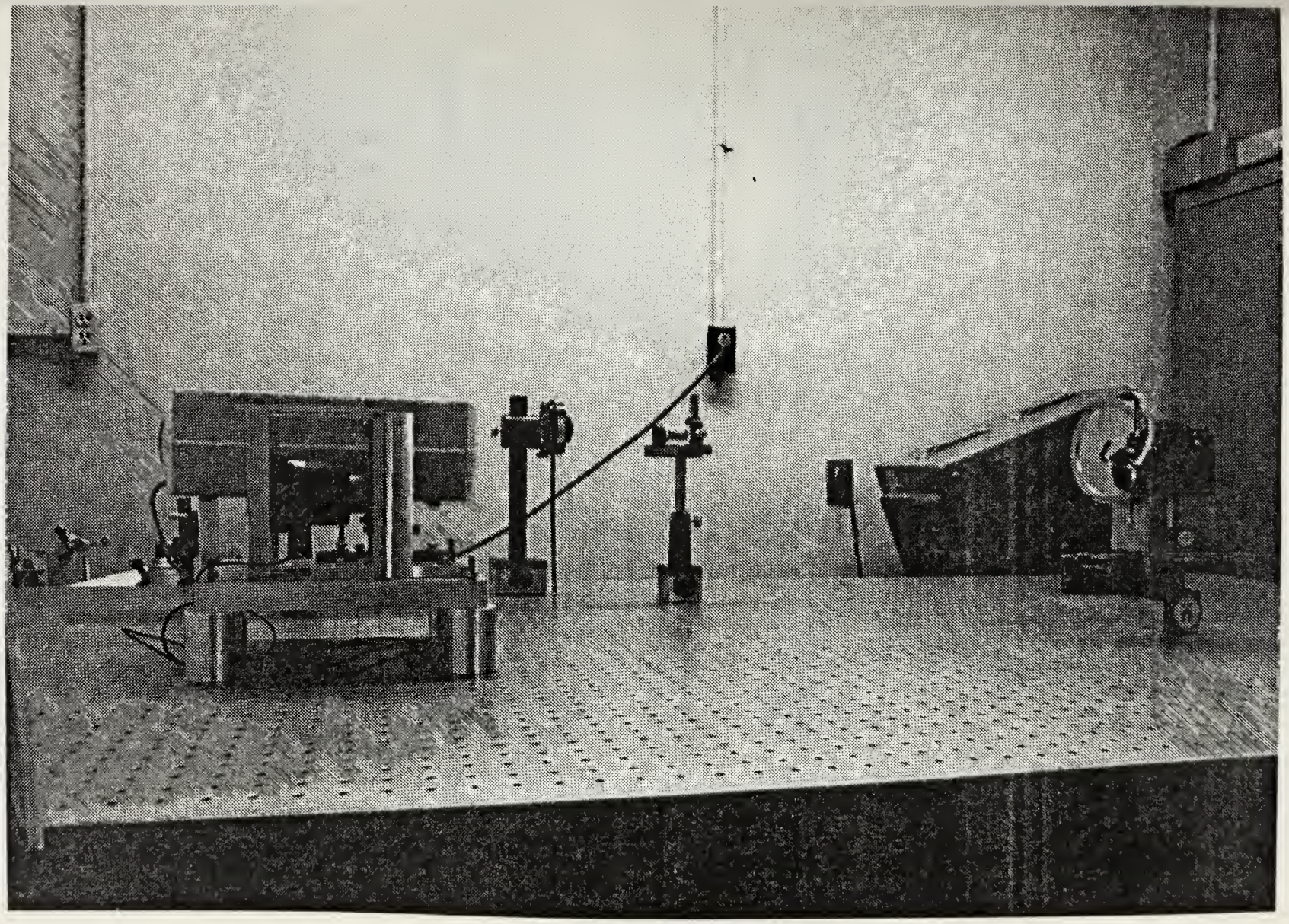

Figure 41. Laboratory equipment arrangement for vibrational analysis using the image shearing camera.

Calculations were made previously by Fahey [A-1] from Leissa [A-2] for the frequency parameters f_n for an all sides clamped rectangular plate.

m	n	$f_{m,n}$
1	1	27.01
2	1	65.50
1	2	41.72
2	2	79.81

The fundamental frequencies calculated by Fahey [A-1] were:

$\omega_{1,1}$ = 327.0 Hz

$\omega_{1,2}$ = 506.2 Hz

$\omega_{2,1}$ = 794.8 Hz

$\omega_{2,2}$ = 968.45 Hz

Fundamental frequencies were found experimentally to be:

$\omega_{1,1}$ = 258 Hz

$\omega_{1,2}$ = 548 Hz

$\omega_{2,1}$ = 752 Hz

$\omega_{2,2}$ = 1047 Hz

Modal amplitude fringes were obtained for the three highest frequency responses, while at 258 Hz fringes were unable to be obtained due to the low amplitude of vibration achieved by the excitor. (See Fig. 42a). A dark ring is observed at

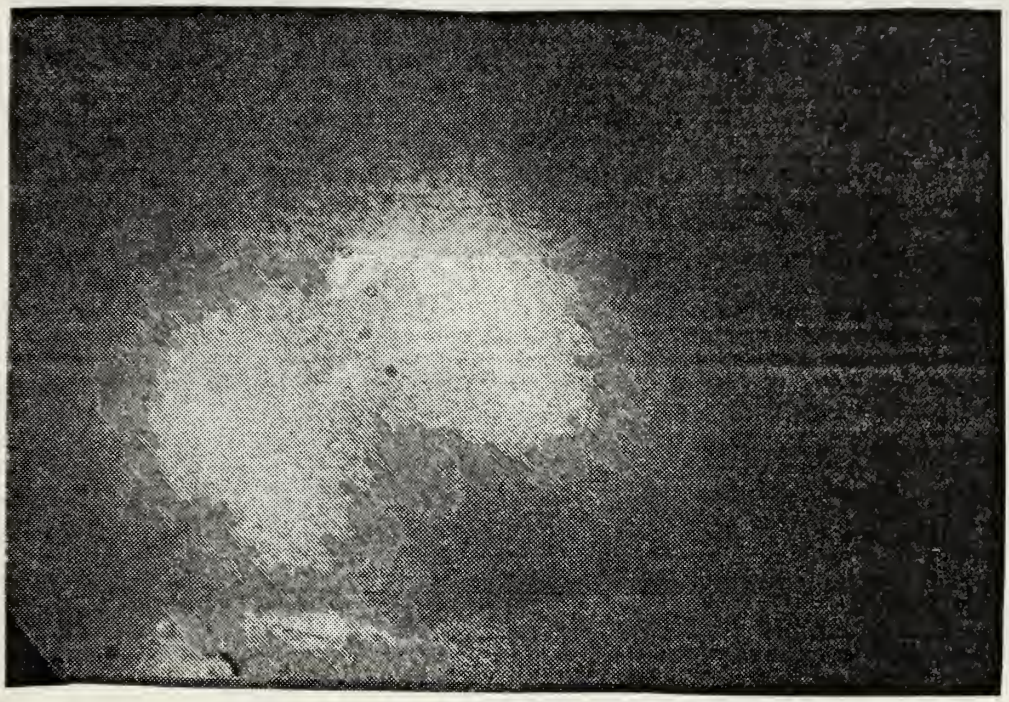

(a) Slope of modal amplitude at 258 Hz.

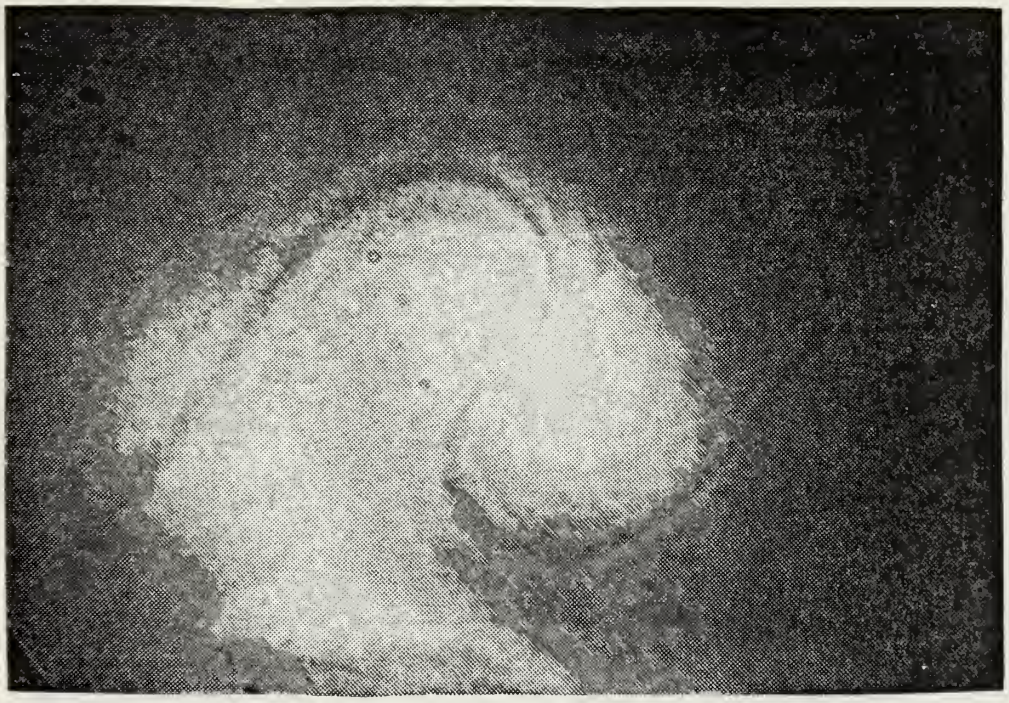

(b) Slope of modal amplitude at 548 Hz.

Figure 42. Slopes of modal amplitudes produced at various resonant frequencies.

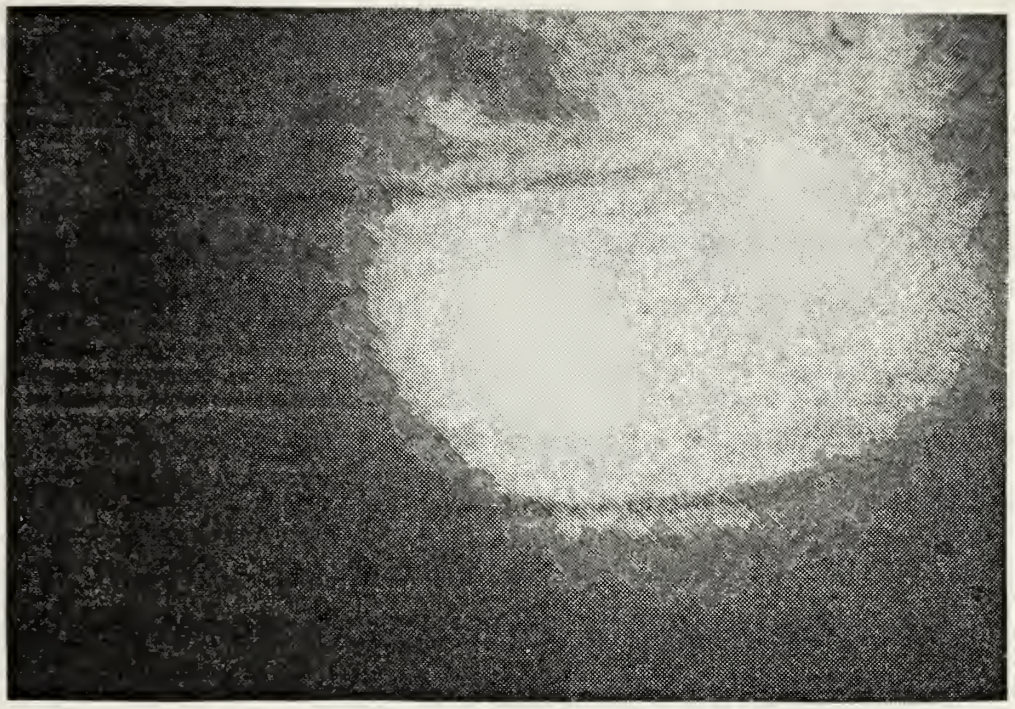

(c) Slope of modal amplitude at 752 Hz.

(d) Slope of modal amplitude at 1047 Hz.

Figure 42 (Continued)

outer plate where the circular first mode fringes would have been seen had a larger amplitude been achieved.

As observed previously, although the fringes produced by holography are much clearer no vibrational isolation is needed nor is the precision optical setup required for speckle photography. A relatively large range of amplitude variation was achieved using the image shearing camera technique.

Further research is definitely required to enable the author to make additional conclusions as to the effectiveness of this technique.

LIST OF REFERENCES

A-1 Fahey, J. M., Vibration Analysis and Nondestructive Testing Using Double-exposure Holographic Techniques, MSME Thesis, Naval Postgraduate School, Monterey, California, 1979.

A-2 Leissa, A. W., Vibration Of Plates, National Aeronautics and Space Administration, pp. 58-65, 1969, SP-160.

BIBLIOGRAPHY

1. Adams, F. D. and Maddux, G. E., Synthesis of Holography and Speckle Photography to Measure 3-D Displacements. Appl. Opt. 13(2) 1974.

2. Air Force Wright Aeronautical Laboratories, Report No. AFDL-TR-75-92, Dual Plate Speckle Photography, by Frank D. Adams and Gene E. Maddux, October 1975.

3. Adams, F. D. and Maddux, G. E., On Speckle Diffraction Interferometry for Measuring Whole Field Displacements and Strains. Air Force Flight Dynamics Lab., Tech. Report 72-123, 1973.

4. Air Force Flight Dynamics Laboratory, Report No. AFFDL-TR-73-123, On Speckle Diffraction Interferometry for Measuring Whole Field Displacement and Strain, by Frank D. Adams and Gene E. Maddux, Dec. 1973.

5. Archbold, E., Burch, J. M., and Ennos, A. E., "Recording of In-plane Surface Displacement by Double-Exposure Speckle Photography," Optica Acta, Vol. 17, No. 12, pp. 883-898, 1970.

6. Archbold, E., Ennos, A. E., and Taylor, Pauline A., "A Laser Speckle Interferometer for the Detection of Surface Movements and Vibration," Division of Optical Metrology, National Physical Laboratory, Teddington, Middx.

7. Archbold, E., and Ennos, A. E., "Applications of Holography and Speckle Photography to the Measurement of Displacement and Strain," The Journal of Strain Analysis, Vol. 9, No. 1, pp. 10-16, January 1974.

8. Archbold, E., and Ennos, A. E., "Measurement by Laser Photography," National Physical Laboratory, Division of Optical Metrology, Teddington, Middlesex, U.K.

9. Archbold, E., Ennos, A. E., and Virdee, M. S., "Speckle Photography for Strain Measurement - A Critical Assessment," Division of Mecnanical and Optical Metrology, National Physical Laboratory Queens Road, Teddington, Middlesex, TW11 OLW, UK.

10. Archbold, E. and Ennos, A. E., "Displacement Measurement from Double-exposure Laser Photographs," Optica Acta, Vol. 19, No. 4, pp. 253-271, 1972.

11. Barakat, Richard, "The Brightness Distribution of the Sum of Two Correlated Speckle Patterns," Optics Communications, Vol. 8, No. 1, pp. 14-16, May 1973.

12. Barker, D. B. and Fourney, M. E., Displacement Measurement in the Interior of 3-D Bodies Using Scattered Light Speckle Patterns. Exp. Mech 16(6) 1976.

13. Born, M. and Wolf, E., Principles of Optics, pp. 370-398, Pergamon Press, 1970.

14. Brdicko, J., Olson, M. D., and Hazell, C. R., "Theory for Surface Displacement and Strain Measurements by Laser Speckle Interferometry," Optica Acta, Vol. 00, No. 0. 0-00, pp. 1-27, 1978.

15. Chiang, F. P. and Khetan, R. P.,"Strain Analysis by one-beam Laser Speckle Interferometry 2: Multiaperture Method," Applied Optics, Vol. 18, Nol 13, p. 2175, 1 July 1979.

16. Cloud, G., "Practical Speckle Interferometry for Measuring In-Plane Deformation,"Appl. Opt. 14(4) 1975.

17. Cowley, J. M., Diffraction Physics, pp. 3-103, North Hollund Publishing Company, 1975.

18. Ballistic Research Laboratories, Report No. 1772, Image Information by Means of Speckle Pattern Processing, by Paul H. Dietz, March 1975.

19. Ditchburn, R. W., Light, pp. 643-677, Academic Press. 1976.

20. Ek, L. and Molin, N. E., "Detection of the Nodal Lines and the Amplitude of Vibration by Speckle Interferometry," Optics Communications, Vol. 2, No. 9, pp. 419 - 424, February 1971.

21. Erf, R. W., Speckle Metrology, Academic Press, 1978.

22. Fowles, G. R., Introduction to Modern Optics, pp. 104 - 121, Holt, Rinehart, and Winston, Inc., 1968.

23. Francon, M., Laser Speckle and Stress Application in Optics, Academic Press, 1979.

24. Linear Systems, Fourier Transforms, and Optics, J. D. Gaskill, John Wiley & Sons, 1978.

25. Goodman, J.W., Introduction to Fourier Optics, pp. 57 - 113, McGraw-Hill 1968.

26. Goodman, J.W., "Some Fundamental Properties of Speckle," Optical Society of America, Vol. 66 No. 11, pp. 1145-1148, Nov. 1976.

27. Gregory, D. A.,"Basic Physical Principles of Defocused Speckle Photography: A Tilt Topology Inspection Technique," Optics and Laser Technology, pp. 201-213, October 1976.

28. George, Nicholas, "Speckle," Optic News, pp. 14-20, January 1976.

29. Hogmoen, Kare, and Pedersen, Hans M., "Measurement of Small Vibrations Using Electronic Speckle Pattern Interferometry: Theory," J. Opt. Soc. Am., Vol. 67, No. 11, pp. 1578-1583, November 1977.

30. Hovanesian, J. D., Hung, Y. Y., and Durelli, A. J., "New Optical Method to Determine Vibration - Induced Strains with Variable Sensitivity after Recording," Report on Contract No. N00014-76-C-0487, School of Engineering, Oakland University, Rochester, Michigan 48063, May 1978.

31. Hung, Y. Y., Daniel, I. M., and Rowlands, R.E., "Full Field Optical Strain Measurement Having Pastrecording Sensitivity and Direction Selectivity," Experimental Mechanics, Vol. 18, No. 2, pp. 56-60, February 1980.

32. Hung, Y. Y. and Taylor, C. E., "Speckle shearing Interferometric Camera - A Tool For Measurement Of Derivatives of Surface - Displacement," Society of Photo-Optical Instrumentation Engineers, Vol. 41, pp. 169-176, August 1973.

33. Hung, Yau Y.,"A Speckle-Shearing Interferometer: A Tool For Measuring Derivatives Of Surface Displacements," Optics Communications, Vol. 11, No. 2, pp. 132-135, June 1974.

34. Hung, Y. Y., and Hovanesian, J. D., "Full-field Surface-Strain and Displacement Analysis of Three-dimensional Objects by Speckle Interferometry," Experimental Mechanics, pp. 454-460, October 1972.

35. Jacquot, Pierre and Rastogi, Pramod K., "Speckle Motions Induced by Rigid-body Movements in Free-space Geometrh: An Explicit Investigation and Extension to New Cases," Applied Optics, Vol. 18, No. 12, pp. 2022-2032, 15 June 1979.

36. Jones, R., "The Design and Application of a Speckle Pattern Interferometer for Total Plane Strain Field Measurement," Optics and Laser Technology, pp. 216 - 219, October 1976.

37. Khetan, R. P., and Chiang, F. P., "Strain Analysis by One Beam Lawer Speckle Interferometry - Part I. Single Aperture Method," Department of Mechanics, College of Engineering and Applied Sciences, State University of New York at Stony Brook, Report No. 252, to appear in Applied Optics. December 1974.

38. Leendertz, J. A., Interferometric Displacement Measurement on Scattering Surfaces Utilising Speckle Effect. J. Phys. E. Sci. Inst., Vol. 3, 1970.

39. Lohmann, A. W., and Weigelt, G. P., "Speckle Motion for the Display of Motion Paths," Optical Society of America, pp. 1271-1276, Vol. 66, No. 11, Nov. 1976.

40. Luxmoore, A. R., Amin, F. A. A., and Evans, W. T., "In-plane Strain Measurement by Speckle Photography: A Practical Assessment of the Use of Young's Fringes," The Journal of Strain Analysis, Vol. 9, No. 1, pp. 26 - 35, January 1974.

41. Air Force Flight Dynamics Laboratory, Report No. AFFDL/FBEC, Photomechanics Facility by Gene E. Maddux, March 1976.

42. McKenchie, T. S., "Image-plane Speckle in Partially Coherent Illumination," Optical and Quantum Electronics, Vol. 8 pp. 61-67, 1976.

43. Introduction To Lasers And Their Applications, Oshea, Donald C., Callen, W.R., Rhodes, W.T., Addison-Wesley Publishing Co., 1977.

44. Parks, V. J., Catholic University of America, "The Range of Speckle Metrology," Paper No. R79-192, presented at 1979 SESA Spring Meeting, San Francisco, Ca., May 20 - 25.

45. Pedretti, M. G. and Chiang, F. P., "Effect of Magnification In Laser Speckle Photography," Optical Society of America, Vol. 68, No. 12, pp. 1742-1747, December 1978.

46. Stetson, Karl A., "The Vulnerability of Speckle Photography to Lens Averrations," J. Opt. Soc. Am. Vol. 67, No. 11, pp. 1587-1590, November 1977.

47. Stetson, Karl A., "Analysis of Double-exposure Speckle Photography with Two-Beam Illumination, Journal of the Optical Society of America, Vol. 64, No. 6, pp. 857 - 861, June 1974.

48. Stetson, Karl A., "A Review of Speckle Photography and Interferometry," Optical Engineering, Vol. 14, No. 5, pp. 482-489, September-October 1975.

49. Stetson, K. A. and Harrison, I. R., "Determination of the Principle Surface Strains On Arbitrarily Deformed Objects via Tandem Speckle Photography," pp. 149-154, VDI-Berichte Nr. 313, 1978.

50. Takahara, Hikaru, "Visibility of Speckle Patterns: Effect of the Optical Guide Length in Coherent Light," Applied Optics, Vol. 15, No. 3, pp. 609-610, March 1976.

51. Tiziani, H. J., "Application of Speckling for In-plane Vibration Analysis," Optica Acta, Vol. 18, No. 12, pp. 891-902, 1971.

52. Tiziani, H. J., "A Study of the Use of Laser Speckle to Measure Small Tilts of Optically Rough Surfaces Accurately," Optics Communications, Vol. 5, No. 4, pp. 271-275, July 1972.

53. Vest, C. M., Holographic Interferometry, pp 1-36 and pp. 396-428, John Wiley and Sons 1979.

54. Vikram, C. S. and Vedam, K., "Measurement of Subspeckle-size Changes By Laser-speckle Photography," Optical Society of America, pp. 406-407, Vol. 4, No. 12, December 1979.

55. Wadsworth, N., Marchant, M., and Billing B., "Real-time Observation Of In-Plane Displacements Of Opaque Surfaces," Optics and Laser Technology, pp. 119-123, June 1973.

INITIAL DISTRIBUTION LIST

		No. Copies
1.	Defense Technical Information Center Cameron Station Alexandria, Virginia 22314	2
2.	Library, Code 0142 Naval Postgraduate School Monterey, California 93940	2
3.	Department Chairman, Code 69 Department of Mechanical Engineering Naval Postgraduate School Monterey, California 93940	1
4.	Professor A.E. Fuhs, Code 67Fu Department of Aeronautical Engineering Naval Postgraduate School Monterey, California 93940	6
5.	LCDR Paul M. Huber, USN Portsmouth Naval Shipyard Portsmouth, New Hampshire 03801	1
6.	Commander Boston Naval Shipyard ATTN: Code 130 Boston, Massachusetts 02129	1
7.	Commander Puget Sound Naval Shipyard ATTN: Code 130 Bremerton, Washington 98314	1
8.	Commander Charleston Naval Shipyard Attn: Code 130 Naval Base Charleston, South Carolina 29408	1
9.	Commander Long Beach Naval Shipyard ATTN: Code 130 Long Beach, California 90801	1
10.	Commander Pearl Harbor Naval Shipyard ATTN: Code 130 Box 400 Pearl Harbor, Hawaii 96860	1

11.	Commander Philadelphia Naval Shipyard ATTN: Code 130 Philadelphia, Pennsylvania 19112	1
12.	Commander Portsmouth Naval Shipyard ATTN: Code 130 Portsmouth, New Hampshire 03801	1
13.	Commander Norfolk Naval Shipyard ATTN: Code 130 Portsmouth, Virginia 23709	1
14.	Commander Mare Island Naval Shipyard ATTN: Code 130 Vallejo, California 94592	1
15.	LT. Phil Hoffman, USN Pearl Harbor Naval Shipyard ATTN: Code 331 Pearl Harbor, Hawaii 96860	1
16.	CAPT. Alfred Skolnick Naval Sea Systems Command PMS 405 Crystal City Washington, D.C. 22202	1
17.	RADM. James W. Lisanby Naval Ship Engineering Center NAVSEA 6000 N.C. 2 Crystal City Washington, D.C. 22202	1
18.	LCDR J.M. Fahey, USN PXO USS THORN (DD-988) c/o FIT (Spruance Class) Ingalls Shipbuilding Co. Pascagoula, Mississippi 93567	1
19.	Professor David Salinas, Code 69Bh Department of Mechanical Engineering Naval Postgraduate School Monterey, California 93940	2
20.	LT. A.B. Lerchbacker, USN 964 Valley Blvd. Elyria, Ohio 44035	10

Thesis
L544
c.1
187529
Lerchbacker
Surface displacement measurements, strain and vibrational analysis using speckle metrology techniques.